Emulsion formulation of electrostrictive materials for energy harvesting devices

Ollin Alan Luna Cornejo

université de BORDEAUX

THÈSE PRÉSENTÉE

POUR OBTENIR LE GRADE DE

DOCTEUR DE

L'UNIVERSITÉ DE BORDEAUX

ÉCOLE DOCTORALE DE SCIENCES CHIMIQUES

SPÉCIALITÉ : CHIMIE -PHYSIQUE

Par Ollin Alan LUNA CORNEJO

FORMULATION DE MATÉRIAUX ÉLÉCTROSTRICTIFS PAR VOIE ÉMULSION POUR LA RÉCUPERATION D'ÉNERGIE

Sous la direction de : Annie COLIN
co-directeur : Philippe POULIN

Soutenue le 5 février 2016

Membres du jury :

M. HADZIIOANNOU, Georges	Professeur au LCPO, Bordeaux 1	Président
M. VIDAL, Fréderic	Professeur au LPPI, Cergy Pontoise	Rapporteur
M. CHAUVET, Olivier	Professeur à l'IMN, Nantes	Rapporteur
M. LALLART, Mickaël	Maitre de Conférences au LGEF INSA Lyon	Examinateur

Titre : Formulation de matériaux électrostrictifs par voie émulsion pour la récupération d'énergie

Résumé :

L'objectif de ces travaux est le développement de réseaux de nanoparticules conductrices telles que les nanotubes de carbone (CNT) ou feuillets de graphene dans une matrice polymère élastique faite de polydimethylsiloxane (PDMS). Une approche par voie émulsion est utilisée pour contrôler de façon précise la structure interne des matériaux. Les dispersions de CNT ou de graphène sont incorporées dans la phase continue d'une émulsion directe composée de gouttelettes de PDMS dans l'eau. Après évaporation, les nanoparticules s'agrègent au niveau de bords de Plateau pour former de réseaux dont la morphologie dépend de la taille de gouttelettes. Les propriétés diélectriques de ces matériaux sont contrôlées par la taille de gouttelettes, la concentration de charges et leur état d'agrégation. L'optimisation de leviers de formulation permet d'atteindre des valeurs de permittivité diélectrique très élevées ($\varepsilon_r' \approx 10^4$ à 100Hz). De plus, nous avons développé une méthode expérimentale adaptée et précise afin d'étudier les propriétés diélectriques du matériau soumis à une contrainte mécanique (i.e. électrostriction). Les propriétés d'électrostriction des matériaux sont étudiées et nous obtenons des coefficients d'électrostriction très élevée ($M_{33} \approx 10^{-11}$ m²/V² à 100Hz). Cette valeur est à ce jour et à notre connaissance la plus élevée dans la littérature. Les matériaux développés au cours de ces travaux peuvent être utilisés dans des capacités variables pour la conversion d'énergie mécanique en énergie électrique.

Les matériaux électrostrictifs développés dans cette thèse sont donc des candidats potentiels pour des applications de récupération d'énergie vibratoire, cependant l'optimisation de certains paramètres reste à étudier.

Mots clés :

Nanocomposites, émulsion, électrostriction, énergie

Title : Emulsion formulation of electrostrictive materials for energy harvesting devices

Abstract :

The aim of this work is to develop near percolated networks of conductive nanoparticles such as carbon nanotubes (CNT) or graphenesheets within an elastic polymer matrix, such as polydimethylsiloxane (PDMS). A novel emulsion formulation route is employed to achieve a fine control over the inner structure of the materials. Graphene or CNT aqueous dispersions are integrated in the continuous phase of an emulsion made of PDMS droplets in water. After water removal, the nanoparticles are segregated in between the PDMS droplets at the Plateau borders of the emulsion. The morphology of the networks formed by the particles is controlled by the size of the emulsion droplets. The dielectrics properties of such materials are governed by (i) the droplets size, (ii) the filler concentration and (iii) the aggregation state. The optimization of such factors by the emulsion approach leads to giant dielectric permittivity ($\varepsilon_r' \approx 10^4$ at 100Hz). In addition, we developed accurate characterization devices to study the material dielectric properties in response to a mechanical stress (i.e. electrostriction). Particularly high electrostrictive coefficients of $M_{33} \approx 10^{-11}$ m^2/V^2 at 100Hz are measured. To our knowledge, these are the highest values in the literature to date. The electrostrictive materials developed in the present work can be implemented in variable capacitors for conversion of mechanical energy into electrical energy. They are promising candidates for ambient mechanical energy harvesting; however, the optimization of some parameters remains to be studied.

Keywords :

Nanocomposites, emulsion, electrostriction, energy

Centre de Recherche Paul Pascal

[UPR, 8641, 115 Avenue du Dr Albert Schweitzer, 33600 Pessac]

"A mi madre por su apoyo incondicional y a mi padre, que en paz descanse"

Cette thèse a été pour moi une véritable expérience de vie, non seulement sur le plan professionnel mais aussi sur le plan personnel, évidemment accompagnée de périodes riches en plaisir et en travail ardu. C'est pourquoi je voudrai remercier tous ceux qui ont participé de loin comme de près à cette étape de ma vie qui s'achève mais qui me permet de poursuivre les prochains chapitres encore mieux armé.

Primo, je tenais à remercier tout particulièrement mes directeurs de thèse qui m'ont permis d'évoluer sur le plan scientifique, notamment grâce à leurs précieux conseils et remarques, aux discussions et aux remises en questions qui m'ont permis d'acquérir un esprit plus critique. Annie COLIN et Philippe POULIN, je vous serai indéniablement reconnaissant pour votre aide, votre soutien, et surtout pour la confiance que vous m'avez témoignée pour mener à terme ce projet de thèse. Travailler dans le cadre de cette thèse a été pour moi un véritable plaisir.

Secundo, je souhaite exprimer ma gratitude envers l'ensemble des personnes avec qui j'ai pu collaborer tout au long de ce projet de thèse. A commencer par mes amis et anciens collègues du L.O.F. qui m'ont accueilli corps et âmes. Je remercie également mes collaborateurs de l'I.M.S. (« Micro-assembled Materials » et « Power » groupes) et I.N.R.I.A. pour leurs soutiens dans le cadre du projet ELENA. Naturellement, je remercie mes amis et collègues du C.R.P.P., notamment le groupe N.T.G., le service de microscopie électronique, également celui d'A.F.M., les ateliers de mécanique, d'électronique ainsi que celui d'« Alibaba » qui m'ont énormément aidé en ce qui concerne les résultats, les montages et les interprétations.

Tertio, je voudrai remercier toutes les personnes qui ont partagé mon quotidien aussi bien au sein du laboratoire qu'à l'extérieur. Merci à tous ceux qui m'ont motivé à faire du football, basketball, squash ou running entre midi et deux ou bien après une bonne journée de travail pour « décompresser ». Comment ne pas remercier également tous ceux avec qui j'ai partagé des moments de souffrance ou de joie lors de différents « raids » ou épreuves de « team building » mais aussi à ceux qui ont complété le « semi-marathon » avec ou sans l'entrainement du « coach ». En parlant d'épreuves à surmonter, je suis très reconnaissant envers ceux qui m'ont réellement soutenu lors de la rédaction. Je pense notamment à mes « co-bureaux » ou à ces personnes qui, comme moi, sont venus au C.R.P.P rédiger leurs thèses pendant les « vacances » d'été 2015.

Last but not least, I will like acknowledge all the « foreign » and « french » crew for the good moments expends inside and outside the laboratory during the coffee breaks or for funnier moments for those few hours expends in mythic places such as "The Central" or "Cubanito" where equations and theorems were less trivial.

"Success is stumbling from failure to failure with no loss of enthusiasm"

-Winston S. Churchill

L'électronique embarquée a connu un fort essor dans les quinze dernières années. De nombreux capteurs sont installés dans de nombreuses situations et transmettent des renseignements (données climatiques, sureté d'un pont, mesure d'usure). Ces capteurs nécessitent une alimentation électrique de faible puissance comprise aux alentours de 1mW. Il en va de même pour les nœuds de transmission d'un réseau sans fil. De façon à rendre ces systèmes autonomes ou à préserver leur autonomie sur des durées plus longues, il est possible de remplacer les batteries conventionnelles par des systèmes récupérateurs d'énergie. L'énergie peut être puisée dans l'énergie solaire, dans les différences de température mais aussi dans les vibrations mécaniques qui nous entourent.

Pour ce faire il existe différentes techniques (matériaux piézoélectriques, bobines électromagnétiques). Les matériaux piézoélectriques et bobines électromagnétiques présentent de bonnes performances de transduction, en revanche leur rigidité et déformation mécanique limité rend leur intégration dans des systèmes électromécaniques à l'échelle micrométrique (MEMS) et utilisation difficiles. Une autre approche consiste à utiliser des capacités variables dont l'entrefer est constitué d'un matériau électrostrictif, c'est-à-dire un matériau dont la permittivité varie en réponse à une déformation mécanique. Ces matériaux sont facilement intégrables dans des MEMS mais le défi consiste à réaliser des matériaux à forts coefficients d'électrostriction. Dans ce domaine les nanocomposites à matrice polymère s'avèrent particulièrement prometteurs.

Les matériaux ici étudiés seront composés par une matrice élastomère, telle que le polydimethylsiloxane (PDMS) chargé par des particules conductrices. De par leurs excellentes propriétés mécaniques et électriques, les nano particules carbonées telles que les nanotubes carbones (CNT) ou les feuillets d'oxyde de graphène (GO) sont d'excellents candidats. Il a été démontré, dans de systèmes aqueux, que l'interaction entre CNT induit par un mécanisme de déplétion induit de grandes variations de la constante diélectrique quand le réseau est proche du seuil de percolation. En incorporant les nanotubes dans un matériau élastique, la même sensibilité sera retrouvée en fonction de la déformation. Le contrôle de ces variations est à priori fortement dépendant de la morphologie du réseau. C'est pourquoi une nouvelle approche utilisant des émulsions est ici proposée. En effet cette approche permet le contrôle de la structuration des nanotubes entre les gouttes d'émulsions. Il est ainsi possible de varier les tailles d'agrégats à l'approche de la percolation. De plus, il est aussi possible de moduler les propriétés mécaniques pour optimiser les coefficients d'électrostriction. La conversion d'énergie sous forme électrique s'effectue en utilisant les variations géométriques et de propriétés diélectriques lorsque le matériau électrostrictif est placé entre deux plaques pour fabriquer un condensateur dont la capacité est variable. Ces variations de capacité sont exploitées par un circuit électronique dit « pompe de charge » qui permet de récupérer et emmagasiner les charges crées par le matériau électrostrictif sous contrainte mécanique.

Afin de synthétiser un tel matériau hybride la première étape consiste à préparer une émulsion directe (O/W) dont la phase huile est constitué de PDMS mélangé à un agent de réticulation (85wt%) afin de former des gouttelettes qui sont dispersées dans une phase continue aqueuse. L'incorporation de la phase huile s'effectue goutte à goutte et par agitation mécanique. Cette technique permet d'obtenir des gouttelettes avec une polydispersité assez large (> 40%). Le diamètre moyen est gouverné par les forces de cisaillement. Afin d'obtenir une distribution de taille et de contrôler le diamètre moyen, nous utilisons une technique « Couette ». Suivant leur méthode nous obtenons des émulsions mieux calibrées (uniformité < 25%), ce qui permet d'obtenir de gouttelettes entre 1µm et 100µm suivant le cisaillement utilisé. Une fois que la taille de gouttelette escomptée est obtenue, nous diluons les émulsions avec des dispersions aqueuses de CNT (respectivement GO). Les CNT (resp. GO) se retrouvent dans la phase continue et la concentration en CNT (resp. GO) est contrôlée aisément. La dernière étape consiste à mouler, puis sécher et finalement réticuler le matériau. Ces différents temps ont été ajustés de façon à ce que le séchage puisse se faire avant que l'émulsion n'ait coalescé ou que la polymérisation ait eu lieu. En effet, lorsque l'évaporation est dite « rapide », les nanoparticules s'agrègent au niveau des bords de « Plateau » pour former un réseau de nano particules de carbone (CNT ou GO). Une étape de réduction thermique *in-situ*, à 200°C pendant 2h, est effectuée uniquement aux matériaux contenant du GO afin d'obtenir de particules d'oxyde de graphène réduit (r-GO) conductrices électriquement.

Les matériaux sont caractérisés par mesure d'impédance avec compensation afin de déterminer les valeurs de permittivité diélectrique ε_r'. Le contrôle de gouttelettes de l'émulsion initiale et du taux de charges carbonées guide les propriétés diélectriques du composite. La stratégie est de se placer proche du seuil de percolation, où les valeurs de permittivité divergent. Des valeurs de permittivité particulièrement élevées et comparables aux meilleurs résultats de la littérature, sont obtenues pour des matériaux dont le taux de nanoparticules se situe autour du seuil de percolation. Les valeurs de permittivité sont de l'ordre de $\varepsilon_r' \approx 10^4$ à 100Hz avec une conductivité relativement faible qui est typiquement 10^{-5} - 10^{-4} S/m pour les nanocomposites chargés en CNT (resp. 10^{-2} S/m pour r-GO). Ces résultats sont obtenus pour de gouttes de gouttes typiquement de 6µm (resp. 20µm) de diamètre et un taux de nanotubes (resp. r-GO) de 0.4wt% (resp. 8wt%). Il a été démontré que la dépendance en fréquence de ces matériaux est obtenue en raison des effets de polarisation de type Maxwell-Wagner. D'autre part, un optimum de formulation est retrouvé de façon expérimentale lorsque la taille moyenne de la goutte $\langle a \rangle$ est environs un ordre de grandeur plus élevé que la longueur moyenne $\langle l \rangle$ de la nanoparticule conductrice. Le procédé de fabrication de nanocomposites via une approche émulsion contrôle la morphologie de façon aisée du réseau interne de nanoparticules et aboutir à des permittivités géantes.

Enfin, de par la versatilité de cette approche émulsion, il est possible d'incorporer d'autres types de charges conductrices sous la forme de dispersions aqueuses.

La deuxième partie du manuscrit porte sur l'étude de propriétés électrostrictives des matériaux composites à base de CNT. Dans la littérature, le phénomène d'électrostriction est évalué en mode actionneur. En effet, le coefficient électrostrictif M_{13} est obtenu à partir de la déflection d'une bicouche composite/PDMS sous l'action d'un champ électrique fort (1 - 10 MV/m). Cependant ces déformations sont dues à la fois au mécanisme d'électrostriction (i.e. variation de propriétés diélectriques sous contrainte mécanique) et à la contrainte de Maxwell (i.e. phénomène de charges en surface). A ce jour à notre connaissance, il n'existe pas dans la littérature une méthode expérimentale capable de découpler ces deux mécanismes. C'est pourquoi, un nouveau montage expérimental a été développé pour déterminer de façon directe le coefficient M_{33}.

Ce montage consiste à mesurer la variation d'impédance quand le composite est soumis à une compression dans le régime élastique. Lorsque les contraintes mécaniques (10^4 N/m^2) sont appliquées sous un potentiel faible (1V), la contribution de la contrainte de Maxwell est largement négligeable devant l'électrostriction. L'étude du coefficient d'électrostriction en fonction du taux de CNT est étudiée suivant les deux approches pour une fréquence donnée (100Hz). Les valeurs de coefficients d'électrostriction obtenus sont en accord, permettant de valider la nouvelle méthode expérimentale et de mettre en évidence que la contrainte de Maxwell est négligeable même lorsque le composite est utilisé en mode actionneur. Les valeurs du coefficient d'électrostriction M_{33} en compression pour de concentrations en CNT sous le seuil de percolation sont de l'ordre de 10^{-15}-10^{-14} m^2/V^2. La valeur maximale du coefficient d'électrostriction M_{33} est obtenue lorsque la teneur en CNT est de 1wt%. Cette valeur est de l'ordre de 10^{-11} m^2/V^2 et se situe parmi les plus élevées de celles rapportées dans la littérature. L'influence de la vitesse à laquelle le composite est comprimé sur les propriétés électrostrictives, a également été étudié. Il est prouvé que pour une variation d'un ordre de grandeur, c'est à dire entre 0.5 et 0.05 mm/min, les valeurs du coefficient M_{33} restent constantes en fonction de la vitesse de compression pour une concentration donnée. Les composites décrits précédemment sont sensibles aux contraintes mécaniques et leurs remarquables propriétés électrostrictives sont liés au contrôle du réseau interne de particules par voie émulsion. Ainsi, leur application en tant qu'actionneurs et capteurs est triviale, cependant leur utilisation en tant que dispositifs pour la récupération reste compromise pour certains composites du fait d'une conductivité électrique relativement élevée (i.e. 10^{-3} S/m) pour ce type d'application. En effet, les matériaux composites qui présent des permittivités diélectriques élevées présentent inévitablement des conductivités électriques élevées.

Un dernier type de matériau à base de GO est développé, dit « papier graphène » présente une permittivité diélectrique ε'_r d'environ 10^6 pour une conductivité électrique de 10^{-2} S/m à 100 Hz. Afin de palier la forte conductivité un compromis doit être envisagé. Les composites sont par la suite élaborés comme des bicouches. La première couche est constitué du composite à base de CNT alors que la deuxième est constituée d'une couche isolante diélectrique, soit du alcool polyvinylique (PVA) soit du GO. Lorsque le matériau composite est associé à une couche de GO, la permittivité comme la conductivité restent autour du même ordre de grandeur. En revanche, la couche de PVA permet de réduire la conductivité (environs 2 ordres de grandeurs) tout en réduisant faiblement la permittivité (un ordre de grandeur) et présente un réel intérêt.

La dernière partie du manuscrit aborde la génération de puissance électrique avec les matériaux électrostrictifs élaborés par la voie émulsion chargés en CNT lorsqu'il est soumis à un stress dynamique. Pour cela, un circuit électronique autonome, dit « pompe de charge » a été conçu sur une machine d'analyse mécanique dynamique (DMA). Afin de valider la preuve de concept, une première étude montre qu'il est capable de restituer une puissance électrique à partir d'une vibration mécanique. La valeur de la puissance générée par un échantillon à 0.05wt% (dont $\varepsilon'_r < 10$) est de 2 nW. Dans le but générer davantage de puissance, il existe deux types d'approches. La première est d'utiliser un composite avec une permittivité, ε'_r, plus élevée (typiquement $\varepsilon'_r > 100$) ou bien d'augmenter la tension appliqué au système. Les tests préliminaires montrant que les matériaux composites avec $\varepsilon'_r \approx 100$, déchargent le système électronique et lorsque la tension est augmenté, le système présente de réactions d'électrochimie. En vue de contourner ses limitations, il est envisageable dans un premier temps d'employer un autre type de système électronique non-autonome et d'autre part de remplacer le système tensio-actif par un système non-ionique.

General introduction

Colloids are a very broad class of material. Foams, sols, gels and emulsions are a few examples of colloidal systems that find wind applications in industry [1]. Colloidal particles refer to a state of subdivision, implying that the particles dispersed in a medium have at least in one direction a dimension roughly between 1 nm and 1μm.

Carbon based nanoparticles such as carbon nanotubes (CNTs) are a well-known example of colloidal particles. There are two main types of nanotubes: Single-walled nanotubes (SWNT) that consist of a single sheet of graphene rolled to form a cylinder with diameter of order of 1 nm and length of up to millimeters. Multi-walled nanotubes (MWNT) consist of an array of such cylinders formed concentrically and similar to the basal plane separation in graphite. Their diameter ranges from 2 to 100 nm. Their lengths are tens of microns. The most common methodology to synthesize carbon nanotubes is the chemical vapor deposition (CVD), however other methodologies such as arc discharge and laser ablation enables well graphitized, defect-free nanotubes. Carbon nanotubes have generated a tremendous interest due their unique mechanical (Young's modulus in the range of 100–1000 GPa), thermal (thermal conductivity up to 6000 W/m K) and electronic (current density up to 100 MA/cm^2) properties. These superlative properties reveal the potential of carbon nanotubes to develop materials with unique properties. The fields of interest for CNT and their nanocomposites are broad and range from mechanical reinforcement, organic electronics, solar cells and energy storage [2, 3].

Emulsions are colloidal systems. They are obtained by shearing two immiscible liquids leading to the fragmentation of one phase into the other. The droplets display a surface tension which is nonzero and requires the use of amphiphilic compounds to stabilize them. An emulsion is denoted by the symbol O/W (i.e. direct emulsion) if the continuous phase is an aqueous solution and by W/O if the continuous phase is an organic liquid (i.e. inverse emulsion). The droplet volume fraction may vary from zero to almost one: dense emulsions present a cellular structure of air-liquid foams, for which the fraction of continuous is very small. The destruction of emulsions may proceed through two distinct mechanisms. The first called Ostwald ripening due to the diffusion of the dispersed phase through the continuous phase. The second one called coalescence consists in the rupture of the thin liquid film between two droplets. When the emulsions achieve a suitable stability, its lifetime ranges the time scale of the year, and they become good candidates for commercial applications. Emulsions are widely used in large fields of applications because of their ability to transport or solubilize hydrophobic substances in a continuous water phase. Many industries take advantage of emulsion technology: painting, paper coating, road surfacing, lubrication, food, cosmetics, pesticides and medicine. [4]

The work developed in this thesis takes advantage of the emulsion versatility combined with the superlative properties of carbon nanotubes to synthesize structure tunable soft nanocomposite devoted to energy harvesting applications. The first chapter is focused on the

theoretical background and state of the art work in the literature that are necessary to the understanding of the latter materials. A particular interest is dedicated to the different types of materials and mechanisms that enable the conversion of mechanical energy into an electric field using ambient vibrations. The second chapter is devoted to the materials and methods used and developed for this particular research work. The chapter pays a particular attention to methodologies for coupling mechanical and dielectric properties. The third and fourth chapters are devoted to the optimization of the internal network formed by carbon nanotubes (third chapter) and graphene colloidal particles (fourth chapter) and its influence on the dielectric properties of the nanocomposites. The fifth chapter is devoted to the study of the dielectric properties of CNT emulsion based nanocomposites under mechanical stress (i.e. electrostriction). A particular attention is attributed to the variation of dielectric properties when the materials are subjected to a mechanical stress. The sixth chapter is focused on the development of an approach to reduce the electrical losses of the system, keeping large variations of dielectric properties in response to a mechanical deformation. Last but not least, the seventh and final chapter is focused on the generated power by an emulsion based nanocomposite filled with carbon nanotubes using a vibrational source. A particular interest is devoted to the mechanisms that enable the conversion of mechanical energy into electrical energy and the improvements that are necessary to increase the power generated.

References

1. *http://old.iupac.org/reports/2001/colloid_2001/manual_of_s_and_t/node33.html*

2. *Iijima S, Ichihashi T. Single-shell carbon nanotubes of 1-nm diameter. Nature 1993; 363(6430):603–5.*

3. *Small but strong: A review of the mechanical properties of carbon nanotube–polymer composites Jonathan N. Coleman , Umar Khan , Werner J. Blau , Yurii K. Gun'ko*

4. *Bibette, Leal-Calderon, Schmitt, Poulin: Emulsion Science, STMP 181, 1–4 (2002)*

Chapter I

Materials and techniques to harvest ambient energies

I. Energy harvesting devices and transducers

1) Introduction

Significant progresses have been achieved in the last decades in energy harvesting technologies for the development of low-consumption, miniaturized and highly efficient devices. Achievement of such devices implies new ways of energy conversion and communication in terms of data transfer, monitoring, sensing, actuating etc. Wireless communication avoids the use of expensive and heavy cables, leading to more autonomous portable systems. The fields of application are wide, ranging from temperature monitoring, location of persons and health factors, sensing pollutants, harmful chemical agents, humidity, fatigue crack formation on aircraft monitoring, industrial machinery and pressure in automobile tires, etc. The energy demand of such systems is generally guaranteed by the utilization of batteries. The size of the devices is limited by the size of the battery [1] and the life span of the entire devices depends on the autonomy of the battery [2] (Figure 1). Other limitations are related to the chemicals used in batteries and to their complex recycling processes [3]. We pointed out, that the main limitation element to produce unlimited life span wireless autonomous systems is the battery. Failures such as structural network damage can be overwhelmed by network re-configuration or by self-organization [4].

Several technologies can be potentially employed to power embedded electronics. Among the new potential sources of energy the most reliable, clean, low cost and efficient ones come from the environment. Extracting energy from the surrounding environment and converting it into electrical energy is known as energy harvesting or power scavenging [5]. The scavenging can come from human activity [6] or derive from ambient energy such as, light, radio, mechanical vibration or heat [7]. Environmental energies are excellent candidates for an imperishable power source for autonomous wireless networks.

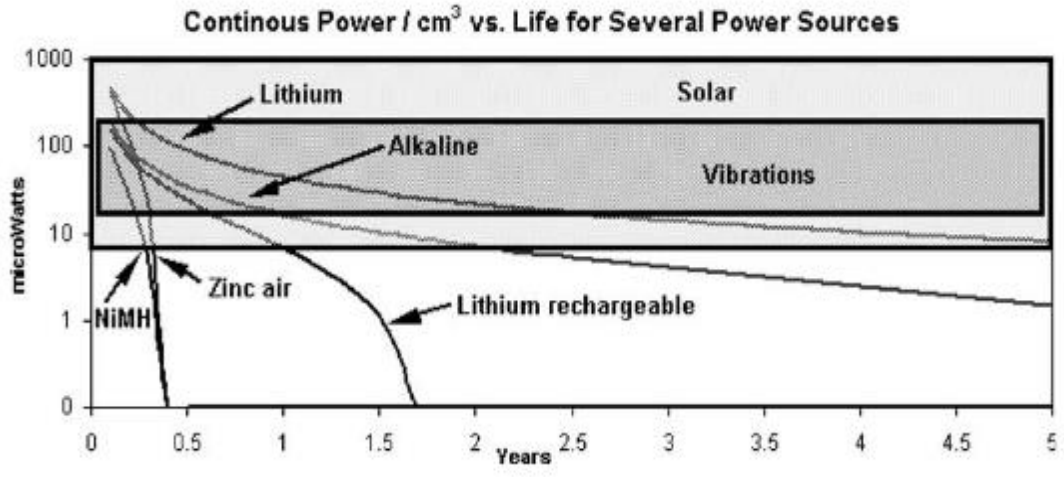

Figure 1 Comparison of the power from vibration, solar and various batteries over life span. The only sources of power reliable enough in the long term are vibrational and solar. These sources are for 100micro watt application is competition [2]

This chapter describes energy harvesting mechanisms and related devices. Non vibratory sources of energy are presented in the first section. In the second section, we provide a particular interest to the most relevant mechanisms of energy harvesting from mechanical vibrations. The third section is devoted to a comparison of these conversion mechanisms, and based on their assessment we will detail our approach based on the use of electrostrictive materials.

2) Environmental energies

Harvesting solar energy is certainly the most common and matured technology in the field. Conversion of light energy into electrical energy is achieved by the use of semi-conductors materials such as silicon. The power density generated in direct sun light by the best devices is about 10mW/cm^3. However the performances are very lightning-dependent [8]. When the intensity is obstructed or decrease, such as in the case of an office room and other indoor environments, the performances decrease by several orders of magnitude [7]. Despite its great interest for large outdoor systems such as solar homes, the use of solar energy in micro-devices is still very limited. Few commercialized examples combine photovoltaic and chemical fuel cells such as the Citizen Eco drive ® watch [9]. We recall that no scavenging is possible in the absence of light; limiting the application fields for autonomous sensor networks.

Another known source of energy is the thermal energy, which can be conveniently transduced into electrical energy by the Seebeck effect. Energy scavenging is here based on a gradient of temperature, $\Delta T=(T_H-T_L)$, across which the thermal generator operates. For optimized conditions, the systems can deliver up to 40µW/cm^3. Typical conversion efficiencies are about 5 to 10 % [6] but are highly dependent on the temperature ranges [10]. Considering the needed large temperature gradients, high temperature range and rather limited efficiency, the technology of thermal energy harvesting is not among the most promising ones to power small electronic devices and autonomous wireless sensors.

Alternative sources such as mechanical energy of ambient or biomechanical vibrations can provide reasonable amount of energy, typically hundreds of µW/cm^3, which is sufficient to power wireless sensors [2;8;11]. Table 1 summarizes some of the human activities and vibrational sources potentially used to fabricate micro generators that convert mechanical energy into electrical energy.

Table 1: Examples of vibration sources and their typical frequencies and accelerations (left), and summary of human activities with their potential associated power output [2]

Vibration source	Acceleration ($m\ s^{-2}$)	$Frequency_{peak}$ (Hz)
Car engine compartment	12	200
Base of 3-axis machine tool	10	70
Blender casing	6.4	121
Clothes dryer	3.5	121
Person tapping their heel	3	1
Car instrument panel	3	13
Door frame just after door closes	3	125
Small microwave oven	2.5	121
HVAC vents in office building	0.2–1.5	60
Windows next to a busy road	0.7	100
CD on notebook computer	0.6	75
Second story floor of busy office	0.2	100

Activity	*Kilocal/hr*	*Watts*
sleeping	70	81
lying quietly	80	93
sitting	100	116
standing at ease	110	128
conversation	110	128
eating meal	110	128
strolling	140	163
driving car	140	163
playing violin or piano	140	163
housekeeping	150	175
carpentry	230	268
hiking, 4 mph	350	407
swimming	500	582
mountain climbing	600	698
long distance run	900	1,048
sprinting	1,400	1,630

3) *Mechanical vibrations*

Sources of ambient mechanical vibrations are diverse. We can distinguish the "high" level vibrations corresponding to large industrial equipment, transports, continuous or natural movements such as ocean waves. The "low" level vibrations include human motions, such as running, movements of structures such as doors, panels, walls or floors. All these different types of vibrations movements deliver enough power to satisfy energy demands of autonomous electronic systems. Table 1 summarizes different vibrational systems with their output power.

Due to the variety of these sources, the amplitude, acceleration and frequency of the corresponding vibrations differ substantially. Williams and Yates [12], proposed a simple model to predict the power generated by mechanical vibrations. The model consists in a housing system displaced by $y(t)$, in which a seismic mass, m, is attached to a spring k . The relative displacement with respect to the housing is $z(t)$.

The conversion of mechanical energy of the oscillating mass into electricity is seen as a linear damper, d_l, independently on the involved mechanism. Figure 2 shows a scheme of the model. The differential equation for $z(t)$ is given by equation (Eq. 1) [13]:

$$m\ddot{z}(t) + d_l\dot{z}(t) + kz(t) = -m\ddot{y}(t) \qquad (1)$$

The analytical expression for the converted power $|P|$ is given by (Eq. 1). Z the displacement magnitude of the housing; ζ_t the damping ratio, ω the input frequency and ω_n is the natural frequency of the spring mass. The present analysis demonstrates that the power output produced is proportional to the cube of the vibration frequency of vibration, and to maximize power generation the mass deflection should be as large as possible.

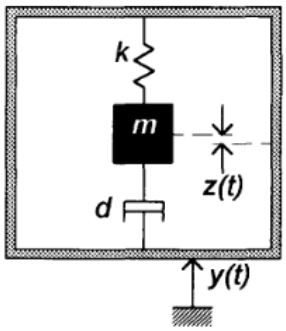

$$|P| = \frac{m\zeta_t \omega_n \omega^2 Z^2 \left(\frac{\omega}{\omega_n}\right)^3}{\left(2\frac{\omega}{\omega_t}\zeta_n\right) + \left(1 - \left(\frac{\omega}{\omega_n}\right)^2\right)^2} \quad (2)$$

$$|P| = \frac{m\zeta_t \omega^3 Z^2}{(4\omega\zeta_t^2)} = \frac{m\zeta_t A^2}{(4\omega\zeta_t^2)} \quad (3$$

Figure 2: Schematic diagram of the model proposed for the conversion of vibration mechanical energy into electrical energy [13]

When the resonant frequency of the spring mass, ω_n, matches the input frequency, ω, Eq.2 is simplified and written as Eq.3. In the expression Eq.3 A is the acceleration magnitude of input vibrations. The potential output power is proportional to A^2/ω and m. The mass is an important parameter controlled in the design of a device. In practice, it may be difficult to considerably increase the mass because of size limitations. The above model provides general information on the main parameters involved in the generation of mechanical energy from ambient vibrations. However the conversion of this energy into electrical energy is also very important to assess. This conversion can be based on three main different mechanisms: electromagnetic, piezoelectric, and electrostatic via a variable capacitance. Details on these mechanisms will be discussed in the following paragraphs.

4) Conversion Mechanisms

i. Electromagnetic Energy Harvesting

Electromagnetic induction, discovered by Faraday in 1831, is the generation of electric current in a conductor located within a magnetic field. The conductor typically takes the form of a coil and the electricity is generated by either the relative movement of the magnet and the coil, or due to changes of the magnetic field. The amount of electricity generated depends upon the strength of the magnetic field, the velocity of the relative motion and the number of turns of the coil. One of the most effective ways to harvest mechanical energy via electromagnetic induction is to use permanent magnets, coils and resonating cantilevers beam. It has been demonstrated [11], [14] that large output power can be delivered but no considerable output voltages. Besides, implementation of the needed elements is difficult. Nevertheless, energy harvesting devices have been developed, such as self-winding watches [15] (Figure 3a) or shaken driven-flashlight [16] (Figure 3b), for which the energy input is low. However no much

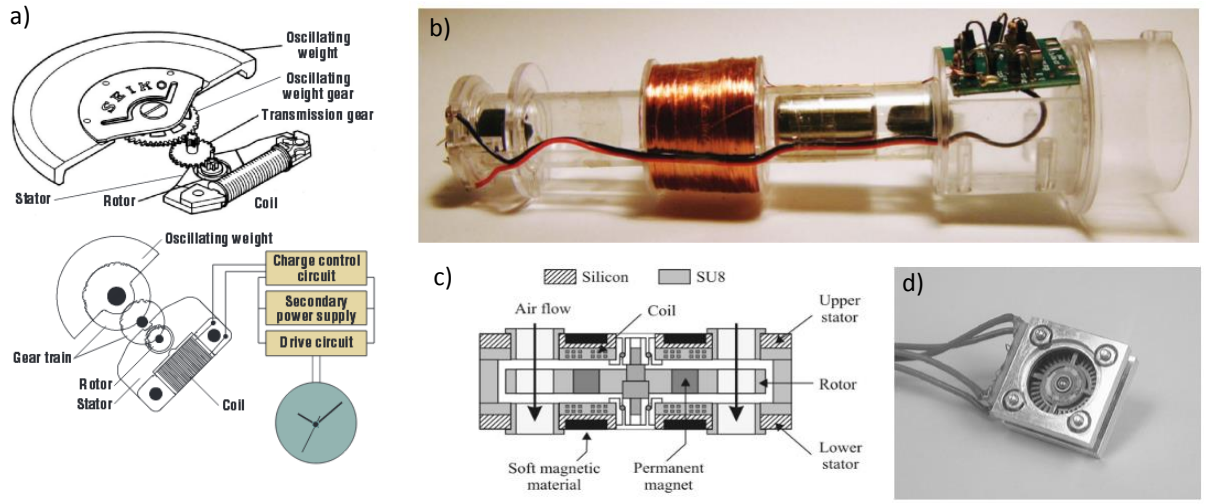

Figure 3: Electromagnetic energy harvesting devices can be found as a) self-winding electric watch , b) inertial solenoid generator from a shake driven light emitting diode flashlight and c) and d) axial flow microturbine with an integrated electromagnetic generator. c) The cross-section of the prototype shows the mechanism to harvest air flow from d) the final assembly. [9, 16,17,18]

work has been devoted to Micro Electro Mechanicals Systems (MEMS). As a matter of fact, electromagnetic induction technology deals with bulky and brittle materials which are complicated to scale-down. Only one device has been reported yet at the micron scale, i.e. for (MEMS). This device was design to harvest electrical energy from airflow though a miniaturized turbine. An output power of 1mW could be theoretically delivered at an airflow speed of about 40 m/s (i.e. 144 km/h) [18] (Figure 3 c and d). Unfortunately such wind flow is achievable only in extreme conditions. As a comparison, the wind flow generated by a hurricane category one is about 120 km/h. [19]

ii. Piezoelectric energy harvesting

The piezoelectric effect was discovered by Jacques and Pierre Curie in 1880 [20]. They found that if certain crystals were subjected to mechanical strain, they became electrically polarized and the degree of polarization was proportional to the applied strain. Conversely, these materials deform when exposed to an electric field. Piezoelectric materials are widely available in many different forms including single crystal (i.e. quartz,) ceramics (i.e. lead zirconate titanate, also called PZT of general formula $Pb\,[Zr_xTi_{(1-x)}]O_3$ or $BaTiO_3$), thin films (i.e. sputtered zinc oxide), screen printable thick-films based upon piezoceramic powders [21-22] and polymeric materials such as polyvinylidenefluoride (PVDF) [23].The equations describing the piezoelectric materials are given by Eq.(3) and (4).

$$S_j = s_{ij}^E \tau_j + d_{im} E_m \tag{3}$$

$$D_m = d_{im}\ \tau_i + \varepsilon_{ik}^\sigma E_k \tag{4}$$

Where S_j is the mechanical strain, τ_i the mechanical stress, D_m the electrical displacement, E_k the electric field, $\varepsilon_{ik}^{\sigma}$ the permittivity and, d_{ik} the piezoelectric strain constant.

The piezoelectric strain constant d_{ik}, is a very important parameter since it quantifies the amount of charges (respectively strain) when a mechanical stress (respectively electric field) is applied to the materials. The so-called coupling coefficient κ, which corresponds to the efficiency of energy conversion, is another important constant used for assessing the interest of piezoelectric materials.

Most piezoelectric materials are anisotropic. In addition, they can be polarized or mechanically loaded in different directions. Different modes can therefore be defined depending on the orientation along which the material is mechanically loaded or polarized. They are associated with different piezoelectric constants d_{ik} to specify the ratio of strain along the *k*-axis to the electric field applied along the *i*-axis, with all external stresses kept constant. Conversely this factor also represent the ratio of charges separated along the *k*-axis when a mechanical stress is applied along the *i*-axis.(Figure 4)

Piezoelectric materials have to be polarized in order to be used for energy conversion. Considering that this polarization is performed along the 3-axis, the materials are often characterized by κ_{31}, d_{31} and κ_{33}, d_{33} (Figure 4) [24-25]. For example, for PVDF, PZT and $BaTiO_3$, the terms d_{33} and κ_{33} are systematically higher than d_{31} and κ_{31}.

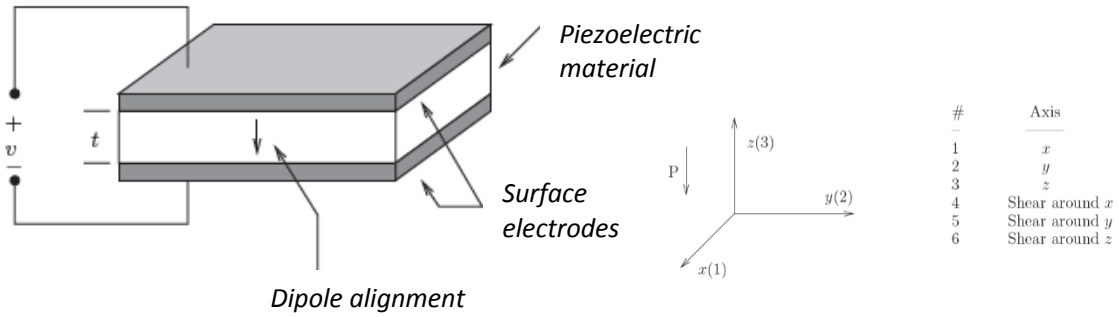

Property	PZT-5H	PZT-5A	$BaTiO_3$	PVDF
d_{33} (10^{-12} C N^{-1})	593	374	149	−33
d_{31} (10^{-12} C N^{-1})	−274	−171	78	23
g_{33} (10^{-3} V m N^{-1})	19.7	24.8	14.1	330
g_{31} (10^{-3} V m N^{-1})	−9.1	−11.4	5	216
k_{33}	0.75	0.71	0.48	0.15
k_{31}	0.39	0.31	0.21	0.12
Relative permittivity ($\varepsilon/\varepsilon_0$)	3400	1700	1700	12

Figure 4: Scheme of the piezoelectric material and the nomenclature of the axis. We define the index k as the direction of the initial polarization which corresponds to the z direction. Table of the properties for different piezoelectric materials: PVDF, $BaTiO_3$ and different types of PZT [24-25]

iii. Applications

A lot of work has been devoted to implement piezoelectric materials employed in cantilevers with an inertial mass at their end. The systems are mechanically stimulated and generate power [26] from a few hundreds of μW to a few mW depending on the size of the devices and conditions. Noteworthy that the power is often given at the resonant frequency of the cantilever system, which is often far from the frequencies of typical ambient vibrations [27]. The use of cantilevers as piezeoelectric generators is largely reported in the literature [28-30]. As a general trend, flexible piezoelectric polymer materials demonstrate to be a more suitable material compared to brittle piezoceramics [31]. Nevertheless, piezoelectric polymers exhibit lower piezoelectric coefficients compared to piezoceramics (Figure 4)

A more realistic scenario was studied by Paradiso and Starner, [32-34] who developed a system to harvest the energy generated by a human being walking. They integrated piezoelectric elements beneath the insole of running sneakers (Figure 5a). They were able to produce an average power of 1.3mW employing a stack of PVDF layers at the toes. A second device was proposed to harvest energy from the heel. A curved bimorph of PZT and aluminum bound together produced 8.3mW as a person walks (Figure 5) [32, 34]. *In vivo* applications were studied by Ramsay and Clay [35] who used a lab on chip to evaluate the power output generated by the change in blood pressures. They predicted a power of about 2.3 μW using an optimized geometry [35]. Another report focused in blood exchange is the one of Sohn *et al* whom employed PVDF membranes that produce experimentally 0.34 μW from a theoretical expected value of 0.64 μW [36].

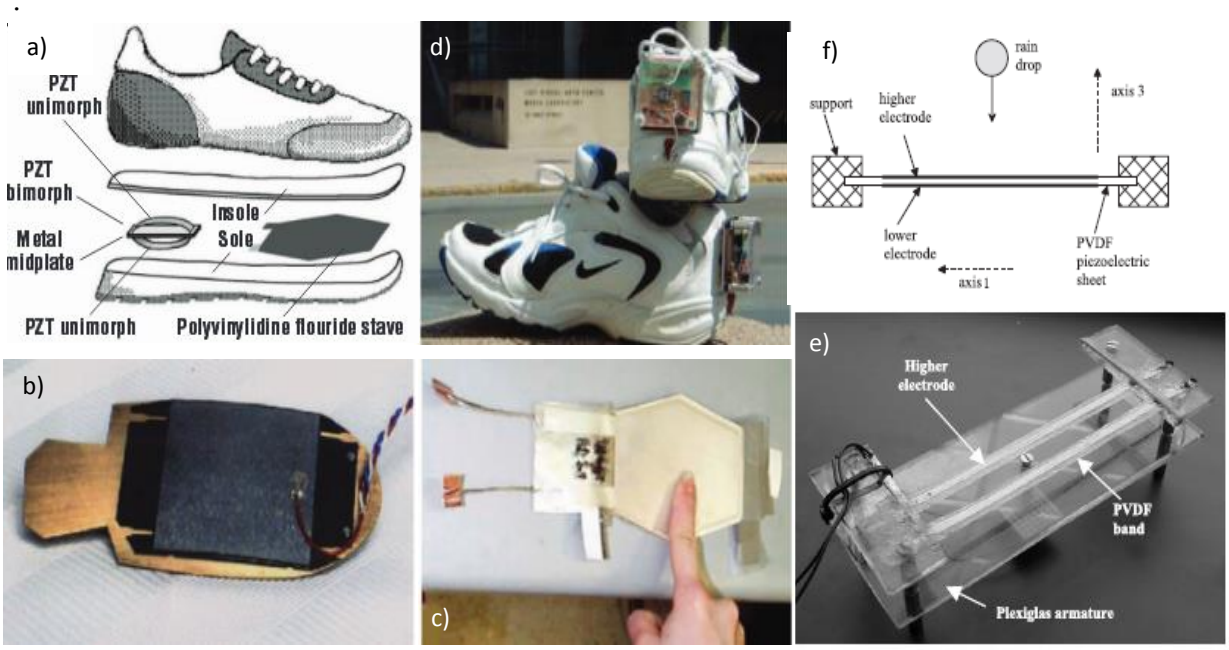

Figure 5: Integration of a) a flexible PZT under a hell and b) a 16-layer PVDF biphorm under the insole of a running shoe, resulting in d) operational power harvesting shoes with heel-mounted electronics for power conditioning, energy storage and transmitter [27-29,32,34]. Scheme of f) the system of raindrop energy harvesting and its corresponding picture of the whole e) mechanical system embedding the PVDF bands [37-38].

Not only human motion can be used as source of mechanical energy, but also natural kinetic energy such as the one arising from falling rain drops. An innovative device was developed by Guigon *et al* [37-38] to harvest this energy. The device is constituted by a piezoelectric polymer. The inertia of a rain droplet being inelastic induces the bending of the material leading to the generation of electrical power. An optimized design of a PVDF cantilever band (10cm long 3mm wide and about 10µm thick) produces about 1µW (Figure 5). The output power is instantaneous and depends on the speed and diameter of the droplets [38].

Piezoelectricity is a very interesting approach because it can deliver sufficient output power to sustain the energy for low consumption sensors. However, the most efficient piezoelectric ceramics are stiff and brittle which limits their implementation in embedded applications. Moreover their properties are downgraded with age and temperature and often this materials required to be polarized at high temperature under a large voltage [30].

A more promising approach to harvest and convert energy from mechanical ambient or biomechanical vibrations is to use variable capacitors. Thus mechanical vibrations induce changes of capacitance which are converted with the suitable electronics into electrical energy.

iv. Variable capacitor

We consider a capacitor constituted of two plates which are electrically isolated from each other by a dielectric material (typically air or vacuum). When subjected to a voltage U, the plates acquire charges with of opposite sign Q. The capacitance C of such system is defined as follows

$$C = \frac{Q}{U} = \frac{\varepsilon A}{d} \tag{5}$$

Where A is the surface of the plates, d the distance between them and ε the dielectric permittivity of the material. The permittivity ε, can be expressed as a function of the permittivity of vacuum ε_0 and of the relative dielectric permittivity of the material $\varepsilon_r' = \varepsilon/\varepsilon_0$. The energy stored in the capacitor is given by Eq.6.

$$E = \frac{1}{2}QU = \frac{1}{2}CU^2 = \frac{Q^2}{2C} \tag{6}$$

Variations of capacitance can be converted into electrical energy. By contrast to piezoelectric and electromagnetic, the conversion mechanism of such electrostatic devices requires an external voltage [39] or electret [40] to initiate the process. Figure 6 summarize the typical geometries for electrostatic generators. The darker zones represent the fixed areas, whilst the lighter zones the released structures that are free to move. For all the configurations, the changes of capacitance are due to pure geometrical effects. For in plane overlap, (Figure 6a), the change of the capacitance is due to the changing overlap area of interdigitated electrodes. For in plane gap (Figure 6b), changes of the capacitance are due to the changes of the gap

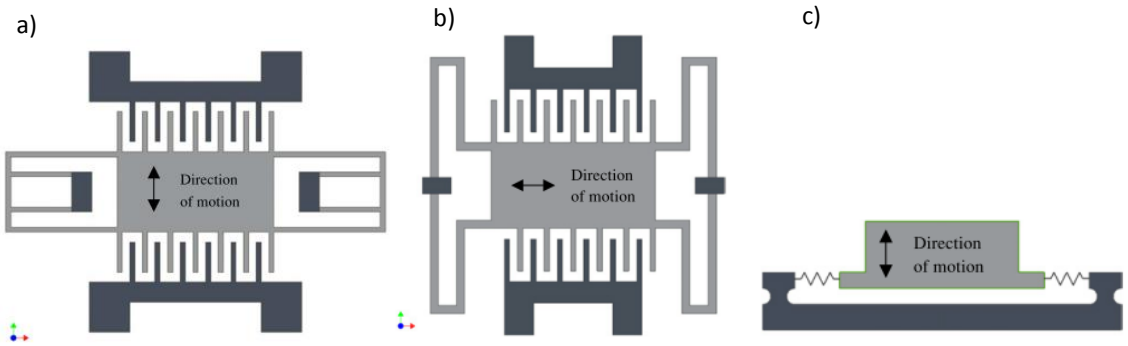

Figure 6: Typical conformations of variable capacitances used to harvest mechanical energy. The standard distance range between the plates is about few microns [31].

between the finger plates. For out of plane gap (Figure 6c), the increase of the capacitance is due to the reduction of the distance between the plates. According to Roundy [41], the power that can be harvested using conventional micro-fabricated systems is about 100μW cm^{-3} and the most efficient geometry is the out-of plane gap closing.

Several energy cycles enable the conversion of mechanical energy in electrical energy using a variable capacitor C_v. The most commonly described cycles are the cycles at constant charge or constant voltage. The charge constrained cycle is an autonomous cycle that does not requires the permanent presence of an external source of energy by contrast to voltage constrained cycles [42].

As a matter of fact, once the electrical charges are brought to the variable capacitance, the charged constrained cycle becomes completely autonomous. Of course, in practice actual devices suffer from losses and completely autonomous operation is not straightforward. Nevertheless, model cycles are still useful to show and discuss principles of energy conversion in variable capacitors. Figure 7 shows the charge constrained cycle of a variable capacitor, C_v. We recall that the capacitance is defined by the slope of the Q-U diagram. Initially, the C_v is electrically neutral and its charge is Q_0 =0 (Figure 7a) and b)). The cycle starts when the system is plugged to an external source of voltage leading to the increase of the charges up to Q_{cst}. In its initial state, the capacitor has a maximum capacitance C_{max}. The electrical charge is stored in C_v under a given voltage U_{min}. The variable capacitor is unplugged from the external source leading to an open circuit at a charge Q_{cst}. A mechanical work is provided in order to change C_v from C_{max} to C_{min} at constant charge. The voltage across the variable capacitor increases in response to this change of capacitance. Lastly the capacitor is discharged and the gained electrical energy collected or used in a resistive device.

The energy output per cycle is express by Eq.7

$$E = \frac{1}{2} Q_{cst}^2 \left(\frac{1}{C_{min}} - \frac{1}{C_{max}} \right) = \frac{1}{2} U_{max} U_{min} (C_{max} - C_{min}) \qquad (7)$$

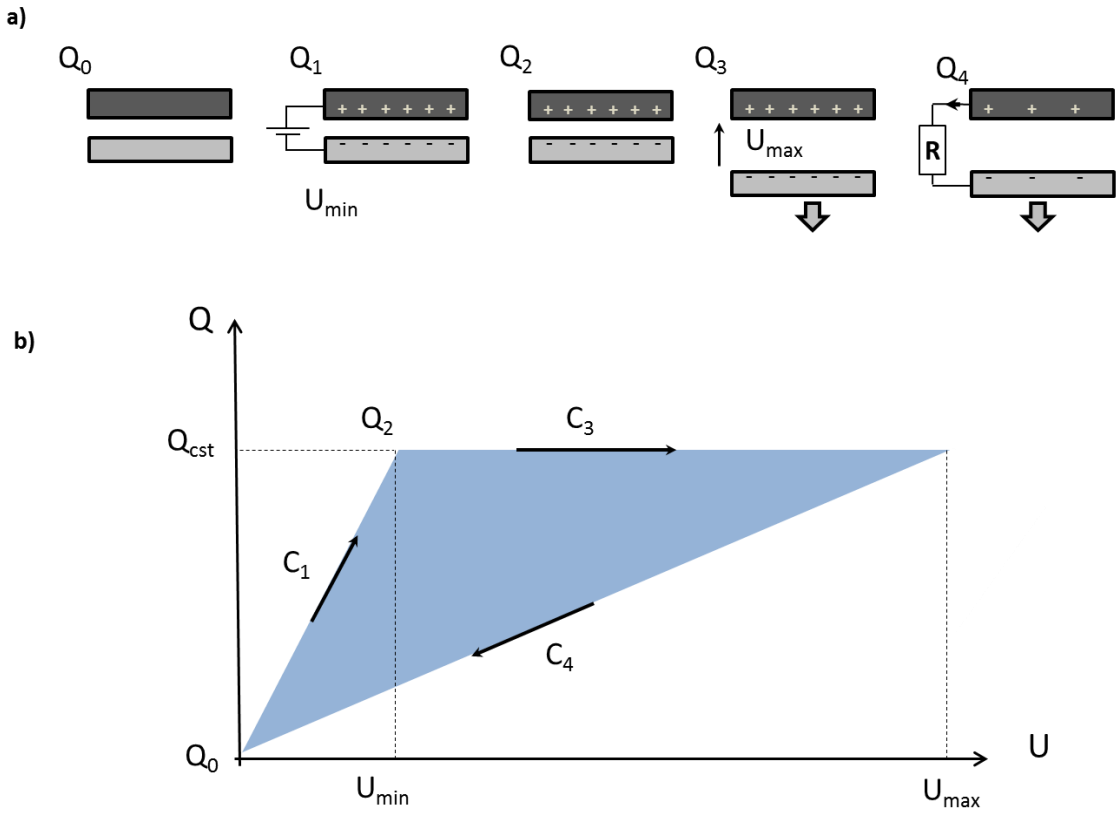

Figure 7: a) Scheme of the energy conversion cycle at constrained charge of a variable capacitor. The dark-grey rectangle represents the fixed electrode whilst the light-grey one represents the mobile electrode. b) Standard energy conversion cycle at constrained charge, the black arrows show the direction of the cycle

This equation shows that the variation of capacitance has to be increased as much as possible for efficient energy harvesting.

Charge pump circuit

The above concept of energy conversion can be realized in practice using a so-called charge pump circuit. The architecture of such a system is shown in Figure 8. It includes a charge pump and a fly back component. The charge pump is responsible for the energy accumulation while the flybak ensures the recharge of a reservoir capacitor [2,43, 44]. The charge pump circuit is constituted by three capacitors and two diodes. C_{res} is a large reservoir capacitor, which provides an initial energy to the whole system. C_{store} is a small storage capacitor, which collects temporarily the electrical charges generated by C_{var} during the electromechanical conversion process. The diodes D_1 and D_2, which are located in between each capacitor, act as unidirectional switches. We recall that the diode D_1 (respectively D_2) is on exclusively when the volages between of C_{res} is higher than C_{var} (respectively C_{var} and C_{store}).

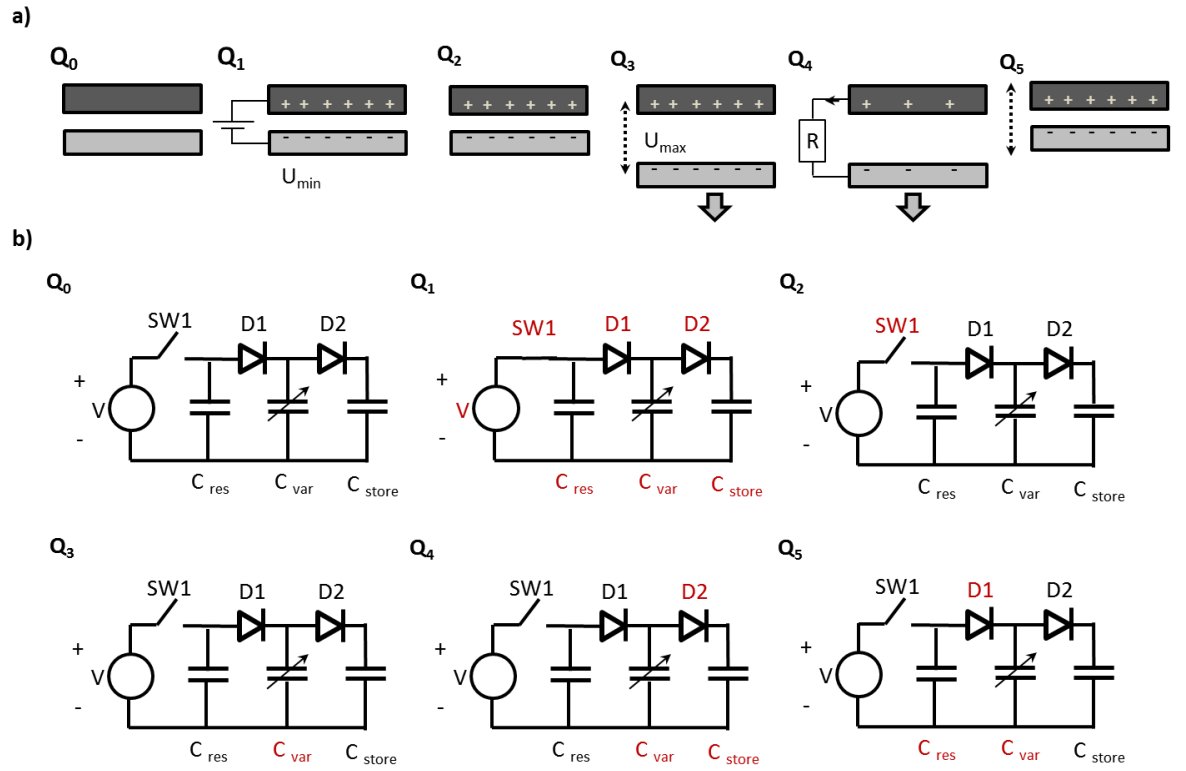

Figure 8: a) Scheme of the energy conversion cycle at charge constrained of a variable capacitor. Dark-grey rectangles represent fixed electrodes whilst light-grey, mobile electrodes. b) Representation of a generator and a charge pump circuit used for harvest the charges from the variable capacitor

The initial condition of the charge pump is when all the voltages of the capacitors $U_{res}=U_{store}=U_{var}=0$ are equal to zero (see Q_0 Figure 8). The generator is then switched on. The switch SW1 enables to transfer the electrical charges from the generator to the charge pump. Since the voltages of the capacitor are null ($U_{res}=U_{store}=U_{var}=0$), the diodes D_1 and D_2 are on and enable the transfer of the electrical charges to all the capacitors (see Q1 in Figure 8). The switch SW1 is then open and the electrical charges are stored in the capacitors (see Q_2 in Figure 8). Consequently the voltages across the capacitors are not equals any more ($U_{res,} \neq U_{store,} \neq U_{var}$). In order to modify the voltage at C_{var} it is necessary to provide a mechanical work to move the electrodes (see Q_3 Figure 8). At constant charge, the mechanical vibrations provoke the increase of the maximal voltage across C_{var} which at some moments exceeds the voltage across $C_{store.}$ In these conditions, D_2 is on, and the charges flow from C_{var} to C_{store} (see Q_4 Figure 8). After reaching its maximum, the voltage across C_{var} starts to decrease. After this decrease, the voltage across C_{var} falls to its minimum. D_1 becomes on and charges from C_{res}, which is much greater than $C_{var,}$ flows again towards C_{var}; completing thereby the cycle (Q_5 in Figure 8). As the mechanical motions continues, C_{var} keeps transferring electrical charges from C_{res} to C_{store}. However after several charge pump cycles, C_{store} reaches its saturation. In order to avoid the loss of further mechanical energy a fly-back system operates and transfers electrical charges from C_{store} to C_{res}.

In order to increase the performances of the system, the dielectric medium can be constituted by a high permittivity and deformable material. The introduction of a material with high

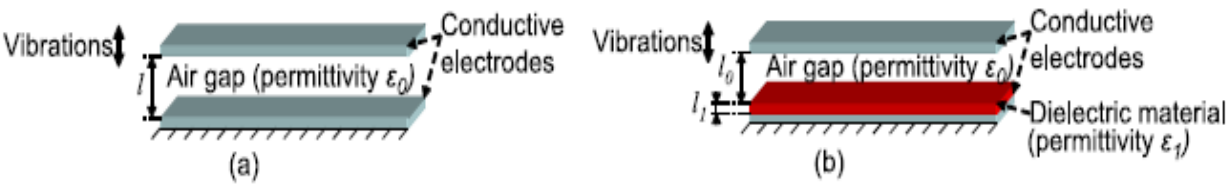

Figure 9: (From the left to the right) Electrostatic energy harvesting using a classical approach (a) and a conversion enhancement using a variable permittivity (b). Lallart et al [45]

dielectric permittivity is expected to lead to high variations of capacitance. Some materials (see Figure 4) exhibit a relative permittivity about three orders of magnitude higher than the one of air. Lallart *el al* [45] compared the amount of output power delivered by an out of plane approach in a variable capacitor with two different dielectric media. In the first case, the inter-plate distance is constituted by an air gap. In the second case, the inter space is constituted by a layer of a high permittivity material plus an air gap $\varepsilon_{air} = 1$ (Figure 9). The simple addition of the high-permittivity material $\varepsilon_r' = 1000$ leads to an improvement of about 50 times of the harvested energy. Ideally the maximum capacitance values would be obtained if no air gap would exist between the electrodes. But in practical applications, the presence of air allows easy deformations and avoids problems of non-perfect electrical contacts [45]. In the followings, we will use high permittivity and soft elastomeric materials. These materials are easily deformable and adhere well to metal electrodes.

5) *Electrostrictive materials*

i. Definition

Electrostriction is defined as the property of non-conductive materials, which develop a quadratic dependency between strain $S_{ij}$and electric polarization P under a constant stress τ_{ij}. The stress does not induce any electric polarization but changes the molecular structure so that its response to a field becomes modified (Figure 10a). Electrostrictive materials are passive materials which need a primary electrical source to convert mechanical energy into electricity. As for piezoelectric materials, electrostriction is described by intrinsic equations based on the thermodynamic potential, i.e. the energy exchange. The general equation of electrostriction is given by (Eq.8) [46-47]

$$D_i = \varepsilon_{ij}^T E_j + 2M_{ijkl} E_j T_{kl}$$

$$S_{kl} = s_{klij}^E T_{ij} + M_{ijkl} E_i E_j \quad (8)$$

Where s_{klij}^E are the elastic compliance coefficients, M_{ijkl} the electrostrictive coefficients, E_j the components of the electric field D_i the components of the electrical flux density and ε_{ij}^T the linear dielectric permittivity coefficients of the material. We note that the general equation can be simplified depending on the characteristics of the studied material.

In the case of an isotropic electrostrictive polymer film subjected to a stress τ_{11} and to an electrical field along its thickness directionE_3, this leads to:

$$D_1 = \varepsilon_{13}^T E_3 + 2M_{13}E_3\tau_{11}$$

$$S_{11} = s_{11}^E \tau_{11} + M_{13}E_3^2 \quad (9)$$

This equation can be re-written as $D_1=\varepsilon_{eff13}E_3$ where ε_{eff} is an effective dielectric permittivity that includes the contribution of mechanical stress. The resulting effective permittivity can be expressed in terms of the variation of the polarization. Consequently, the electrostrictive coefficient M_{13} is defined by Eq. 10 as the variation of the dielectric constant when mechanical stress is applied [48].

$$M_{13} = \frac{\Delta\varepsilon'_{r13}\varepsilon_0}{2\tau_{11}}, \qquad for\ \vec{E} = E_3\overrightarrow{e_3}, \qquad and \qquad \vec{\tau} = \tau_{11}\begin{pmatrix}1 & 0 & 0\\ 0 & 0 & 0\\ 0 & 0 & 0\end{pmatrix} \quad (10)$$

Where, ε_0 is the permittivity of the vacuum, $\Delta\varepsilon'_r$ is the variation of the relative dielectric permittivity due to an external mechanical stress τ_{11} and an electrical field in the 3 direction.

Same analysis in the situation of an isotropic electrostrictive polymer film subjected to a stress τ_{33} and to an electrical field along its thickness direction E_3, leads to:

$$M_{33} = \frac{\Delta\varepsilon'_{r33}\varepsilon_0}{2\tau_{11}}, \qquad for\ \vec{E} = E_3\overrightarrow{e_3}, \qquad and \qquad \vec{\tau} = \tau_{33}\begin{pmatrix}0 & 0 & 0\\ 0 & 0 & 0\\ 0 & 0 & 1\end{pmatrix} \quad (11)$$

Note that the coefficients M_{33} and M_{13} are equal in the case of an incompressible isotropic material.

ii. Measurement of the electrostrictive coefficient

Electrostriction is ascribed to the intramolecular dipoles in the polymer chains. The application of an external electric field induces the reorientation of the polar chains, resulting on a bulk deformation (Figure 10a), which persists until the electric field is removed. The measurement of this precise bulk deformation is a way to determine the electrostrictive properties of some polymers materials. Classical electrostriction experiments are generally performed on thin polymer samples coated with conducting metallic or organics layers on their two opposite faces and acting as compliant electrodes.

Figure 10 a) and b) show an electro-active polymer material in between two compliant electrodes. When an electrical field *E* is applied, with an intensity equal to typically 10V/µm, the thickness is reduced and consequently the width is increased in all directions. The variation of the thickness is recorded by a sensor on top of the materials enabling the

determination of the strain. The electrostrictive coefficient M_{33} is obtained by dividing the strain over the square of the electric field $M_{33}=S_{33}/E_3^2$ [49].

Figure 10 c) shows the scheme for the measurement of the electrostrictive coefficient M_{13} (i.e. when the applied electric field is perpendicular to the strain). In this configuration the material is composed by two layers and two compliant electrodes. Due to their different thicknesses and affinity to the electric field, the layers display different states of elongation or compression, resulting in the bending of the multilayer material. The resulting deflection of the tip is employed to calculate the electrostrictive coefficient M_{13} [50].

The bending and thickness actuation (i.e. Figure 10 b) and c)) are the most commonly used characterization techniques that enables the determination of the electrostrictive coefficients, M_{33} and M_{13} respectively.

Nevertheless these methods suffer from some drawbacks.

The actuation that is measured to compute these coefficients arises from the Maxwell stress and from the electrostriction effect [51]. The Maxwell stress is driven by the interaction between free charges on the electrodes, leading to the modification of the internal electric field distribution inside the dielectric material. The electrostriction is driven by the interaction between dipoles induced inside the material (Figure 10a). Besides, these mechanisms are difficult to separate experimentally because both induce bulk deformations that display a quadratic dependence with the electrical field. According to Kofod *et al* [52] the actuation for elastomeric materials with low permittivity $\varepsilon'_r \approx 1$, such as silicones, natural rubber latex and acrylates results mainly from Maxwell stress. On the other hand, for high permittivity $\varepsilon'_r \approx 10$ polar polymers, such as PVDF and PU, the actuation is dominated by the electrostriction mechanism [53].

The most reliable procedure to verify that the actuation is due to a pure electrostrictive effect is to corroborate that the bulk dielectric permittivity of the material is modified when the

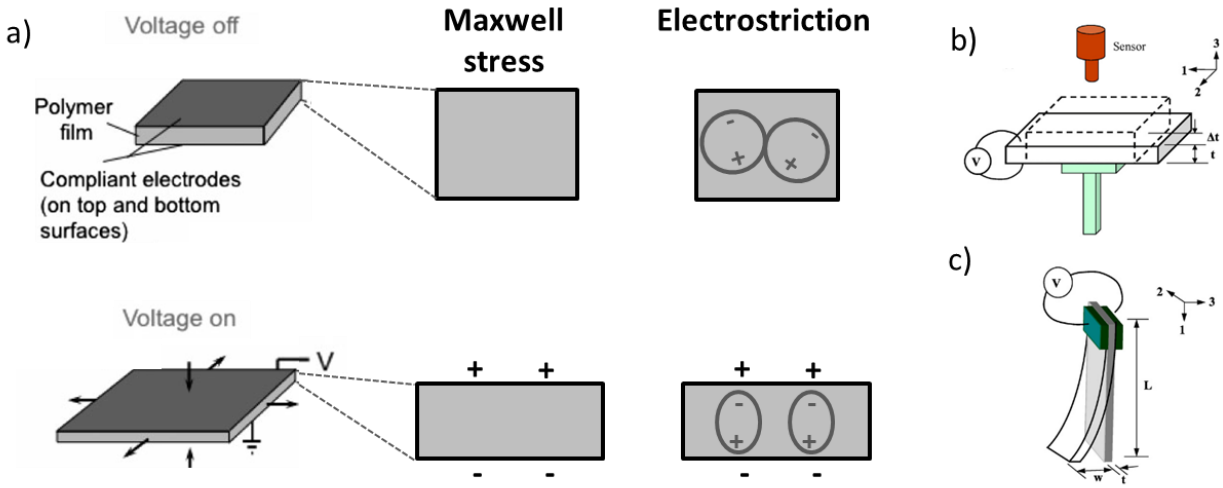

Figure 10: The strain of an electro-active polymer material can be due to different a) electromechanical mechanism: Maxwell stress (i.e free charges on the electrodes) or electrostriction (i.e. interaction between dipoles within the material). Scheme of the two characterization techniques to determine the electrostrictive coefficient Mij via an indirect approach: b) thickness (M_{33}) or c) bending actuation (M_{13}). Deshmukh et al [63]

material is subjected to a mechanical stress [51, 54]. Indeed in this case, the free charges will not be involved in the variation of the dielectric constant. We anticipate that the dielectric constant has to be measured at high frequency in order to avoid polarization at the electrodes. There does not exist, to our knowledge, such experimental determination reported in the literature.

Last but not the least, the accuracy of the measurements may be biased by the heat produces due to the high values of the electric field, by the remaining polarization on the electrodes or even by the methodology to determine the deflection of the tip.

We conclude this section by noting the necessity to develop a more direct characterization technique, using a low voltage, for the assessment of the dielectric properties while a mechanical stress is applied (i.e. electrostrictive properties).

iii. Intrinsically electrostrictive polymers

Neat polymers have been tested with bending or thickness actuation, to explore their potential as electromechanical harvesters. Cheng *et al* [55] and Huang *et al* [56] studied the electrostrictive properties of neat polyvinylidene fluoride (PVDF) polymer polyvinylidene fluoride, trifluoroethylene (PVDF-TrFE) copolymers and polyvinylidene fluoride, trifluoroethylene, and 1, 1-chlorofluoroethylene P(VDF-TrFE-CFE) terpolymer(exclusively Values measured for M_{33} are about $1.9x10^{-19}$ m^2xV^{-2} at 1Hz, while M_{13} values go up to $5x10^{-18}$ m^2xV^{-2} at the same frequency. Zhang *et al* [57], studied the influence of the temperature on the electrostrictive coefficient values of PU polymers. At 100 Hz the value of M_{33} of PU, increases from 5 $x10^{-19}$ m^2xV^{-2} at 20°C to 3.5 $x10^{-18}$ m^2xV^{-2} at 80°C. Guillot *et al* [53] also performed thickness actuation in PU polymers to determine the electrostrictive coefficient M_{33} at 2 kHz. The values are broadly distributed: the lowest one is about $9x10^{-19}$ m^2xV^{-2} and the highest one of about $7x10^{-17}$ m^2xV^{-2}. The huge difference between the values is explained by the incorporation of several average molecular weight chains within the polymer. In summary, the electrostrictive properties of neat polymer can be increase by improving the polarization at the intramolecular scale [47]. However the obtained electrostrictive coefficients M_{ij} remain typically below 10^{-16} m^2xV^{-2}. In spite the relatively low electrostrictive coefficients for such materials, it has been proved that the induced polarization is used at large scale applications to perform harvesting devices. [53,55-57]. We expect that an enhancement on the electrostrictive properties can scale down the size of such devices. Thus, smaller energy harvesting devices can be produced, typically at the micron scale.

iv. Electrostrictive nanocomposites

A very efficient approach to increase both the permittivity and electrostrictive coefficients of polymers consists in adding conductive inclusions in insulating polymers. The presence of

conductive particles enhances the ability of the nanocomposites to be polarized due to the Maxwell-Wagner polarization mechanisms. Wongtimnoi *et al* [51] included conductive carbon black (CB) particles to a PU matrix using a co-solvent such as DMF. As expected the M_{33} increases by about two orders of magnitude compared to the neat polymer. The optimized material reaches a value of M_{33} of about 1,2 x10^{-14} m^2xV^{-2} for a 1.5 v % of carbon black fillers at 0.1Hz. Guiffard *et al* [58] reported a similar value for a PU matrix but instead of CB, the fillers incorporated were SiC particles. The modification of the filler leads to an average M_{33} value of about 2.5 x10^{-15} m^2xV^{-2} at 0.1Hz (Figure 11).

The improvement of M_{ij} has been proved for PU polymers but also for other dielectric matrixes. Cottinet *et al* [59] incorporated CB to a PVDF-TrFE copolymer matrix. Herein, the value reaches 2 x10^{-15} m^2xV^{-2} at 0.1Hz, corresponding about to 3 orders of magnitude greater than that of the neat fluorinated polymers [55-56]. Noteworthy that the applied electric field to cause electromechanical actuation is reduced by an order of magnitude (i.e. 1V/μm) compared to neat polymers. Most of the works focused on the electrostrictive properties of nanocomposites reported values of about 10^{-15} m^2xV^{-2} [60]. These values are significantly higher those of neat polymer. These values are significantly higher than neat polymer (about three orders of magnitude) but we believe that optimizing the fillers distribution and the structure of the matrix can increase the electrostrictive coefficient M_{13} or M_{33} even more.

The use of single wall carbon nanotube –polyimide (PI-SWNT) composites seems to yield greater results than the rest of the composites reported in the literature. As a matter of fact, Park *et al* [50] improved the electrostrictive properties of a PI by including a highly uniform dispersion of single wall carbon nanotube SWNT to the polymer. The uniformity of the dispersion is possible due the donor-acceptor interaction between the SWNT and the PI. [61,62]. The electrostrictive coefficient M_{33} and M_{13} were determined using thickness and bending actuation respectively. The optimization of the M_{ij} values was carried out by adjusting the SWNT concentration. The optimized composites display a huge M_{33} value of 1.2x10^{-13} m^2xV^{-2}at 0.02Hz. The M_{13} value is calculated using four layers bending actuation and is about the same order of magnitude. Deshmukh *et al* [63] developed a similar composite system where the out of plane and the extensional strain are used to determine the M_{33} and M_{13} coefficients. The optimized composite is found to be at 1% SWNT. The M_{13} value is as high as 5x10^{-14} m^2xV^{-2}at 1Hz. When this composite material is studied employing thickness actuation at 1Hz, the value of M_{33} is about 9x10^{-13} m^2xV^{-2}, the highest ever reported to our knowledge. The PI-SWNT electrostrictive coefficients are about six to seven orders of magnitude higher than those of neat polymers. Deshmukh *et al* [63] stress that the high electrostrictive coefficient

Polymer	Fillers	Content (vol %)	Dielectric Constant	Frequency Measurement of Permittivity (Hz)	M_{33} (m^2/V^2) 10^{-15}	Frequency Measurement of M_{33} (Hz)
PU	No		6.8	0.1	−1	0.1
PU	SiC	0.5	10.9	0.1	−2.5	0.1
PU	CB	1	15.4	0.1	−4	0.1
P(VDF-TrFE-CFE)	No		65	0.1	−1.1	0.1
P(VDF-TrFE-CFE)	CB	1	95	0.1	−2.4	0.1
P(VDF-TrFE-CFE)	PANI	23	2,000	100	−0.15	1
P(VDF-TrFE-CFE)	PANI	12.7	600	100	−0.02	1

SiC, silicon carbide; CB, carbon black; PANI, polyaniline.

Figure 11: The table summarizes the effect of the fillers on dielectric and electrostrictive properties for PU and PVDF (c). [60]

results from the creation of micro and nanocapacitors formed by the carbon nanotubes (CNT) [64]. In addition the donor acceptor interactions between the fillers and the matrix bring additional polarization to the system. The π–electron from the aromatic molecules of the polymer chains interacts with the SWNT. We note that this polarization effect leads to an additional structuration of the dipoles at the nano-scale.

v. Applications

Due to their low cost, lightweight, ease of processing, low stress needed, and sensitivity at low frequencies, variable capacitors provide a promising route towards mechanical energy harvesters from a wide range of mechanical sources of energy [65]

Enhanced with the use of electrostrictive materials, variable capacitors can target small, medium and large-scale application systems that are not easily attainable with piezoelectric or electromagnetic materials.

Large-scale applications require low cost and robustness. Among the large scale applications, we can cite a very interesting, clean and renewable energy: ocean waves. The wave energy converters (WEC) can effectively harvest the hydrodynamic energy into electrical power through the strain of electrostrictive materials. The transducers is set in a oceanographic buoy based on a suspended proof mass that stretches the electrostrictive materials as the buoy heaved the waves (Figure 12a). The oceanographic buoy was tested in real conditions and the mechanical deformation of the electro-active material generated more than 11 Joules for about 220g of materials within the buoy. The WEC is not practical for power generation to feed an

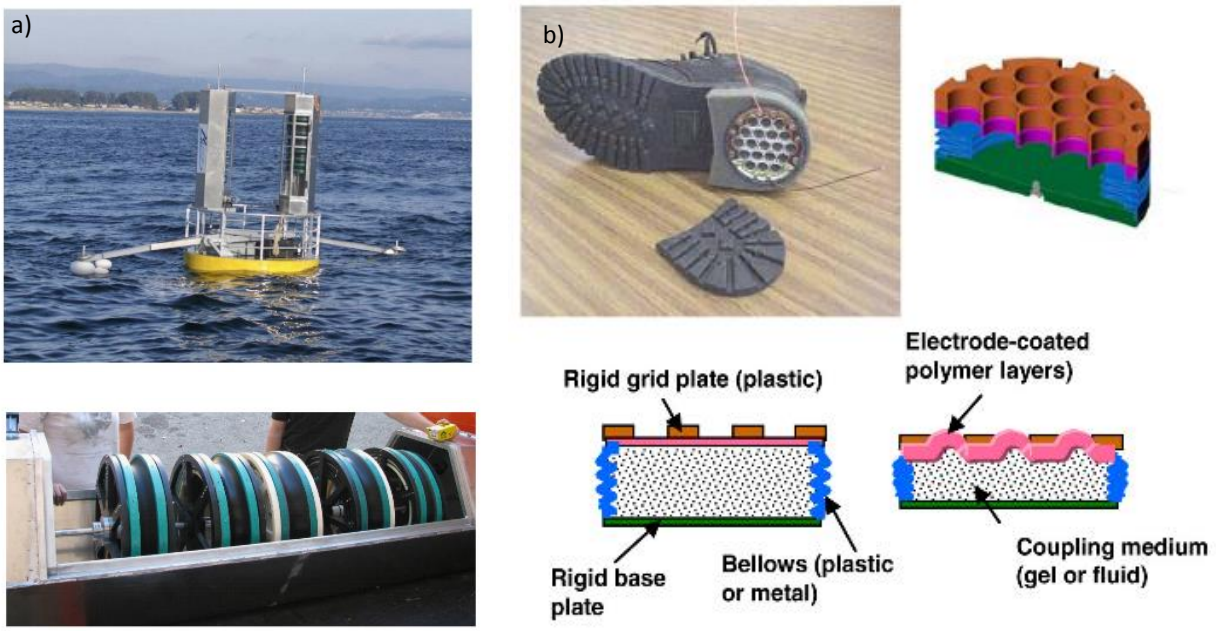

Figure 12: Image of a) a Dielectric elastomer ocean wave power generator set on an articulated, multi-body system buoy (top) and concatenated rolls in a generator module (bottom). Images and schemes of a b) heel-strike generator base on the principle of a dielectric elastomer. Photo of the device installed in a boot (top left) and cross section (top right and bottom) [66-68].

entire harbor, but it is definitely a fully autonomous system capable to harvest the energy needed to power its on board lighting, instrumental or communication systems [66,68]. This proof of concept is not limited to large-scale applications. With the propagation of mobile communication devices, the need for extending life of batteries has increased. In order to overcome this problem, Kornbluh *et al [68]* developed an electrostatic generator in a boot heel. This device uses the compression of the heel during walking to harvest power from human walk. This device is composed by a stack of electro-active films (Figure 12b). The generator uses a fluid to transfer the compression of the heel to the stretching the electro-active polymer. When the heels press down, an elastomer membrane is compressed. The device can produce up to 800mW. [68]

The shoe generator can deliver enough energy to power night vision goggles or charge batteries of mobile phones. We recall that most of the portable wireless devices need power outputs about 1 to 100mW, mobiles phones requires about 1W. Compared with other state of the art harvesters, the amount of energy exceed the one generated by piezoelectric shoe elements of Paradiso *et al* [9].

Electrostrictive materials are a promising approach to improve the energy conversion of mechanical sources into electrical energy due to their unique properties. In spite these promising results, key challenges and improvement remain to be solved. Indeed, there is a need to develop new materials operating at lower voltages and that could be easily integrated into small scale devices (i.e. MEMS technology).

Moreover, the major challenge in the field consists in achieving large changes of capacitance under mechanical deformation. An exciting approach is based on the use of elastic polymers filled with conductive nano-inclusions. The presence of the nanoparticles leads to an increase of the dielectric constant of the material. Nevertheless, the potential of this technology is far from being optimized because the permittivity of materials that have been investigated is not yet sufficiently large and the sensitivity to stress of the materials (electrostriction coefficient) remains limited. Electrostrictive composites are generally made of random dispersions of particles without any structural optimization.

Our aim in this thesis is to bypass this bottleneck and to synthesize new, easy to process, electrostrictive materials displaying a high sensitivity to the mechanical stress that can yield huge electrostrictive coefficients.

6) Our strategy

i. Emulsion template composites

We propose to add conductive or high permittivity nano-fillers to soft elastomeric polymers. Addition of such particles is expected to yield enhancements of the permittivity of the polymer. The permittivity of composites made of conductive inclusions in an insulating matrix theoretically diverges at the percolation threshold. Actual divergence is not observed in actual experiments because of finite size effects of the samples. Nevertheless, a large increase of permittivity is still observed in the vicinity of the percolation threshold [68]. Near-percolated networks are also expected to be highly sensitive to external stimuli, such as materials near a critical point with enhanced susceptibility. These predictions make near percolated nanocomposites particularly promising for applications based on electrostriction mechanisms.

Nanocomposites are typically synthesized by processing techniques such as melt-mixing, extrusion, or copolymerization, which provide randomly distributed particles. In this project, we propose to make self-assembled near-percolated networks of conductive carbon nanotubes (CNT) in elastomers (poly-dimethyl-siloxane). This approach offers opportunities to control the stiffness, level of connectedness and morphology of the networks of CNTs segregated in between the emulsion droplets [69, 70].

In addition nanocomposites can be relatively inexpensive, mechanically robust, chemically stable and easily processable from small to large scales.

Considering the great potential of nanocomposites as electrostrictive materials and their side advantages for future applications, the work of the present thesis is focused on nanocomposites made of nanocarbon inclusions in PDMS.

ii. Bilayer structure composite materials

Our aim is to build a system displaying large variations of capacitance under mechanical strain. Bilayer structures can be used as an alternative method to combine properties not otherwise met in a single component, for example, low losses, high permittivity and deformability. For example some electrostrictive materials with giant permittivities suffer from large losses. These losses include dielectric losses but also conduction from free charges present in the systems. Of course the relative contribution of capacitive and resistive behavior in the material can be quite complex. In addition, it can depend on the mechanical load applied to the systems. The phase and magnitude of the impedance can in fact vary. In particular, one can consider electrostrictive-piezoresistive materials which essentially act as a capacitor for some mechanical load, but which behave as resistor in other conditions of load. The above

concepts will be clearer with a more detailed description of the systems studied in the thesis work.

The present bilayers are prepared as follows. The first layer is an electrostrictive material made using the emulsion approach (Figure 13a). The second layer is constituted by a dielectric material which is presently a dielectric polymer film or a graphene oxide film. Ultrathin layers are achieved via spin coating / drop casting methods (Figure 13b). These layers are chosen to be thin on purpose in order to form large capacitances. The thin layer of dielectric polymer (respectively GO) will be considered as the one with the capacitance C_1 (respectively C'_1). A so called bilayer structure is obtained when the dielectric layer is placed on top of the electrostrictive material. The bilayer structured can be modeled in first approximation as a simple electrical circuit shown in Figure 13.

The electrostrictive material is represented by a parallel resistor-capacitor circuit element RC_2 (see Figure 13a). The pure dielectric material is represented by a capacitor C_1 (or C'_1 for GO) element (see Figure 13b). The whole equivalent circuit for the bilayer structure is a capacitor C_1 or C'_1 in series with a RC_2 in parallel. We note that the electrostrictive material is formulated to be as sensitive as possible to the mechanical stress. Therefore its dielectric and resistive properties change with the mechanical strain. Here we consider materials that act as insulating dielectrics in absence of load. The equivalent electronic circuit for the bilayer structure can be therefore viewed as two capacitors in series (C_2 in series with C_1 or C'_1). The value of the equivalent capacitor C_{eq} is close to the capacitor with the lowest capacitance value (see Figure 13c). Under mechanical loading, the electrostrictive material acts as an electrical conductor. The equivalent electronic circuit for the bilayer structure is henceforth a resistor R, in series with a capacitor C_1 or C'_1. The equivalent capacitor C_{eq}, is equal to the capacitor in series with the resistor. In brief, the amplitude and phase of the impedance can be tuned by tuning the

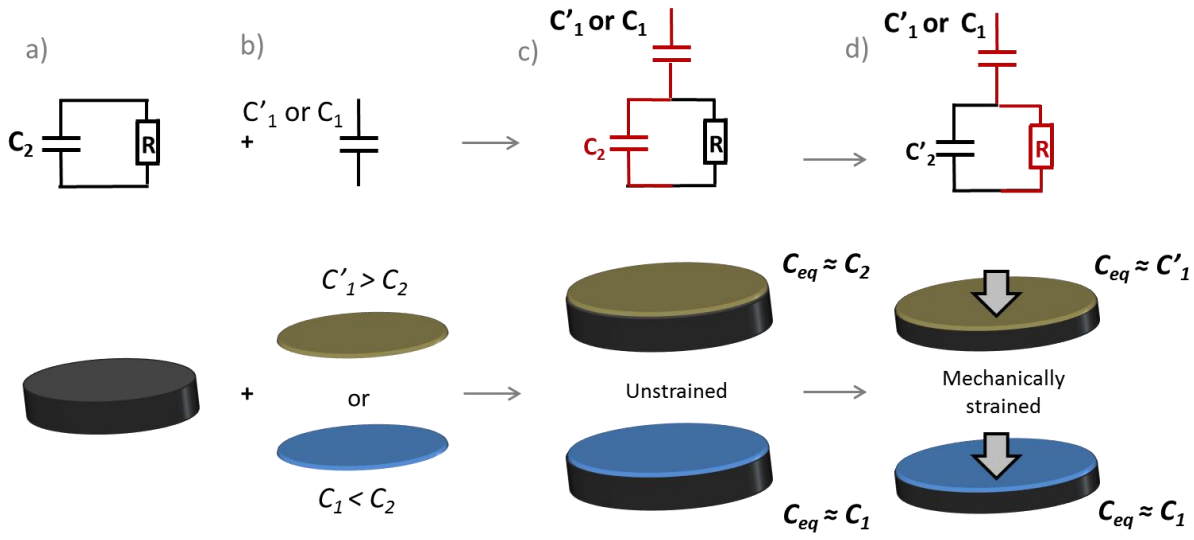

Figure 13: Scheme of the composition of the bilayer structure composite material: a) the black block represents the composite material prepared with a polymer matrix and anisotropic conductive particles. b) Blue and brown disks represent a thin-layer of polymer and graphene oxide respectively. The electrical properties of the bilayer material change when subjected to a mechanical strain. It can acts as a capacitor c) or as resistor d). The upper part shows the equivalent electronic circuits for each material and situation.

capacitance values of the layers and by taking advantage of the sensitivity to stress of the "electrostrictive-piezoresistive" layer. We see that the above concept offers an opportunity to induce large variations of capacitances by appropriately optimizing the chosen materials and their thickness.

iii. Our plan

The present thesis is structured as follows. In Chapter II we detail the synthesis of the composite materials and the development of characterization techniques to simultaneously study mechanical and dielectric properties. In Chapter III and IV we show the design and fabrication of high permittivity materials employing elastic matrices. The materials are made using an emulsion approach. We characterize their dielectric properties in unstrained conditions. Results for CNT based composites are given in Chapter III. Those for graphene oxide are presented in Chapter IV. Chapter V is devoted to the electromechanical characterization of the composite materials loaded with CNTs. Chapter VI is devoted to the study of multilayer materials for which the structuration is conceived to reduce the electric losses and enhance electrostrictive properties. In chapter VII we discuss preliminary results dealing with energy harvesting applications.

References :

1. Mitcheson, P.D., E.M. Yeatman, G.K. Rao, A.S. Holmes, and T.C. Green. « Energy Harvesting From Human and Machine Motion for Wireless Electronic Devices. » Proceedings of the IEEE 96, no 9 (2008): 1457-86.

2. Roundy, Shad, Paul K. Wright, et Jan Rabaey. « A study of low level vibrations as a power source for wireless sensor nodes. » Computer Communications, Ubiquitous Computing, 26, n° 11 (1st July 2003): 1131-44.

3. Woias P, "Energy Harvesting Scientific course "FSRM –workshop, ZUerich 2015

4. Seah, W.K.G., Zhi Ang Eu, and H. Tan. « Wireless sensor networks powered by ambient energy harvesting (WSN-HEAP) - Survey and challenges. » In 1st International Conference on Wireless Communication, Vehicular Technology, Information Theory and Aerospace Electronic Systems Technology, 2009. Wireless VITAE 2009, 1-5, 2009. doi:10.1109/WIRELESSVITAE.2009.5172411.

5. Chalasani, S., and J.M. Conrad. « A survey of energy harvesting sources for embedded systems. » In IEEE Southeastcon, 2008, 442-47, 2008. doi:10.1109/SECON.2008.4494336.

6. Thad Starner, et Joshep A. Paradiso. « Human-generated-power-for-mobile-electronics.pdf. ». http://www.cc.gatech.edu/~thad/p/books/human-generated-power-for-mobile-electronics.pdf.

7. A. Mehra, X. Zhang, A.A. Ayron, I.A. Waitz, M.A. Schmidt, C.M. Spadaccini. A six –wafer combustion system for a silicon micro gas turbine engine, Journal of Microelectromechanical Systems 9 (4) 2000 517-526

8. Schmidhuber H. and Hebling C. "First experiences and measurements with a solar powered personal digital Assistant " Proc. 17th European Photovoltaic Solar Energy Conf. ETA-Florence and WIP-Munich, 2001, 658-662

9. Paradiso, J.A., and T. Starner. « Energy scavenging for mobile and wireless electronics. » IEEE Pervasive Computing 4, no 1 (January 2005): 18-27. doi:10.1109/MPRV.2005.9.

10. J. Lebet, "Living on air-history of the atmos clock" Jeager-LeCoultre 1997

11. Necula, Christian, Bogdan Gramescu, Daniel C Comeaga, Octavian Dontu, et Constantin Nitu. "A survey of energy harvesting as power supply for mechatronic systems." 20179-184.pdf.

12. Willimas, C.B., et R.B. Yates. "Analysis of a micro-electric generator for microsystems". Proceedings of the Transducers 95/Eurosensors IX (1995) 369-372.

13. Stephen N.G.2006. "On energy harvesting from ambient vibration" J. Sound Vib.293.409-25

14. Chandrakasan, A.P., et R. Amirtharajah. « Self-powered Signal Processing Using Vibration-based Power Generation - Solid-State Circuits, IEEE Journal of - 1998_amirtharajah_jssc.pdf. »

15. A. Chapuis and E. Jacquet , "The History of the self watch, roto – sadag,1956

16. K. Matsuzawa and M. Saka. Seiko human powered quartz watch. In M. Rose, editor, Prospector IX: Human-Powered Systems Technologies,pages 359–384, Auburn, AL, November 1997. Space Power Institute, Auburn Univ

17. S.R. Vetorino et al., Renewable Energy Flashlight, US patent 6,220,719, to Applied Innovative Technologies, Inc., Patent and Trademark Office, 2001

18. A. S. Holmes, G. Hong, K. R. Pullen, andK. R. Buffard,B Axial-flow microturbinewith electromagnetic generator:Design, CFD simulation and prototypedemonstration,[in Proc. IEEE MEMS,2004, pp. 568–571

19. http://www.nhc.noaa.gov/aboutsshws.php

20. http://gallica.bnf.fr/ark:/12148/bpt6k2282p

21. White, Na0m. M., and J. D. Turner. « Thick-Film Sensors: Past, Present and Future. » Measurement Science and Technology 8, no 1 (1997): 1. doi:10.1088/0957-0233/8/1/002.

22. Baudry H 1987 Screen printing piezoelectric devicesProc.6th European Microelectronics Conf. (Bournemouth) pp 456–63

23. Information, National Center for Biotechnology, U. S. National Library of Medicine 8600 Rockville Pike, Bethesda MD, et 20894 Usa. « Ferroelectric polymers. - PubMed - NCBI. ».

24. Piezoelectric Ceramics Data Book for Designers Morgans Electro ceramics

25. Piezoelectric transducers for vibration control and damping Moheimani and Fleming

26. Jeon Y.B. Sood R., Jeong J-hand Kim S.G. "MEMS power generator with a traverse mode thin film PZT" Sensors Actuators A, 2005, 122, 16-22

27. Sodano H.A. Park G. and Inman D.J. "Use of piezoelectric energy harvesting devices for charging batteries. Proc.SPIE 10th Annual Int. Symp. On Samrt Structures and Materials , 2003, p101-108

28. White N.M., Glynne-JonesP and Beeby S.P. "A novel thick-film piezoelectric microgenerator Smart Mater. Struct. 2001, 10,850-852

29. Glynne-Jones P., Beeby S.P., and White N.M. "Towards a piezolectic vibration powered micro-generator" IEE Proc. – Sci. Meas. Technol 2001.148 68-72

30. Beeby S.P, Tudor M.J. White N.M " Energy Harvesting vibration sources for microsystems applications" Meas. Sci. Technol .2006 , 17 R175-R195

31. Torah R. Beeby S and White N. "An improved thick film piezoelectric material by powder blending and enhanced processing parameters IEEE Trans. UFFC 2005 52, 10-16

32. N.S. Shenck and J.A. Paradiso, "Energy Scavenging with Shoe-Mounted Piezo-electrics," IEEE Micro, vol. 21, no. 3, 2001,pp. 30–42

33. Kymissis J., KendallC., Paradiso J.A. and Gershenfeld N., "Parasitic power harvesting in shoes " Proc 2nd IEEE Int. CONf. wearable Computing, 1998, 132-139

34. Dynamoelectric Shoes, US patent 5,495,682, Patent and Trademark Office, 1996

35. Ramsay M.J. and Clark W.W. "Piezoelectric energy harvesting for bio MEMS applications " Proc. SPIE, 2001, 4332 , 429-436

36. Sohn JW, Choi SB, Lee DY An investigation on piezoelectric energy harvesting for MEMS power sources. Proceedings of the IMechE Part C: Journal of Mechanical Engineering Science (2005) 219:429–436.

37. Guigon R., Chaillout J.J., Jager T.and Despesse G. Harvesting raindrop energy: experimental study Smart Mater. Struct. 17 (2008) 015039

38. Guigon R., Chaillout J.J., Jager T.and Despesse G. Harvesting raindrop energy: theory Smart Mater. Struct. 17 (2008) 015038

39. Michenson P, Stark B., Miao P, Yeatman E., Holmes A., Green T." Analysis and optimization of MEMS on chip power supply for self powering slow moving sensors" Proc. Eurosensors XVII

40. Sterken T., Fiorini P., BaertK., Borghd S. "Power extraction from ambient vibration " Proc 3rd Workshp on semiconductor sensors and actuators"pp 680-683

41. Roundy S. "Energy scavenging for wireless sensors nodes with a focus on vibration to electricity conversion" PhD Thesis University of California, Berkeley

42. Boisseau S. Despesse G., Seddik B.A. "Electrostatic Conversion for vibration Energy Harvesting", Small-Scale Enregy Harvesting , Intech 2012

43. Yen B.C., Lang H. J. , " A variable capacitance vibration to electric harvester", IEEE Transaction on circuits and Systems –I: Regular Papers IEEE, 2006 53,2 pp 288-295

44. Dudka A., Galayko D and Basset P., "Design of integrated smart adaptive conditioning circuit for capacitive vibration energy harvester " in Workshop of Energy and Wireless Sensors, Besancon , France 2012.

45. Lallart M., Pruvost S., Guyomar D., "Electrostatic energy harvesting enhancement using variable equivalent permittivity" Physics Letters A 375 (2011) 3921–3924

46. Jean-Mistral, C., S. Basrour, et J.-J. Chaillout. « Comparison of Electroactive Polymers for Energy Scavenging Applications ». Smart Materials and Structures 19, nº 8 (6 juillet 2010): 085012. doi:10.1088/0964-1726/19/8/085012.

47. Ren, K, Y Liu, H Hofmann, et Q.M. Zhang. « An active energy harvesting scheme with an electroactive polymer ».Appl. Phys. Lett. 91, 132910 2007

48. Liu, Liwu, Yanju Liu, Zhen Zhang, Bo Li, et Jinsong Leng. « Electromechanical stability of electro-active silicone filled with high permittivity particles undergoing large deformation ». Smart Materials and Structures 19, nº 11 (4 octobre 2010): 115025. doi:10.1088/0964-1726/19/11/115025.

49. Guyomar, D., P.-J. Cottinet, L. Lebrun, C. Putson, K. Yuse, M. Kanda, et Y. Nishi. « The Compressive Electrical Field Electrostrictive Coefficient M33 of Electroactive Polymer Composites and Its Saturation versus Electrical Field, Polymer Thickness, Frequency, and Fillers ». Polymers for Advanced Technologies 23, nº 6 (1 2012): 946-50.

50. Park Cheol, Kang Jin Ho, Harrison, Joycelyn S. Costen Robert C. ,and Lowther Sharon E. «Actuating Single Wall Carbon Nanotube–Polymer Composites: Intrinsic Unimorphs» Adv. Mater. 2008, 20, 2074–2079

51. K. Wongtimnoi, B. Guiffard, A. Bigner-Van de Moortele, L. Severyrat, C Gauthier, J.Y. Cavaille « Improvement of electrostrictive properties of a polyether-based polyurethane elastomer filled with conductive carbon black - 1-s2.0-S0266353811000704-main.pdf ».K. Composites Science and Technology 71 (2011) 885–89.

52. Kofod G, Sommer-Larsen P, Kornbluh R, Pelrine R. Actuationresponse of polyacrylate dielectric elastomers. J Intell Mater SystStruct 2003;14:787–93.

53. Guillot, F. M., et E. Balizer. « Electrostrictive Effect in Polyurethanes ». Journal of Applied Polymer Science 89, nº 2 (11 juillet 2003): 399-404. doi:10.1002/app.12096

54. Zhao X, Suo Z. Electrostriction in elastic dielectrics undergoing large deformation. J Appl Phys 2008;104, 123530/1–7.

55. Cheng, Z.-Y., Vivek Bharti, T.-B. Xu, Shexi Wang, Q. M. Zhang, T. Ramotowski, F. Tito, et R. Ting. « Transverse strain responses in electrostrictive poly(vinylidene fluoride-trifluoroethylene) films and development of a dilatometer for the measurement ». Journal of Applied Physics 86, nº 4 (15 août 1999): 2208-14.

56. Huang, C., R. Klein, Feng Xia, H. Li, Q.M. Zhang, F. Bauer, et Z.Y. Cheng. « Poly(vinylidene fluoride-trifluoroethylene) based high performance electroactive polymers ». IEEE Transactions on Dielectrics and Electrical Insulation 11, nº 2 (avril 2004): 299-311. doi:10.1109/TDEI.2004.1285901.

57. Zhang, Q. M., J. Su, Chy Hyung Kim, R. Ting, et Rodger Capps. « An experimental investigation of electromechanical responses in a polyurethane elastomer ». Journal of Applied Physics 81, nº 6 (1997): 2770-76.

58. Guiffard, B.; Seveyrat, L.; Sebald, G.; Guyomar, D. J. Phys. Enhanced electric field-induced strain in non-percolative carbon nanopowder/polyurethane composites Appl. Phys. 2006, 39, 3053–3057.

59. Cottinet, P.-J., Guyomar, D., Guiffard, B., Putson, C., and Lebrun, L.,. (2010). Modeling and Experimentation on an Electrostrictive Polymer Composite for Energy Harvesting IEEE Transactions on ultrasonics, ferroelectrics, and frequency control, Vol. 57, No. 4, pp., 0885-3010.

60. Lallart M., Cottinet P.J., Guyomar D., Lebrun L. "Electrostatic Polymers for Mechanical Energy Harvesting Journal of Polymer Sciencence part B: polymer Physics 2012, 50, 523–535

61. Park, Cheol, Zoubeida Ounaies, Kent A Watson, Roy E Crooks, Joseph Smith Jr., Sharon E Lowther, John W Connell, Emilie J Siochi, Joycelyn S Harrison, et Terry L. St Clair. « Dispersion of single wall carbon nanotubes by in situ polymerization under sonication ». Chemical Physics Letters 364, no 3-4 (4 octobre 2002): 303-8.

62. Wise, Kristopher E., Cheol Park, Emilie J. Siochi, et Joycelyn S. Harrison. « Stable dispersion of single wall carbon nanotubes in polyimide: the role of noncovalent interactions ». Chemical Physics Letters 391, no 4-6 (2004): 207-11. doi:10.1016/j.cplett.2004.04.096.

63. Deshmukh, Sujay, et Zoubeida Ounaies. « Single walled carbon nanotube (SWNT)–polyimide nanocomposites as electrostrictive materials ». Sensors and Actuators A: Physical 155, no 2 (octobre 2009): 246-52. doi:10.1016/j.sna.2009.07.007.

64. Z. Ounaies, C. Park, K.E. Wise, E.J. Siochi, J.S. Harrison "Electrical properties of single wall carbon nanotube reinforced polyimide composites" Compos. Sci. Technol., 63 (11) (2003), pp. 1637–1646

65. Carpi F., DeRossi D., Kornbluh R, Pelrine R., Somer-Larsen P. « dielectric elastomers as electromechanical transducers. Fundamentals, Materials, Devices,Models, and applications of an emerging electroactive polymer Technology, Elsevier, Amsterdam,2008.

66. Kornbluh R.D., Eckerle J., McCoy B., "A scalable solution to harvest kinetic energy" Newsroom ,2011 SPIE, 10.1117/25.1201106.003749.

67. Kornbluh R.D., Pelrine R., Prahlad H., Wong-Foy A.,McCoy B. Kim S., Eckerle J.,"From boots to boys: promises and challenges of dielectric elastomer energy harvesting", Porc SPIE 7976, p797605,2011

68. Kornbluh R.D."Elastomers: applications of dielectric elastomer Transducers for actuation, generation, and smart structures, "Smart structures and materials 2002: Industrial and commercial applications of smart structures technologies, Proc SPIE, vol4698 ,2002, 254-270.

69. Grossiord N, Loos J, Laake LV, Maugey M, Zakri C, Koning CE, et al. High conductivity polymer nanocomposites obtained by tailoring the characteristics of carbon nanotube fillers. Adv Funct Mater 2008;18 (20):3226–34.

70. Grossiord, N.; Kivit, P. J. J.; Loos, J.; Meuldijk, J.; Kyrylyuk, A. V.; van der Schoot, P.; Koning, C. E., On the influence of the processing conditions on the performance of electrically conductive carbon nanotube/polymer nanocomposites. Polymer 2008, 49 (12), 2866-2872.

-Mechanical ambient energy sources are a promising and alternative source of energy to develop new light-weight transducers and autonomous sensors networks.

-In order to develop the latter transducer it is necessary to synthesize composites with high permittivity and electrostrictive values.

-The main challenge is to develop morphology controlled nanocomposites which are sensitive to the mechanical stress. However it is also crucial to develop an adapted methodology to study such properties (dielectric properties under dynamic strain).

-We propose to synthesize such materials using an emulsion approach which enables finely control of the inner conductive network and a mechanical sensitivity due to the softness of the matrix.

- The optimization of such materials is study using the emulsion formulation and we propose different strategies to increase the electrostrictive coefficient and reduce the electrical losses

- We expect to develop an innovative energy harvesting device. There is not to our knowledge works that are able to develop, integrate and preform the application from a material conception.

Chapter II

Materials and methods for the development of electroctrictive nanocomposites

Requirements

We remind that the main challenge of the thesis is to develop sensitive electrostrictive materials. In order to bypass this bottleneck we developed an emulsion synthesis procedure that enables the fine control of the network of the conductive particles within the composite. In addition it is crucial to fully understand the electrostrictive properties of the materials. Consequently, we developed a specific characterization technique to study the mechanical and dielectric properties simultaneously. Finally, to study the potential of the emulsion based electrostrictive composites developed by the emulsion approach as energy harvesting devices, we build an electronic circuit based on the principle of the charge pump. The chapter is described as follow. In the first section we will described the materials and methods that were used in order to synthesize the nanocomposites materials. The second is devoted to the characterization techniques enabling the determination of the dielectric properties in rest (i.e. electrostriction). The third section is focused on the description of two different methodologies performed to describe the dielectric properties under mechanical stress. The first one is performed using an actuator while the second one is performed directly by the compression of the material. In addition, for techniques, the sample preparation, the mechanism, the calculations and the experimental set-up need it to determine the electrostrictive coefficient are detailed. The fourth section is devoted to the mechanisms and the experimental devices used for the study of the generated current when the samples are subjected to low frequency mechanical stress. The fifth and final section is devoted to the mechanism and experimental set-up that enables the determination of the power generated by electrostrictive materials when subjected to high frequency mechanical stress.

I. Synthesis of the emulsion based electrostrictive nanocomposite materials

1) Materials

The PDMS, Sylgard 184, was purchased from Dow Corning as a kit of PDMS base and curing agent. We recall, that the range of temperature for stable performances is [-55°C; 220°C]. This parameter is essential to avoid any degradation of the composite materials during the thermal reduction treatment.

The sodium dodecyl sulphate (SDS) was purchased from Sigma Aldrich and used as received.

The aqueous solution of graphene oxide (GO) monolayers was purchased from Graphenea® and the GO concentration is about 0.4 wt%. The mean GO sheet size is about 2-3 μm [1]. The solution was centrifuged in order to increase the GO concentration. Centrifugation was performed with a Sorval RC 6+, rotor SE-12, centrifuge at 22000 rpm (i.e. 50 000 g) for 45 minutes. After centrifugation, the supernatant was removed. The bottom phase that contains GO monolayers was collected. The solid content in the material was determined by dry extracts after evaporation of the water under vacuum at 100°C. The mean final weight fraction

of GO was 5.8%.

Thin multiwall CNTs (MWCNTs) were purchased from Nanocyl under the reference Nanocyl 7000 and used as received. The average diameter of the nanotubes is about 10 nm and the average length is about 1.5 microns. Their dispersion was carried out in 10mL flat-bottom flasks by respectively mixing 0.9 wt% and 1.2 wt% of CNT and SDS. Tip sonication using a Branson Sonifier 450A is performed during 1h at 135 Watts to unbundle and homogeneously disperse the CNTs. The sample is cooled down during sonication employing an ice bath. Carbon nanotubes are cut during the sonication treatment and their length decreases down to an average length of about 500nm [2,3].

2) Methods

The present route consists in building networks of carbon based fillers in between emulsion droplets of cross-linked PDMS polymer. Direct emulsions are made of oil droplets dispersed in an aqueous phase. As liquid drops are deformable, they can pack efficiently with a very small amount of remaining water continuous phase.

The possibility to use water based dispersions which are well controlled and which can be stabilized with commercial surfactants is a major advantage of this approach. A mixture of PDMS and curing agent (10% in weight with respect to the PDMS phase) is first prepared as the oil phase. Emulsions are prepared by progressively adding the oil phase to an aqueous solution of SDS surfactant under mechanical stirring provided by a mechanical mixer (IKA Eurostar 40 digital). The gap between the paddle and inner wall of the container is about 7.5 mm. The surfactant weight fraction in the water phase is 4 wt%. Oil is added drop wise until

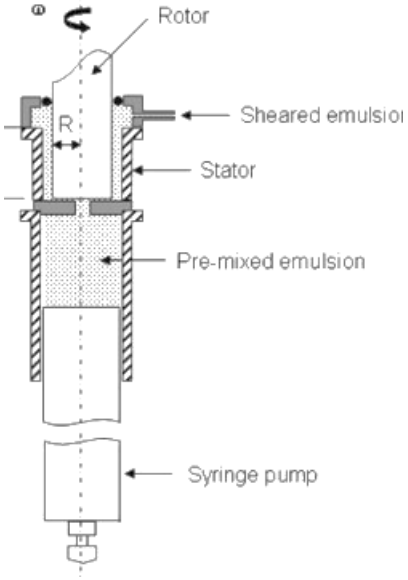

Figure 14: Scheme of the cross section of the Couette injection-shearing system. The premix emulsion contained initially in the syringe is pumped into the thin gap (few 100µm) between the rotor and the stator. The shearing induced the rupturing of the droplet leading to a mono dispersed emulsion.

its weight fraction reaches 85 wt%. Shear can be increased by raising the rotational speed of the mixer in order to form smaller droplets. The size of the obtained droplets is characterized using a Mastersizer Malvern 2000 particle size analyzer. Different mean droplets sizes were achieved by modifying the shear stress applied to the emulsion. The droplet sizes are broadly distributed using the mechanical stirring. They range from 80μm to 15μm. In order to obtain smaller droplets, higher shear stress has to be applied to the emulsions. Smaller emulsion droplets are produced using a Couette emulsification instrument [4,5]. The Couette mixer consists in a rotor stator system that enables the production of small and monodisperse emulsions due to high shear induced droplet rupturing. In this method, a premixed emulsion of large, polydisperse droplets is first introduced into a syringe. The premixed emulsion is prepared manually. It is pushed by a piston into the gap between the rotor and the stator. The sheared monodisperse emulsion is recovered at the top of the mixer (Figure 14.). The mean droplet size depends on the shear rate and on the oil volume fraction. Experimentally, we decided to shear emulsions at a fixed volume fraction (85%wt). Therefore the obtained mean droplet sizes are ranging in between 10 and 3 μm. We produce principally emulsions for which the mean droplet size is about 5μm.

Using different instruments we are able to produce emulsions for which the mean droplets size can vary of about 3 orders of magnitude. Once the desired mean droplet size is obtained, the emulsions are then gently mixed with a carbon based aqueous dispersion of CNTs or GO. In both cases three different mean droplet sizes are studied. In addition, the amount of fillers is varied in order to obtain different filler loadings in the final composites obtained after drying. The emulsions loaded with the carbon based fillers are placed in circular homemade Teflon molds. The diameter of the Teflon molds is Ø 46mm. Solid materials are obtained by evaporating water from the emulsion and by curing the PDMS polymer. The obtained samples are under the form of elastomer disks with a black color. They look perfectly homogeneous on macroscopic scale. The systems made from emulsions loaded with CNT are detailed in Chapter III, while systems made from emulsions loaded with GO are described in Chapter IV.

II. Measurements of electrostrictive materials at rest

1) Methodology

The complex impedance is measured under a voltage of 1V applied in the frequency range of 10-10^6 Hz using a computer-controlled impedance analyzer (Materials Mates 7260). The average thickness of the samples is about 500µm and each sample is removed from its edges using a Ø 40mm circular cutter Figure 15. This step avoid to planarity problems due to the edges during the dielectric measurements. The diameter of the steel electrodes is Ø 38mm. All the experiments are performed at room temperature. A classical calibration procedure, the so called compensation procedure [6] is used in order to determine the impedance of the sample. This procedure allows parasite contributions from the wiring, cables and electrode polarization to be removed from the measured data. Consequently, the electric conductivity and the relative dielectric permittivity can be calculated.

2) Compensation procedure

When the samples are characterized by the impedance analyzer, the measured complex impedance, Z includes the impedance of the sample Z_{sample} but also includes parasitic impedances. Unfortunately, the parasitic impedances are experimentally unavoidable. The parasitic impedances Z_Q include the impedance generated by polarization at the electrodes (generally found at low frequencies) Z_{excess}, and the noise impedance generated by experimental device such as plugging and cables $Z_{Q'}$. Figure 16 shows the equivalent circuit of the experimental device. The parasitic impedances are represented by the equivalent circuit Q. The noise impedance generated by the cables and plugging are represented by the equivalent circuit Q'. The compensation procedure allows to get rid of the parasitic impedances Z_Q and determine the complex impedance Z_{sample}. The complex impedance is defined as:

$$Z = Z_{Re} + jZ_{Im} = V/I \qquad (0)$$

Where Z_{Re} is the real part and Z_{Im} the imaginary part of the impedance, V is the voltage and I, is the electric current.

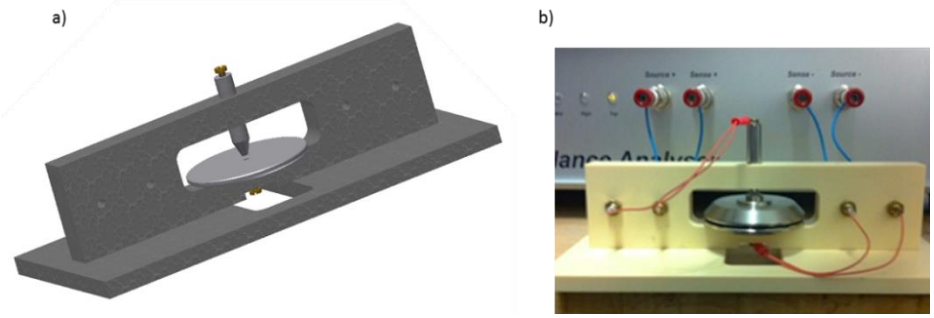

Figure 15: a) Scheme of the home made set-up for the characterization of the dielectric properties without mechanical stress. B) Image of the real set-up plugged into an impedance meter for the characterization of dielectric properties.

Thus the complex impedance of the sample enables the calculation of the electric conductivity (from the real part) and the relative dielectric permittivity (from the imaginary part).

The parasitic impedances Z_Q are located between the input reference plan (Z_i, V_i, I_i) and the electrodes used for the measurement (Z_o, V_o, I_o). The noise impedance $Z_{Q'}$ can be reduced by shortening the length of the cables leading to the electrodes used for measurements. In addition, the impedance produced by polarization at the electrodes Z_{excess} is embraced in the circuit. This consideration is valid since we suppose that the polarization at the electrodes is the same no matter the nature of the sample. In our case we deal exclusively with dried solid materials. We are able to determine the different terms of the equivalent circuit *Q* by solving the matrix *M* (Eq.1) defined as follows:

$$\begin{pmatrix} V_i \\ I_o \end{pmatrix} = \begin{pmatrix} H_{11} & H_{12} \\ H_{21} & H_{22} \end{pmatrix} * \begin{pmatrix} I_i \\ V_o \end{pmatrix} \quad (1)$$

Where, H_{ij} are the terms of the hybrid matrix. V_i and I_i are the input voltage and current. V_o and I_o are output voltage and current.

We note that the power is preserved within the circuit Q, therefore $H_{12}=H_{21}$. The matrix can be written by the following system of equations.

$$V_i = H_{11} * I_i + H_{12} * V_o \quad (2)$$

$$I_o = H_{12} * I_i + H_{22} * V_o \quad (3)$$

If we considered that $V_o = Z_{sample} * I_o$, we can re-write the systems as follows:

$$\frac{V_i}{I_i} = Z_i = H_{11} + \frac{H_{12}^2}{\frac{1}{Z_{sample}} - H_{22}} \quad (4)$$

In order to determine the different element of the hybrid matrix, we carry out three measurements with samples of known properties:

- One ***short circuit*** measurement. In this situation the complex impedance Z_{sample} is null ($Z_{sample} = 0$), enabling the determination of the first element of the matrix $Z_i = V_i/I_i = H_{11}$. To measure the short circuit, we let the two electrodes in contact.

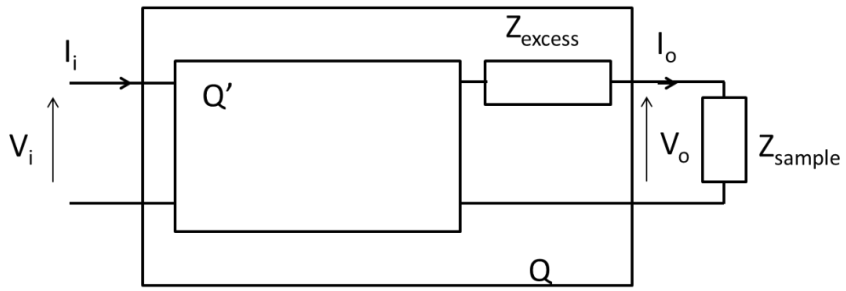

Figure 16: Scheme of the equivalent electric circuit for the experimental impedance device. It is characterized (from left to right) by the reference plane of the impedance analyzer to the measured sample Z_{sample}

- One ***open circuit*** measurement. In this situation the complex impedance Z_{sample} approaches infinity ($Z_{sample} \approx \infty$), therefore $Z_i = (H_{11}\text{-}H_{12}^2)/H_{22}$. To measure the open circuit, we create a large air gap in between the two electrodes.

- One ***reference*** material measurement. In this situation and for accuracy reasons, the chosen sample should preferentially be chemically reminiscent of the samples to be investigated. This ensures a better compensation of the electrode polarization which essentially depends on the chemical composition of the material in contact with the electrode. We therefore decided to use a PDMS neat polymer sample as reference material.

The terms H_{ij} are frequency dependent and hold the entire information concerning the polarization of the electrodes, additional impedances concerning plugging and cables, and the corrections related to the circuit.

The composite materials are modeled as a RC parallel equivalent circuit. Using the terms H_{ij} and the impedance Z_i, we are able to determine Z_{sample}. Therefore the resistance R and the capacitance C values of the sample can be calculated as follows:

$$R = Z_{Re_{sample}} * \left(1 + \left(\frac{Z_{Im_{sample}}}{Z_{Re_{sample}}}\right)^2\right) \tag{5}$$

$$C = -\frac{Z_{Im_{sample}} * \left(1 + \left(\frac{Z_{Im_{sample}}}{Z_{Re_{sample}}}\right)^2\right)}{R^2 + 2\pi f} \tag{6}$$

Where, f is the frequency of the electric field. $Z_{Re_{sample}}$ is the real part, and $Z_{Im_{sample}}$ is the imaginary part of the complex impedance of the sample.

Henceforth, the relative dielectric permittivity ε_r', and the electrical conductivity σ are calculated using the following equations from the known values of R and C.

$$\varepsilon_r' = \frac{C * d}{S * \varepsilon_0} \tag{7}$$

$$\sigma = \frac{1}{\rho} = R * \frac{S}{d} \tag{8}$$

Where ρ is the resistivity, ε_0 is the permittivity of the vacuum, S is the surface and d the thickness of the sample.

III. Measurements of electrostrictive materials under dynamic stress

1) Determination of the electrostrictive coefficient in actuator mode

i. Composite material and preparation of the multilayer stack

The objective is to obtain the electrostrictive coefficient M_{13} of an emulsion based composite by analyzing the bending of a system made of stacked layers in response to an electrical field. These layers are represented in Figure 17. The two outer layers (i.e. layers 2 and 3) act as compliant electrodes. They are made of gold using a coating sputtering technique. Their thickness is of about 100nm. The layer 1 is composed by the emulsion based electrostrictive material. The layer 4 is prepared with a pure dielectric PDMS neat polymer. The layer 1 and 4 are expected to respond differently to the electric field. If individually considered both layers would be compressed in their thickness and expand laterally under an electrical field. But here the two layers are mechanically coupled. One will expand whereas the second one will contract, or at least display a smaller expansion compared to the other layer, resulting in a bending of the whole system. The bending is in fact dictated by the layer that has the greater electrical energy. This dominant layer is the layer 1 because of its much greater permittivity and thickness compared to layer 4.

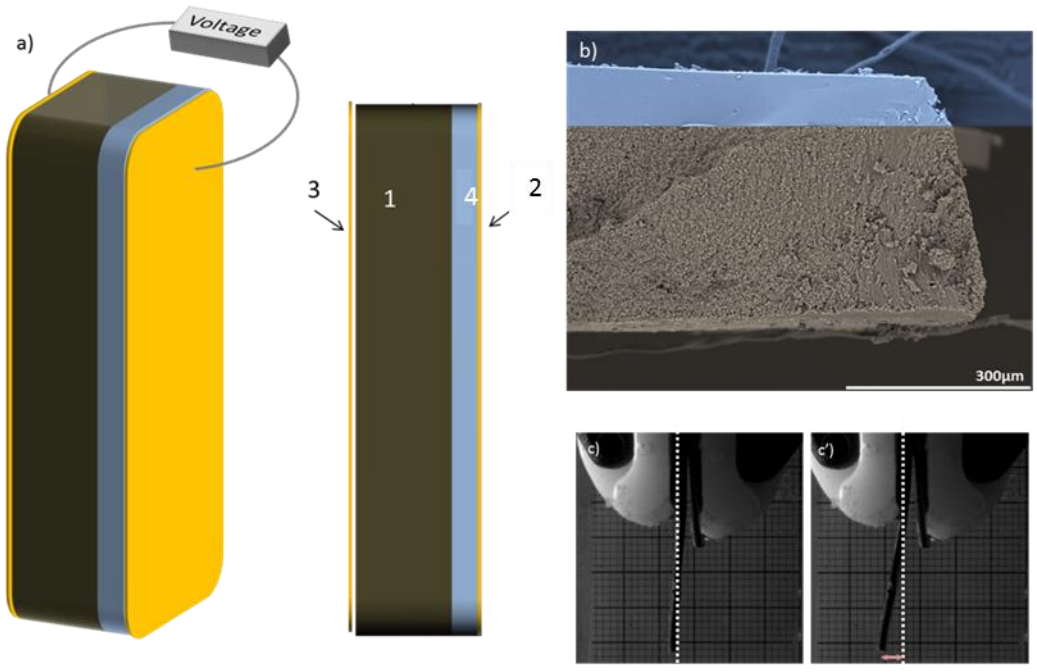

Figure 17: a) Scheme of the actuator set-up for the determination of the electrostrictive coefficientM_{13}. The four-layer material is composed of a nanocomposite layer (1), an inactive dielectric layer of PDMS(4) and two conductive layers of gold used as electrodes (2 and 3). b) SEM image of the cross section of the of the bilayer material. Blue represents the inactive layer while grey the nanocomposite one. c) and c') images of the multilayer system holed by copper electrodes hidden within tweezers when the electric field E=0 and E= 0.5 MV/m respectively

We note that the PDMS base and curing agent ratio for layer 4 is modified to a 7:1 ratio. The ratio used for the electrostrictive material is 10:1. The difference of ratio between the two layers enables a better adhesion of the two inner layers of the stack and prevents possible delamination problems upon bending.

A mechanics model is used to calculate the electrostrictive coefficient M_{13} from the induced curvature K and the mechanical properties of the four-layer material [8].

ii. The experimental set-up

A set-up that is reminiscent of those commonly used to characterize electrostrictive coefficients M_{13} of polymer films was implemented. It is shown in Figure 18. The strip composite material is subjected to a triangular AC electric field, produced by a TTi-TGA 1230 waveform generator (Figure 18 A) and amplified by a TREK high voltage amplifier model 609E-6 (Figure 18 F). We use plastic tweezers (Figure 18 C) to hold the sample and the electrodes. A high voltage is applied between the two copper electrodes. The voltage was kept below 1.5V/µm to avoid air and dielectric breakdown. The strip composite material is enlightened by a light emitting diode, LED, (Figure 18 B) to ensure a reliable video recording. The bending of the strip composite material induces by the electric field is monitored by a PHANTOM high speed camera MR110 (Figure 18 D). The influence of the frequency was evaluated in the range of 0.5Hz -10Hz under electrical fields ranging from 0 to 1.5V/µm.

iii. The bending strip mechanism and the M_{13} calculation

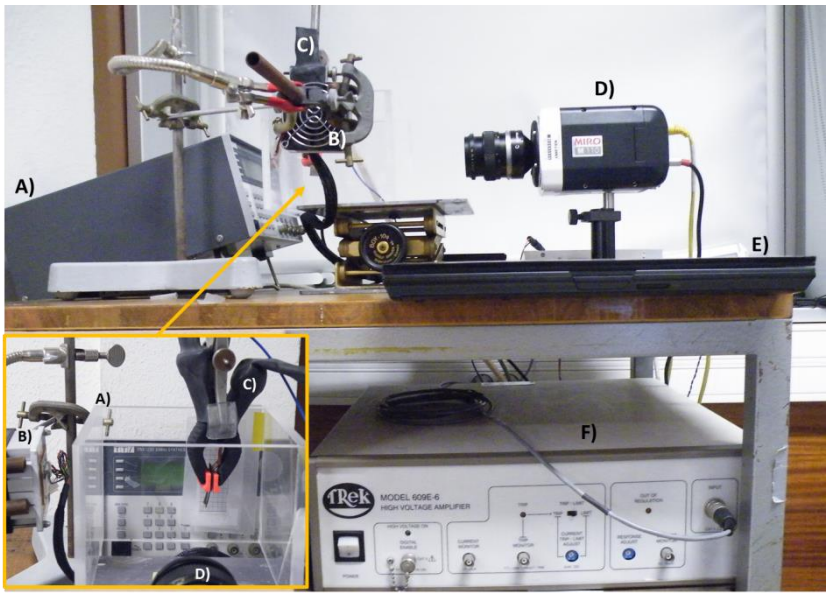

Figure 18: Picture of the set-up for the bilayer composite actuator system. It is composed by a generator A) of voltage which is increase by an amplifier F). The voltage is delivered though copper electrodes hidden within tweezers C) which hold the sample. The deflection of the material is recorded by a camera D), a lamp B) and computer E).

The strain induced by the electric field is the result of two mechanisms: the Maxwell stress and the true electrostriction. The first one is due to the interaction between free charges on the electrodes while the second one is due to the interaction between dipoles induced inside the material. The combination of both is sometimes called "effective electrostriction". But the separation of their distinctive contribution is therefore not straightforward because they both depend on E^2, with E the electrical field. Nevertheless, in a number of cases, one mechanism largely dominates over the other.

According to Wongtimnoi *et al* [9], we can assume that the contribution of the Maxwell stress is negligible in materials with high electrostriction coefficients, such as the ones presently investigated. Thus, the measurement of the effective electrostriction can provide a reasonable measurement of the true electrostriction coefficient M_{13}

$$\varepsilon_a = M_{13}E^2 \tag{9}$$

Where ε_a is the induced in plane strain of the electrostrictive layer 1. E is the applied electric field perpendicular to the plane.

The bending mechanism is generalized for layers presenting different thicknesses (h_1, h_2, h_3, h_4) and widths (b_1, b_2, b_3, b_4) with the restriction that $b_2 \geq b_1$ and $b_3 \geq b_1$ so that the applied electric field permeates the full width of the electrostrictive layer 1.

The applied electric field is given by

$$E = \frac{V}{h_1 + h_4} \tag{10}$$

Where V is the voltage applied between the compliant electrodes 2 and 3.

According to Singer [8], the curvature K if a multilayered strip can be written as:

$$K = \frac{1}{r} = \frac{M_a}{Y_2 I_{ce}} \tag{11}$$

Where r is the radius of curvature, M_a is the applied moment, Y_2 is the Young' modulus for layer 2 and I_{ce} is the cross-sectional moment of inertia of the strip made of material 2.

We note that in the neutral zero-field state, the strip is flat and its length is L, as shown in Figure 17. When the voltage V is applied, we consider that the electrostrictive layer 1 is free to slip as it expands to a length $L+\Delta L_a$. Where ΔL_a is defined by $\Delta L_a = L*\varepsilon_a$. As a consequence, of the applied voltage layer 1 is compressed in its width and we stretch layers 2,3 and 4. In its final state, the strip has a length $L+\Delta L_c$ defining the combined longitudinal strain $\Delta L_c = L*\varepsilon_c$.

The layers of the strip material are henceforth attached, resulting on the preservation of the longitudinal forces $F_i = Yi*\varepsilon_i*b_i*h_i$

$$F_1 + F_2 + F_3 + F_4 = 0 \tag{12}$$

The above equation is known as the balance equation are states that the negative force (compression) F_1 is equal to the sum of the resulting forces (extension).We note that the strain for the layer 1 is given by $\Delta L_c = \Delta L_c - \Delta L_a$. Resulting on $\varepsilon_1 = \varepsilon_c - \varepsilon_a$

If we combined Eq 12 taking into accounts the combined and free strain we obtain.

$$\varepsilon_c = \frac{Y_1 b_1 h_1 \varepsilon_a}{G} \tag{13}$$

Where G is a lighter form of the sum defined as $G \equiv \sum_{i=1}^{4} Y_i b_i h_i$

The force of compression in the layer 1 can be written as $F_1 = -\varepsilon_c \sum_{i=2}^{4} Y_i b_i h_i$

In order to deduce M_a, we sum the moments of the forces about the center of layer 1

$$M_a = \frac{\varepsilon_c}{2}[Y_2 b_2 h_2(h_1 + h_2 + 2h_4) + Y_3 b_3 h_3(h_1 + h_3) + Y_4 b_4 h_4(h_1 + h_4)] \tag{14}$$

The cross-sectional moment of inertia I_{ce} of the equivalent strip about the central longitudinal axis is calculated by summing the moments of inertia of the equivalent layers about the longitudinal axis. According to Singer [8] the moment of inertia of equivalent layer 1 about the longitudinal axis is given by

$$I_{ce} = -\frac{Num}{4Y_2 G} + \frac{1}{3Y_2}(A + B + C) + \frac{b_2 h_2}{3}(D) \tag{15}$$

Where:

$$Num = \left(Y_1 b_1 h_1(h_1 + 2h_3) + Y_2 b_2 h_2(2h_1 + h_2 + 2h_3 + 2h_4) + Y_3 b_3 h_3^2 + Y_4 b_4 h_4(2h_1 2h_3 + h_4)\right)^2$$

$A = Y_1 b_1 h_1(h_1^2 + 3h_1 h_3 + 3h_3^2)$, $B = Y_3 b_3 h_3^3$;

$C = Y_4 b_4 h_4(3h_1^2 + 3h_3^2 + h_4^2 + 6h_1 h_3 + 3h_1 h_4 + 3h_3 h_4)$;

$D = Y_2 b_2 h_2(3h_1^2 + h_2^2 + 3h_3^2 + 3h_4^2 + 3h_1 h_2 + 6h_1 h_3 + 6h \quad h_1 + 6h \quad h_3 + 3h \quad (h \quad + h_3))$

Into the curvature formula Eq11, we substitute the combined stress Eq.13, the applied moment Eq.14, and the moment of inertia Eq. 15 and solve for the free strain ε_a of the electrostrictive layer 1,

$$\varepsilon_a = -\frac{K(Num)}{2Y_1 b_1 h_1(Den)} + \frac{2KG}{3Y_1 b_1 h_1(Den)} * A * B * C * D \tag{16}$$

Where:

$Den = Y_2 b_2 h_2(h_1 + h_2 + 2h_4) - Y_3 b_3 h_3(h_1 + h_3) + Y_4 b_4 h_4(h_1 h_4)$;

Finally, the electrostrictive coefficient of the layer1 is obtained as a function of the curvature K and the free strain ε_a

$$M_{13} = \frac{\varepsilon_a (h_1 + h_4)^2}{V^2} \tag{17}$$

2) Direct determination of the electrostrictive coefficient

i. Composite material and its preparation

The following paragraph is devoted to the development of a methodology to determine the electrostrictive coefficient M_{33}. We refer to this set-up as the direct characterization methodology. Here, by contrast to the previous method, we apply a mechanical stress and measured the modification of the dielectric properties of the sample. The composite materials are characterized as obtained after their synthesis. Contrary to the actuator mode methodology no further preparation is needed.

ii. The mechanism and the M_{33} calculation

We remind that the electrostrictive composite materials are modeled by an RC parallel circuit. When the mechanical stress is applied, the material is strained leading to the change of the distance separating the conductive particles. Henceforth the capacitance of the material varies. The mechanical stress is controlled and cycled by a traction machine; inducing mechanical loads and unloads cycles to the material. These cycles provokes an increase and decrease of the capacitance of the electrostrictive material, which can be represented as a variable capacitance. In addition, the traction machine enables the determination of the stress, strain and Young's modulus during the entire experiment. Measurements of the dielectric properties are started at the same time as the mechanical cyclic loadings. Consequently, we can obtain the desired information for the determination of M_{33}.

$$M_{33} = \frac{\Delta\varepsilon_r' \varepsilon_0}{2\tau_3} \qquad (18)$$

Where $\Delta\varepsilon_r'$ is deduced from the study dielectric properties and τ from the analysis of the mechanical properties.

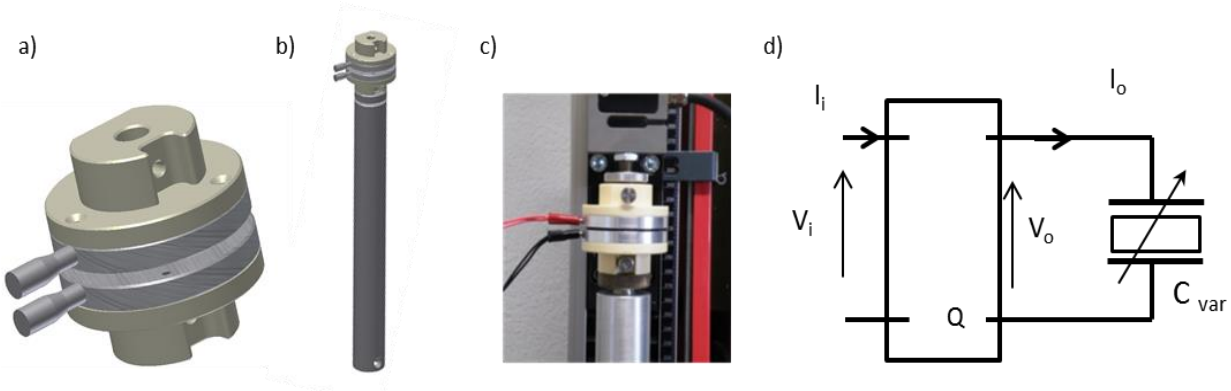

Figure 19: a) Scheme of the electrodes and b) a rigid support that are fixed to the traction machine. c) Picture of the real device once attached to the traction machine. d) Scheme of the equivalent circuit of the experimental device.

iii. The experimental set-up

We use two homemade metal electrodes that enable the study of the dielectric properties and application of the mechanical stress at the same time. The experimental set-up relies on assembling two electrodes into a traction machine (Figure 19 and Figure 20). The home-made aluminum electrodes (Ø 40mm) were equipped with a PVC-insulator adaptor (Figure 19). Its main role is to insulate the measurement performed by the electrode from the rest of the ZWICK 2.5 traction machine. Not forgetting that it ensures a reliable mechanical contact with the force sensor and the steel base of the traction machine (Figure 19). The electrodes are connected to a Materials Mates 7260 impedance analyzer enabling the characterization of the dielectric properties under a mechanical stress imposed by traction machine. We note that the electrostrictive material under mechanical stress acts as a variable capacitor. The dielectric properties at rest are studied keeping the same parameters (section 1 above). The dielectric properties under dynamic stress are studied at a constant frequency (f=100Hz), at 1V and following the typical compensation procedure. An electrical contact is found when the force sensor detects a non-null positive force. For all the characterized samples we apply a pre-strain force of about 0.5N. We note that the pre-strain is to ensure a good contact between the electrodes and the sample. We define a mechanical cycle as the mechanical step for which the strain goes from 0% to 8% and back to 0% strain. This cycle is repeated successively 20 times and studied. The measurements were carried out at room temperature of about 20°C.

We focused on the impact of the filler concentration on the electrostrictive coefficient M_{33}. Moreover, we study the influence of the mechanical frequency on M_{33}. Herein the mechanical frequency is defined by the speed at which the mechanical strain is applied. We evaluate two different strain rates, 0.5 and 0.05 mm/min.

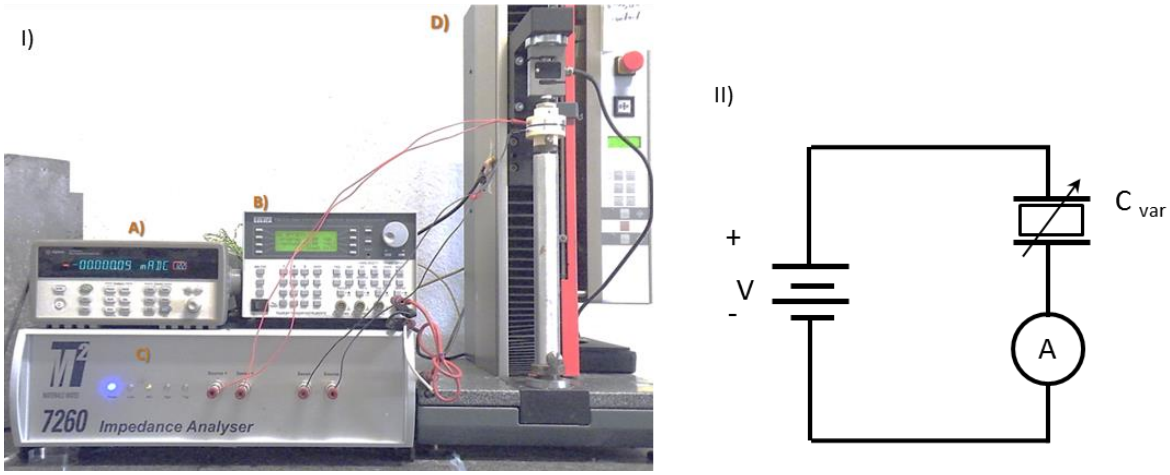

Figure 20: I) Picture of the current and electrostriction characterization techniques using a electrostricitve material as a variable capacitor. The electrostrictive properties are determine by an impedancemeter C) when mechanical stress is apply to the sample by a traction machine D).The current generated under mechanical stress is measured by an amperemeter A). The bias electric field E is provided by a voltage generator B). II) Scheme of the equivalent circuit of the experimental device to study the current generated using an electrostrictive material as a variable capacitor.

IV. The current generated by the electrostrictive material

Thanks to the development of the above mentioned experimental device, we are able to study several electromechanical properties. We measure in particular variations of electrical current generated by an electrostrictive material under a bias voltage and during a periodic mechanical loading and unloading. Inspired by Lallart *et al* [10], we modified the experimental device developed for the study of the electrostrictive properties. We used an experimental device, in which an amperemeter is connected in series to the variable capacitor made by the electrostricitve material. Figure 20 shows the experimental device and the equivalent electronic circuit. A DC electric bias field of about 1V using a TTi-TGA 1230 waveform generator (Figure 20B) is used to polarize the capacitor. This electric field applied and the mechanical stress are applied to the sample placed in between the two home-made electrodes assembled in the ZWICK 2.5 traction machine (Figure 20D). The current is measured by a 34790 Agilent amperemeter (Figure 20A) and recorded in a laptop computer using the Labview software.

This method allows estimates of the electrical power generated from the variable capacitor [10]. It is therefore a valuable tool to evaluate the potential interest of the investigated materials for future energy harvesters. Nevertheless, it is important to note that such methodology cannot be applied to actually make an energy harvesting device because of the need of a high bias voltage.

V. Measurements of the power generated by electrostrictive materials under dynamic stress

1) The mechanism and the power calculation

The previous characterization techniques and devices enable the study of the electrical current and the dielectric properties of electrostrictive materials under dynamic mechanical stresses. Unfortunately, the latter techniques are limited by the frequency of the mechanical stress imposed by the traction machine. We recall that a number of ambient vibrations have frequencies above 1Hz. The aim of the present characterization device is to evaluate the energy delivered by the electrostrictive material in more realistic conditions using an electronic circuit card. This card allows the energy harvesting system to run autonomously using a cycle driven conditioning circuit.

The electrostrictive material is subjected to mechanical frequencies close to the one encountered in real environnemental ambient sources (i.e. 100Hz) by a Dynamic Mechanical Analysis (DMA) machine. The electronic card includes the charge pump [11,13] and the fly-back [12,13] electronic circuits and an interface to measure and control the parameter of the electronic circuit. Figure 21 represents the electronic card used to evaluate the power generated. We note that the variable C_{var} is not embedded in the electronic card. However, the power that it generate can be integrated to the circuit due to an intended input (orange square Figure 21). We remind that the capacitors C_{res} to C_{store} and diodes D_1 to D_2 (red square Figure 21) enable the control of the charges flow through C_{var} [11]. Once initially charged (blue square Figure 21), C_{res} provides charges to C_{var} when it voltage is minimal (D_1 on). Due to the mechanical stress the voltage across C_{var} increases and provides the generated charges due to the change of the capacitance to C_{store} (D_2 on). When the charges are given to C_{store}, therefore the voltage across C_{var} decreases and C_{res} provides again charges to C_{var} (D_1 on). In order to improve the efficiency of the system, the charges accumulated in C_{store} are returned back to C_{res} via the fly-back circuit (purple square Figure 21). After several cycles, the voltage across C_{res} should increase if the electrostrictive material within C_{var} generates energy. In order to evaluate this energy, we follow the voltage across C_{res} and C_{store} thanks to the measurement interface (green square Figure 21).

2) *The experimental set-up*

The following section is devoted to detail the characterization technique enabling the evaluation of electrostrictive materials as variable capacitor C_{var} under mechanical stresses in conditions close to those encountered in ambient environments. Therefore the latter materials are subjected to mechanical compression about few percent of strain at frequencies above 10Hz. These mechanical deformations are provided by a DMA/SDTA861e (Figure 22IA and II). In order evaluate the energy delivered by the electrostrictive materials, we monitor the voltages across C_{res} and C_{store} using an oscilloscope Textronik DP4054B (Figure 22C). The power

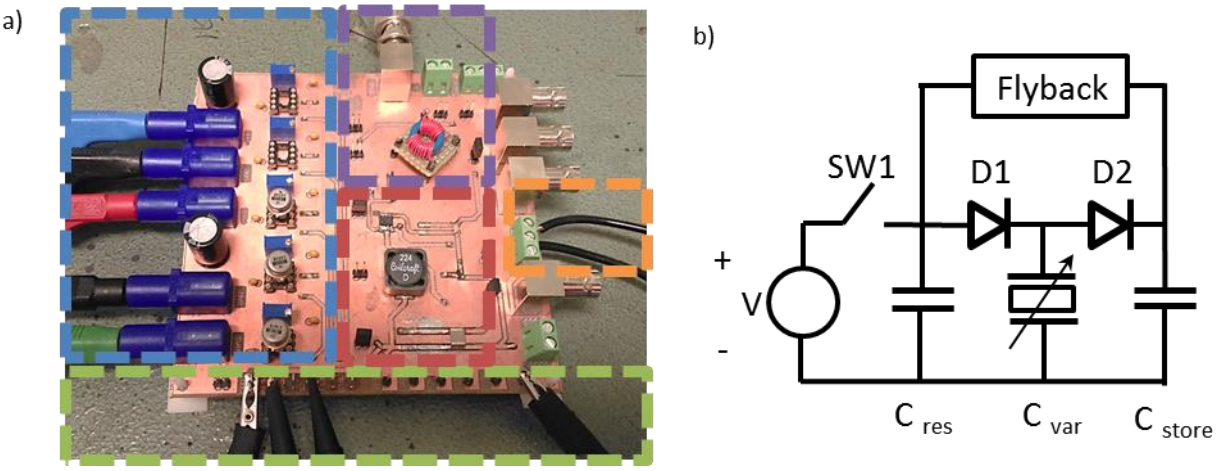

Figure 21 : a) Picture of the electronic card circuit that evaluates the energy generated by a variable capacitor using an electrostrictive material. The blue square is the input for power supply of voltage followers. The green square is the measurement interface. The orange square is the input of the variable capacitance. The purple square is the external control for the fly-back circuit. The red square is composed by the core of the charge pump but C_{var} and fly-back circuits. b) Scheme of the equivalent circuit of electronic card.

supply is a generator Hameg HMP4040 (Figure 22D). The frequency and the pulse of the fly-back return electronic circuit is regulated by a wave generator Agilent 33500B.

We note that the maximal mechanical strain/force applied to the samples are about 5% / 15N depending on the DMA instrument limits. The investigated samples are under the form of thin disks and studied in M_{33} mode. The thickness of a sample is 1mm and its diameter is 20mm. We recall that the sample must be electrically isolated from the DMA machine. Henceforth we manufacture a home-made sample holder that is attached to the mobile part of the DMA (Figure 22II and III). The sample holder is constituted by an aluminum support connected to the DMA, an insulating polyether-ether-ketone (PEEK) polymer and an aluminum electrode on top (Ø= 20mm).

Due to the high Young's modulus of the PEEK polymer, we consider that the entire strain is due to the deformation of the soft PDMS based sample which has a Young's modulus smaller by three orders of magnitude compared to the PEEK.

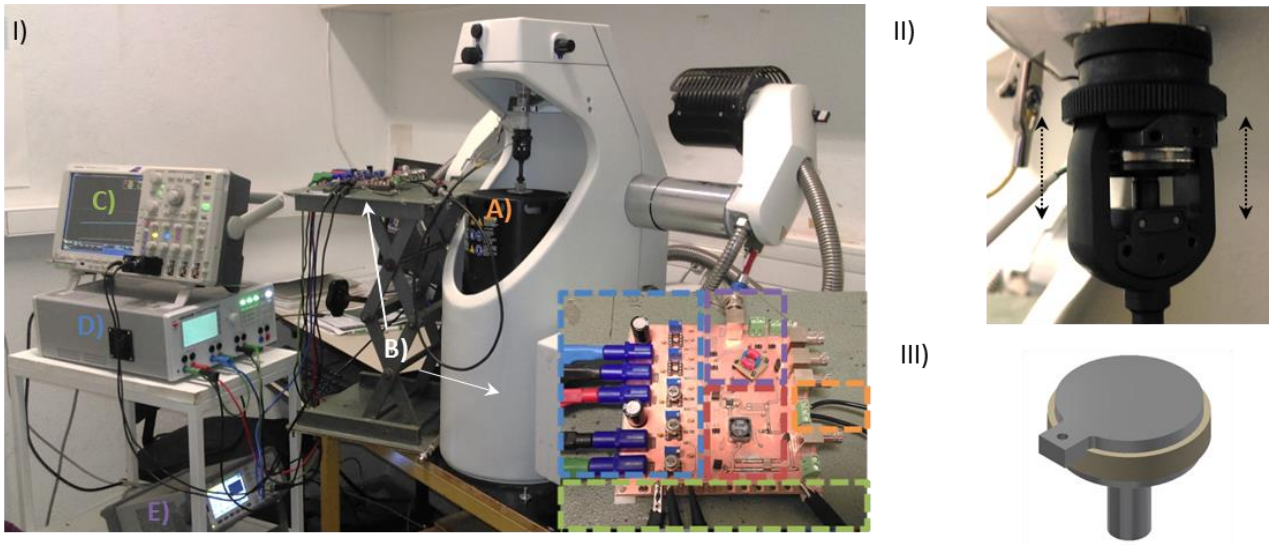

Figure 22: I) Picture of the experimental device to evaluate the energy generated by an electroctrictive material as a variable capacitor using a DMA machine. The color of the squares is correlated to the color of the letters on the picture. It corresponds to the necessary plugging between the machines and the electronic card circuit. II) Picture of the home-made DMA sample holder electrical properties of the variable capacitor under mechanical stress. III) Scheme of the home-made sample holder.

References:

1. *J. Yuan, A. Luna, W. Neri, C.Zakri, T. Schilling, A.Colin & P. Poulin «Graphene liquid crystal retarded percolation for new high-k materials »NATURE COMMUNICATIONS DOI: 10.1038/ncomms9700*

2. *A. Lucas, C. Zakri, M. Maugey, M. Pasquali, P. van der Schoot, P. Poulin Kinetics of Nanotube and Microfiber Scission under Sonication',. J. Phys. Chem. C 2009 113, 20599–20605*

3. *Pagani, G.; Green, M. J.; Poulin, P.; Pasquali, M. 'Competing mechanisms and scaling laws for carbon nanotube scission by ultrasonication', PNAS 2012, 109 (29), 11599-11604.*

4. *T. G. Mason*, † and, et J. Bibette‡. « Shear Rupturing of Droplets in Complex Fluids ». Research-article, 20 août 1997.*

5. *C. Mabille, * V. Schmitt, Ph. Gorria, F. Leal Calderon, V. Faye, and B. Deminière, et J. Bibette. « Rheological and Shearing Conditions for the Preparation of Monodisperse Emulsions ». Research-article, 27 novembre 1999.*

6. *Alibert I. Coulon C. Dielectric study of the dilute part of a SDS/brine/alcohol system: A new sequence of phases?, Europhys. Lett.,1997, 39 (5) 563-568*

7. *Park Cheol, Kang Jin Ho, Harrison, Joycelyn S. Costen Robert C. ,and Lowther Sharon E. «Actuating Single Wall Carbon Nanotube–Polymer Composites: Intrinsic Unimorphs» Adv. Mater. 2008, 20, 2074–2079*

8. *Singer, Ferdinand L. «Strength of Materials», Harper &Brso. , 1951, 469*

9. *Wongtimnoi, K., B. Guiffard, A. Bogner-Van de Moortèle, L. Seveyrat, C. Gauthier, and J. -Y. Cavaillé. « Improvement of electrostrictive properties of a polyether-based polyurethane elastomer filled with conductive carbon black ». Composites Science and Technology 71, n° 6, 885-92.*

10. *Lallart, Mickaël, Pierre-Jean Cottinet, Laurent Lebrun, Benoît Guiffard, et Daniel Guyomar. « Evaluation of energy harvesting performance of electrostrictive polymer and carbon-filled terpolymer composites ». Journal of Applied Physics 108, 3,2010*

11. *S. Roundy, P. K. Wright, and J. Rabaey, "A study of low level vibrations as a power source for wireless sensor nodes," Computer Communications, vol. 26, no. 11, pp. 1131–1144, Jul. 2003.*

12. *B. C. Yen and J. H. Lang, "A Variable-Capacitance Vibration-to-Electric Energy Harvester," IEEE Transaction on Circuits and Systems–I: Regular papers IEEE, vol. 53, no. 2, pp. 288–295, 2006.*

13. *A. Dudka , P. Basset , F. Cottone , E. Blokhina , D. Galayko"Wideband Electrostatic Vibration Energy Harvester (e-VEH) Having a Low Start-Up Voltage Employing a High-Voltage Integrated Interface" Journal of Physics: Conference Series, Volume 476, conference 1*

-We developed a new route to synthesize electroactive nanocomposites via the curing of a direct emulsion loaded with carbon based nanoparticles. This method allows the characteristic size of the conductive domains to be tuned and controlled.

-We developed a characterization methodology for the measurement of the electrostrictive coefficients. Such methodology is more direct than frequently reported analyses using actuators.

- We developed a second characterization technique which enables the measurement of the power generated by the above mentioned nanocomposites in conditions close to those met in ambient environment. This method provides an evaluation of the potential of the investigated materials for future energy harvesting applications.

Chapter III

Giant permittivity carbon nanotube–polymer nanocomposites obtained by curing a direct emulsion (O/W).

I. Introduction

High dielectric permittivity materials are key components in a number of electrical and electronic applications [1-5]. Those include energy storage devices, active vibration control systems, energy conversion technologies, capacitive sensors and actuators. There is currently a fast growing interest in polymer based high permittivity materials because of their flexibility, low cost, easily tunable properties and versatile processing [5]. Polymers nanocomposites made of conducting particles embedded in an insulating polymer matrix are among the most promising systems. They indeed exhibit a large increase of dielectric permittivity in the vicinity of their percolation threshold [5-7]. The increase of permittivity is physically explained by the formation of large conducting clusters, which are separated by small distances in near percolated networks. This effect creates locally large capacitors, which contribute to the increase of permittivity of the material [7]. Perfect and infinite samples are expected to exhibit a divergence of permittivity at percolation. In practice, finite size effects and resistive contacts between the conducting particles make the achievement of high permittivity materials still challenging. In addition, the polymer composite technology suffers from a weakness due to the substantial increase of losses near and above percolation. These losses arise from dielectric losses related to the motion of bound charges of the dielectric medium and from the intrinsic conductivity brought by the free charges of the conducting particles. The main challenge in the field consists in finding compromises that allow high permittivity and low losses in frequency ranges of interest. Such compromises are expected to be found by developing a fine degree of the structuration of the nanoparticles within the polymer matrix. Progresses towards this goal have been achieved in the recent years. Several examples of composites made of metal or carbon nanoparticles in polymers have been shown to exhibit very high permittivity at low frequency [5, 8-13]. In addition some of them exhibit relatively low losses. Carbon nanotubes (CNTs) based nanocomposites are particularly promising. Because of the CNT large aspect ratio these composites exhibit a low percolation threshold [14-17]. This is the opportunity to achieve large permittivities with a low fraction of conductive inclusions. Nevertheless, the dispersion of nanotubes in polymer matrices is not straightforward, and controlling the structure of the aggregates they form remains a difficult task. Examples of fine CNT dispersions were achieved by in situ polymerization of monomers in the presence of CNTs [13], by mixing polymer beads and CNTs [14, 15], by melt processing of polymers and CNTs [10] or by solution casting where the polymer matrix and CNTs are dispersed in a common solvent followed by evaporation [9]. For comparing materials properties, we consider the so-called relative dielectric constant ε_r' which is the real part of the permittivity divided by the vacuum permittivity $\frac{\varepsilon'}{\varepsilon_0}$, and the net conductivity σ which includes the contribution of the imaginary part of permittivity $\omega\varepsilon''$ and the conductivity provided by free charge σf: $\sigma = \omega\varepsilon'' + \sigma f$. Note that losses in the literature are either characterized by the value of the net conductivity or by the so-called loss tangent defined as $\tan\delta = \frac{\sigma}{\omega\varepsilon'}$. Properties obtained in the above contributions are summarized in Figure 23. The data include the properties of functionalized multi-walled carbon nanotube (MWCNT/poly(vinylidene fluoride) (PVDF)

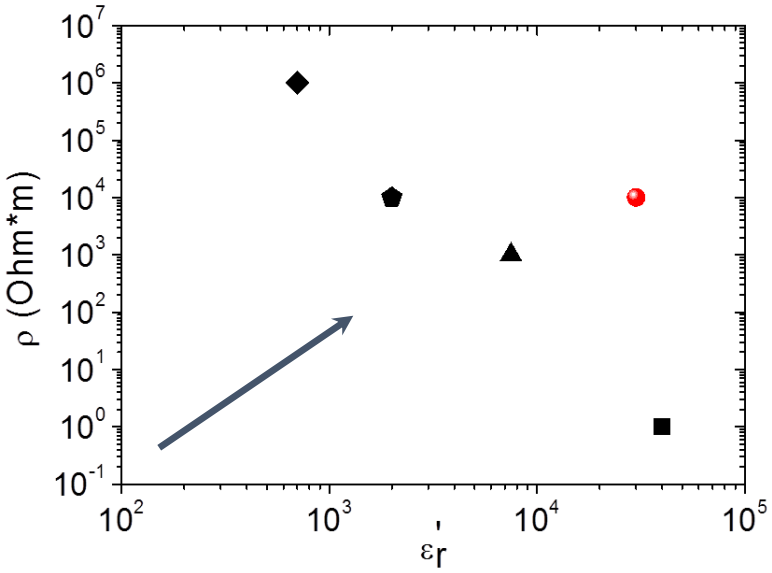

Figure 23: Comparison of properties of binary CNT polymer composites. The blue arrow indicates the direction towards high permittivity and low losses materials as required in applications. The black symbols represent data extracted among the best results of the literature: black diamond [19], black pentagon [20], black triangle [9], black square [18]. The red point represents the properties of the presently achieved materials. All the data are given for the same frequency of 100Hz

composites made by solvent casting [9] or melt mixing [19, 20]. They also include data for MWCNT-polystyrene (PS) composites [18]. Bulk polymerization of styrene monomer in presence of MWCNTs and polystyrene (PS) beads led to very low percolation threshold, of only 0.08 wt% [18]. The length of the nanotubes was greater than the diameter of the beads, but the latter still affected the structuration of the composite by providing an excluded volume for the CNTs; explaining thereby a low percolation threshold

These recent results clearly demonstrate the potential of CNT-polymer composites to achieve high permittivity materials. But a greater degree of control of the structuration of the conductive inclusions is still needed to achieve improvements of properties. We show in this work that the fabrication of composites using an emulsion approach provides such a control and yields unprecedented performances. The emulsion droplets are greater than the length of the carbon nanotubes. As a consequence the CNTs remain literally segregated in between the emulsion droplets. The polymer is cross-linked after the composite has been molded and dried in order to end up with a solid state nanocomposite. Varying the size of the emulsion droplets allows the tuning of the average separation between conducting clusters. The drying and curing conditions as well as the droplet size are factors that enable large variations of properties for exactly the same chemical composition. Optimized materials exhibit a relative dielectric permittivity of 2.5×10^4 along with an electrical resistivity of only 10^4 Ωm at 100Hz (Figure 23). Description and discussion of the present results are provided in the followings. The first section of the article is devoted to the preparation and the characterization of the samples. In the second section, we discuss the influence of the drying-curing conditions. The last section presents the effect of the emulsion droplet size on the electrical properties.

Optimization of the dielectric properties for high permittivity and low losses materials are discussed.

II. Materials and Methods:

I. Materials

Thin multiwall CNTs (MWCNTs) were purchased from Nanocyl under the reference Nanocyl 7000 and used as received. The average diameter of the nanotubes is about 10 nm and the average length is about 1.5 microns. The dispersions of CNTs were carried out in a 10mL flat-bottom flask by respectively mixing 0.9 wt% and 1.2 wt% of CNT and sodium dodecyl sulphate (SDS) purchased from Sigma. Tip sonication using a Branson Sonifier 450A is performed during 1h at 135 Watts to unbundle and homogeneously disperse the CNTs. The sample is cooled down during sonication employing an ice bath. Carbon nanotubes are cut during the sonication treatment and their length decreases down to an average length of about 500nm.[21,22].

The latex, DS910, was purchased from Momentive and used as received. The particles consist of acrylic ester and styrene butadiene copolymer beads and have an average diameter of 180 nanometers and a polydispersity of 19.9%.

The polydymethyl-siloxane (PDMS), Sylgard 184, was purchased from Dow Corning as a kit of PDMS base and curing agent. It has a relative dielectric permittivity of about 2.7 independent of frequency in the range of the present study from 10 to 10^6 Hz.

II. Methods

i. Preparation of the samples

The present route consists in building CNT networks in between emulsion droplets of cross-linked PDMS polymer. Direct emulsions are made of oil droplets dispersed in an aqueous phase. As liquid drops are deformable, they can pack efficiently with a very small amount of remaining water continuous phase.

The possibility to use water based dispersions which are well controlled and which can be stabilized with the commercial surfactants is a major advantage of this approach. The direct dispersion of CNTs in PDMS would be more difficult. In addition, and as explained latter, the use of emulsion droplets greater than the CNT length allows the structure of near percolated networks to be controlled. A mixture of PDMS and curing agent (10% in weight with respect to the PDMS phase) is first prepared as the oil phase (Figure 24a). Emulsions are prepared by progressively adding the oil phase to an aqueous solution of SDS surfactant under mechanical

stirring provided by a mechanical mixer (IKA Eurostar 40 digital). The gap between the paddle and inner wall of the container is about 7.5mm. The surfactant weight fraction in the water phase is 4 wt% (Figure 24b). Oil is added drop wise until its weight fraction reaches 85 wt% (Figure 24c). Shear can be increased by raising the rotational speed of the mixer in order to form smaller droplets. The size of the obtained droplets is characterized using a Mastersizer Malvern 2000 particle size analyser. Medium and large droplets sizes were respectively achieved by shearing the emulsion at rotational speeds of 300rpm and 125rpm. An average droplet size of 24 microns and a polydispersity of 40.7%, respectively 85 microns and 36.7%, were obtained for the medium, respectively large, droplets. Smaller emulsion droplets are made using stronger shear in a Couette emulsification instrument [23]. A premix made of large droplets (~85 microns) is introduced in the instrument, which consists in a Couette cell with a thin gap of only 100 microns. The rotation speed of the rotor is set at 681rpm. Droplets with a mean size of 6 microns and a polydispersity of 29.6% are thereby obtained. Composites made

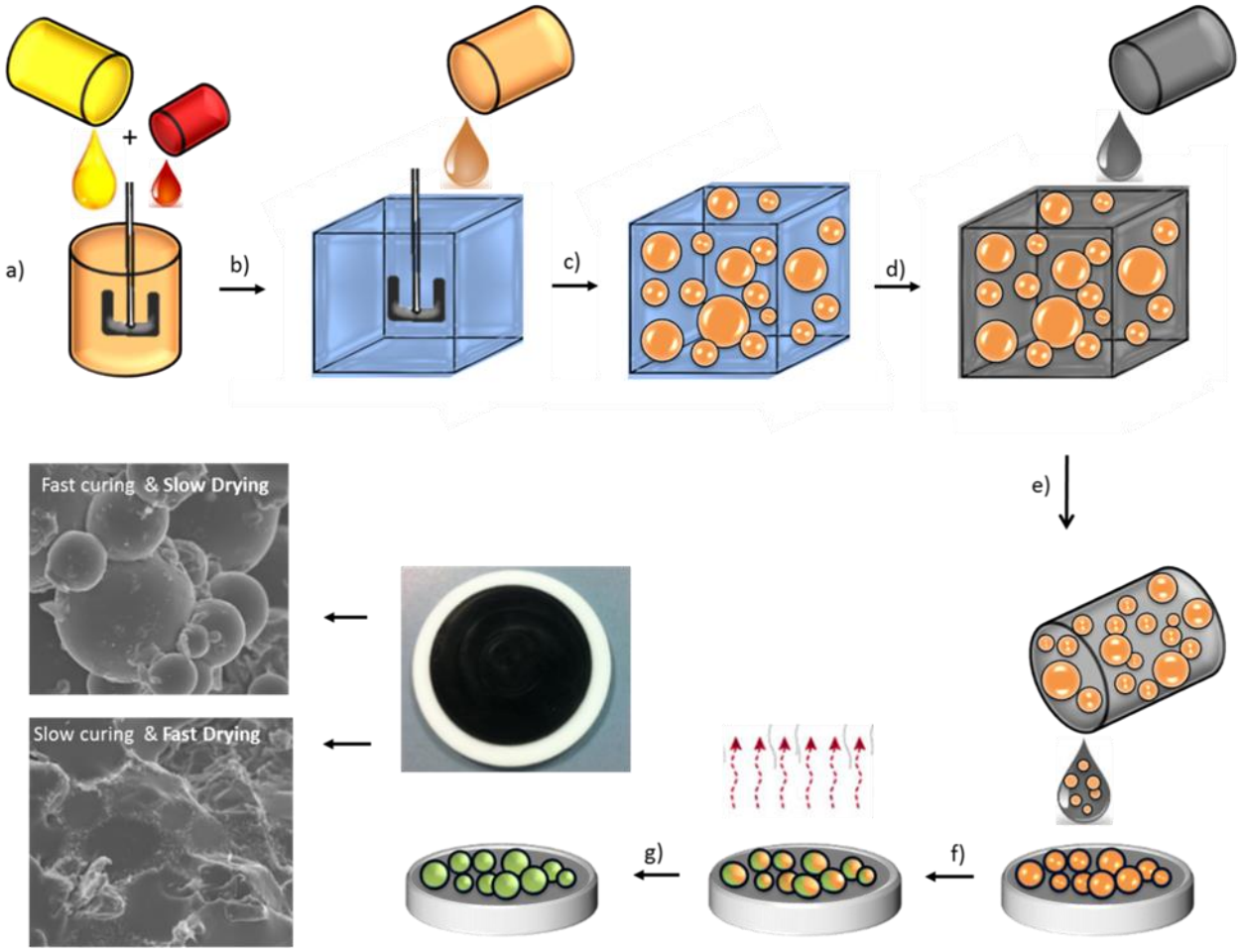

Figure 24: Scheme of the manufacturing process of the emulsion methodology. Curing agent (red) and PDMS (yellow) base are mixed (a) to form an oil phase (orange). The oil phase is then mixed (b) to an aqueous phase (blue) to form an emulsion (c). The CNT dispersion (dark grey) is added to the emulsion (d). The loaded emulsion is molded (e), to get rid of the solvent by evaporation (f). During the solvent evaporation the polymer of the oil droplets start to be cross linked (orange-green) to eventually solidify (green) and form a solid nanocomposite.(g) Scanning electron micrographs of a obtained samples in conditions of fast curing/slow drying and slow curing/ fast drying conditions are shown in the bottom left

from the above emulsions are shown in Figure 25 and display morphology differences due the distinct characteristic size of the parent emulsion droplets. The emulsions or latex suspensions are then gently mixed with an aqueous dispersion of CNTs. The amount of added CNT dispersion is varied in order to obtain different CNT loading in the final composites obtained after drying (Figure 24d). Emulsions loaded with CNTs are placed in circular homemade Teflon molds that have a depth of 0.5 mm and a diameter of 19 mm (Figure 24e). Solid materials are obtained by evaporating water from the emulsion and by curing the PDMS polymer. Drying and curing are critical stages as they take place simultaneously (Figure 24f). The final morphologies depend strongly on the competition between the two mechanisms. As intuitively expected and as shown further, fast curing along with a slow drying leads to spherical drops. Indeed the droplets have ample time to solidify in their original spherical shape before the composite is dried. By contrast, fast drying and slow curing conditions lead to the formation of faceted drops. Because of the slow curing, the droplets have time to highly pack and deform before their solidification (Figure 24g).

In order to determine the role of the composite morphology, two limit procedures are presently used. They are respectively named fast drying or fast curing. In the fast drying conditions, the mold is set in an oven at 30°C for 16h. The hygrometry is controlled by the use of $CaCl_2$ as hygroscopic compound. The average relative humidity is about 30%.In the fast curing conditions, the emulsion is first placed in a closed vial at 60°C for 20 minutes in order

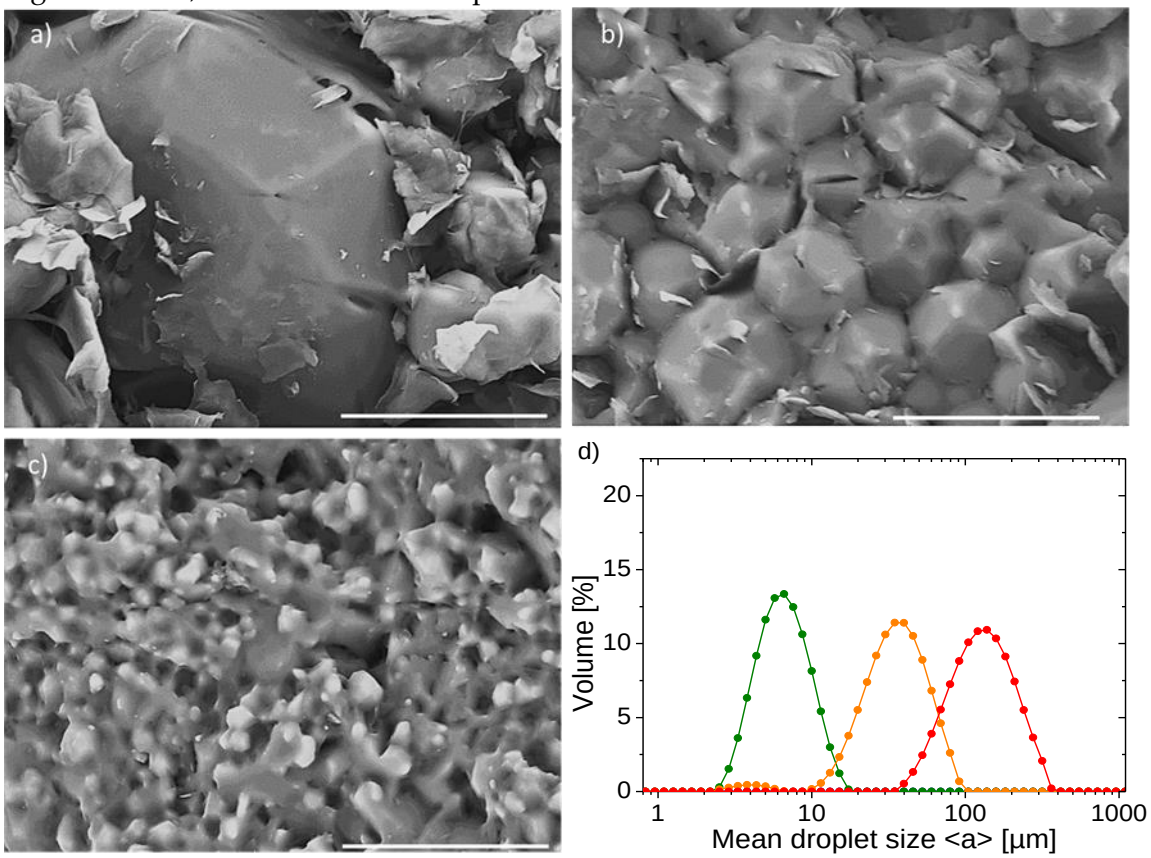

Figure 25: SEM images of nanocomposites for: a) large, b) medium, c) small, droplets formed in the absence of nanotubes in fast drying conditions as defined in the text. Scale 30µm. d) Size distribution of the corresponding emulsion droplets: a is the mean diameter of the emulsion defined as <a>=d43=<d4>/<d3>. The size distribution is log normal and the standard deviation is defined as std=Δd43/d43. Green circles correspond to <a>=6 µm, std=0.30, yellow squares to <a>=24 µm, std=0.41. red triangles to <a>=85 µm, std=0.37

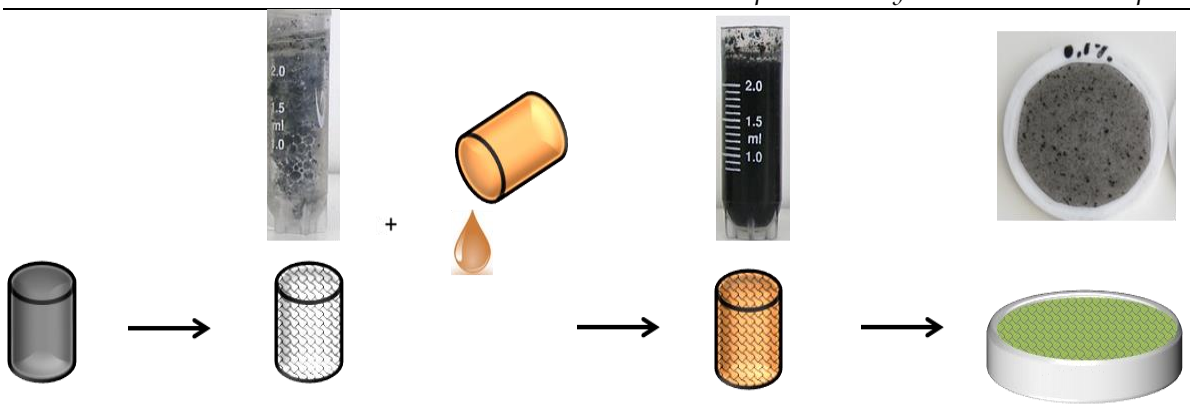

Figure 26: Scheme of the direct manufacturing process of a conventional nanocomposite of PDMS and CNT-SDS coated materials. An aquous dispersion of CNT (black) is freeze-dried to sublimate water. The freeze-dried material (withe hatched) is added to the oil phase (orange). Thematerials are vigorously stirred to form a rough slurry mixture (orange hatched). Finally the slurry is cured to form a solid nanocomposite (green hatched).

to initiate cross-linking without water evaporation. The material is then introduced in an oven at 30°C in the absence of any hygroscopic compounds. The relative humidity in these conditions is about 40%

ii. Preparation of the directly processed reference

In order to highlight the role of the emulsion on the properties of the material, we prepare a reference material using a classical procedure. An aqueous dispersion of CNTs stabilized by SDS is prepared. The aqueous suspension is then freeze-dried to yield a homogenous and light powder of CNT and surfactants. Freeze-dried mixtures can be more easily processed and re-dispersed than classically dried nanotubes [24]. The freeze-dried mixture is then directly mixed with the PDMS base and curing agent under mechanical stirring provided by a mechanical mixer (IKA Eurostar 40 digital). The obtained mixture is placed in a circular homemade Teflon mold that has a depth of 0.5 mm and a diameter of 19 mm. Solid conventional nanocomposite materials are obtained by curing the PDMS polymer (Figure 26)

The following characterization techniques are carried out in order to assess correlation between microstructure and electrical properties of the above described samples. The sample composition is specified by considering the weigh fraction of CNT *i.e.* the mass of CNT divided by the total mass of the sample including PDMS, SDS and CNT.

iii. Characterization of the samples:

***Dielectric measurements*:**

The alternating current (AC) electrical conductivity measurements were performed across the thickness of the molded disc samples of 19 mm in diameter and 0.38 mm in thickness. The sample is loaded between two metallic disc electrodes that have the same diameter than the samples. The electrical conductivity was measured under a voltage of 1000 mV applied in the frequency range of 10-10^6 Hz using a computer-controlled impedance analyzer (Materials Mates 7260). A classical calibration procedure removing the contribution of the polarization of the electrodes [25] is used to determine the dielectric permittivity and the conductivity of the sample as a function of the frequency. All the experiments are performed at room temperature.

***Scanning Electron Microscopy (SEM) analysis*:**

All samples were prepared as follows. Each composite was cut at its edge then quenched in liquid nitrogen to be finally broken apart using pliers. This procedure reveals a clear view of the composite's inner structure. The sample surface is coated with a thin (2 nm) conductive layer of Au/Pt using an Emitech SC7620 Mini Sputter Coater for better resolution of SEM imaging. A low magnification tabletop SEM Microscope Hitachi TM1000 was used to analyze the structure of the emulsion on large scale. The CNT network was visualized using a high resolution Jeol JSM 6700F SEM.

III. Results

1) *Emulsion based composites properties as a function of the drying condition compared to references*

We prepared nanocomposites loaded with 0.3%CNT using the fast drying conditions and two references.

The first reference is a mixture of SDS,CNT, PDMS obtained by direct processing without emulsion templating as described in section ii.

The second reference is a blank emulsion of PDMS with SDS without nanotubes. The size of the droplets is 24 microns (polydispersity of 41%).

The two others samples are composite materials made with emulsion droplets. The initial size of the emulsion droplets is 24 microns (polydispersity of 41%)

The CNTs are barely dispersed in the first reference and the material is not homogeneous. The relative permittivity of the first reference nanocomposite material is about 4.25 and independent of frequency. This value is only slightly higher than that of the neat PDMS (2.7). It reflects the presence of a surfactant and CNTs but the low value results from a lack of structuration within the matrix.

The conductivity is found to be 1.9×10^{-10} S/m at 100Hz as expected for an insulating polymer meaning that the aggregates of nanotubes are not connected.

At 0 wt% concentration, the relative dielectric permittivity is about 6 and independent on the frequency. Again this value is only slightly higher than the neat PDMS (2.7). This is likely due to the presence of remaining SDS in the bulk material.

The conductivity is found to be 1.9×10^{-9} S/m, a value as expected for an insulating polymer. We note that the process conditions or drying of curing do not modify the electrical properties of the reference material (0 wt%).It can be concluded that both reference materials do not display any particularly interesting dielectric properties.

Table 2: Comparison of the dielectric and electrical properties of nanocomposites at 100Hz prepared in fast curing and fast drying procedures as defined in the text

CNT (wt)%	Relative dielectric permittivity ε_r'		Electrical conductivity σ (S/m)	
	Fast curing	Fast drying	Fast curing	Fast drying
0%	6.1	6.0	1.9×10^{-9}	2.0×10^{-9}
0.3% ref 1	4.25	-	1.9×10^{-10}	-
0.3%	4.1×10^{1}	1.1×10^{3}	8.7×10^{-7}	1.8×10^{-4}

Figure 27 displays the structure of the nanocomposites. For the samples prepared using an emulsion , in both procedures, the solidified droplets have roughly the size (24 microns) of the parent liquid droplets of the emulsion materials; meaning that the droplets don't coalesce during the drying and curing stages.However, the inner morphology of the nanocomposites is different depending on the processing conditions.

The nanocomposites prepared using the fast curing conditions present round droplets and the nanotubes are spread in the whole matrix around the droplets. By contrast, fast drying conditions lead to composites that contain facetted droplets. In these structures the nanotubes are literally segregated in the Plateau borders and nodes of the foam-like structure (by analogy with classical foam in which air is here replaced by PDMS) formed by the highly packed emulsion. Modifications of the morphology are expected to result in different electrical properties. This is confirmed by the data shown in Table 2.

An increase by a factor 180, respectively 7, of the relative dielectric permittivity at 100 Hz compared to the reference sample is achieved for the fast drying, respectively fast curing conditions. The AC conductivity measured at 100 Hz is significantly increased by the presence of the carbon nanotubes. But the effect is much more pronounced in the fast drying conditions. The conductivity of materials obtained in fast drying conditions is indeed 200 times greater than the conductivity of materials obtained in fast curing conditions.

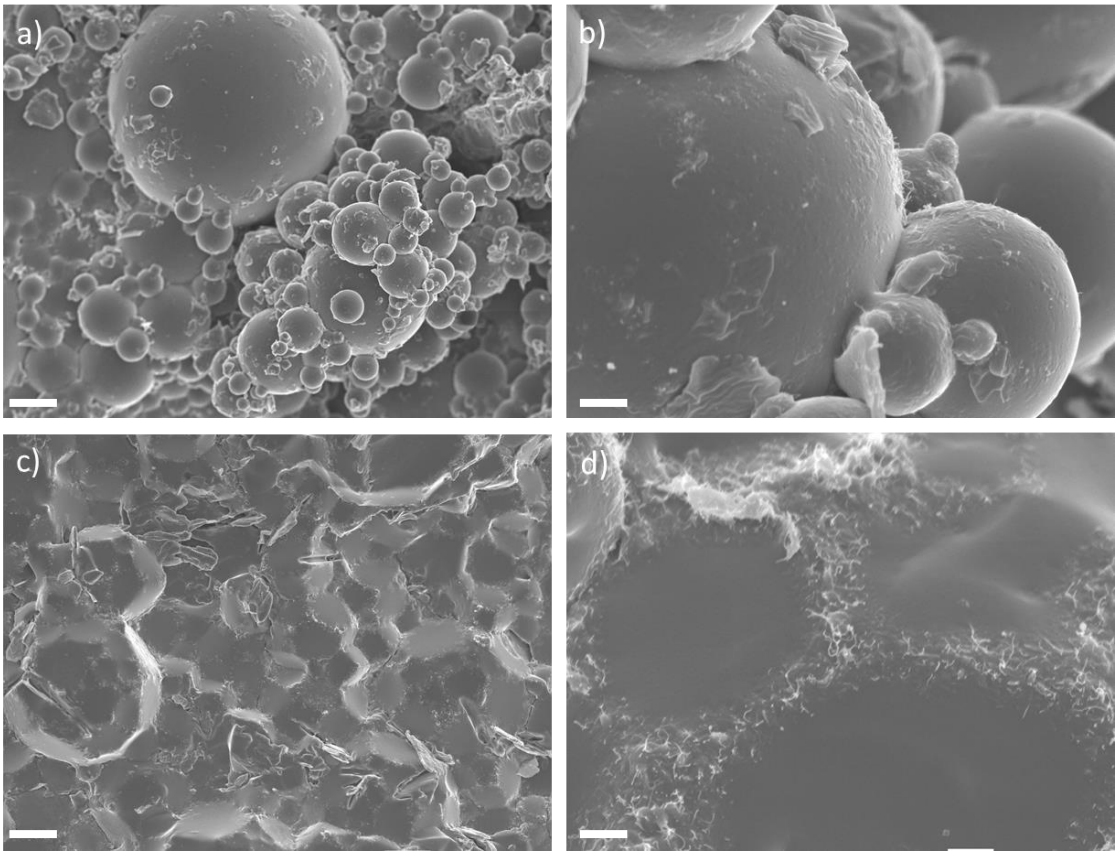

Figure 27: SEM images of the inner structure of PDMS-CNT nanocomposites using an emulsion with droplet of average size <a>= 24 μm (polydispersity of 41%) and manufactured following two procedures: a fast curing condition (a) and b)) and a fast drying conditions (c) and d)) as defined in the text. The carbon nanotube weight fraction is 0.3%.The scale bars represent 10 μm for images a) and c) and 1μm for b) and d).

.

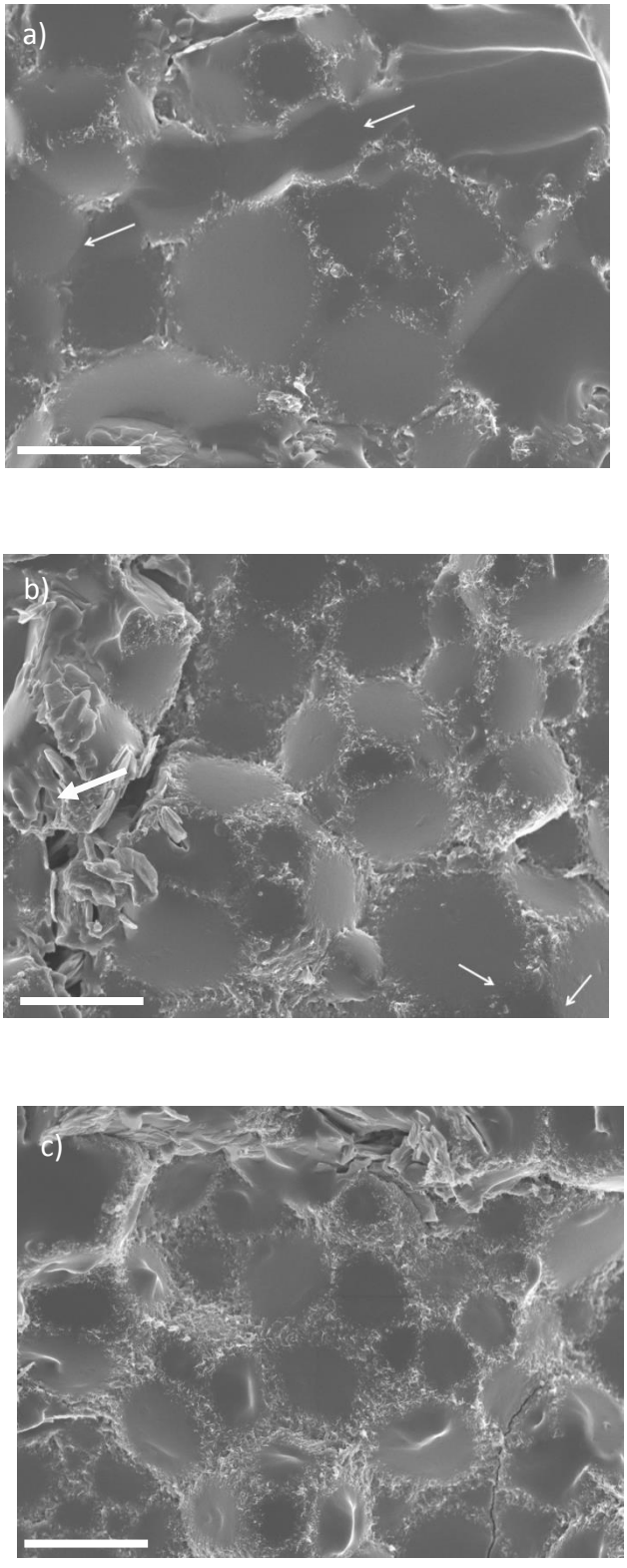

Figure 28: SEM images of the CNT networks for 0,1wt% (a), 0.3wt% (b) a near-percolated and 0,5wt% (c) a fully percolated one (c). The systems at 0.1wt% and 0.3wt% seem to be in a near percolated regime with some CNT aggregates in the Plateau borders and nodes of the foam structure formed by the PDMS droplets. But disconnections and bare zones can be notice as pointed by the white arrows of the images. At 0.5wt% the system seems to be well above percolation with all the aggregates fully connected. All the scales bars represent 10µm

2) *Emulsion based composites properties as a function of the carbon nanotube concentration in the fast drying conditions.*

Considering the above findings, it was decided to focus the investigation of the role of the CNT concentration in fast drying conditions, which are the conditions inducing the best electrical properties. The scanning electron micrographs in Figure 28 show the evolution of the carbon nanotube network as a function of the carbon nanotube fraction. At low concentration the carbon nanotubes are dispersed and scattered. Some aggregates appear in the network with increasing the concentration. They fill the nodes and some of the Plateau borders of the foam structure formed by the droplets. Filling of the network is homogeneous but bare zones are clearly visible for the less concentrated materials. At higher concentration, all the conductive paths are continuous and no bare zones are present. These observations suggest that the less concentrated systems are presumably in a near-percolated regime whereas the material with a concentration of 0.3 wt% is already above percolation. This is actually confirmed by electrical characterizations. Figure 29 shows the dielectric permittivity and the electrical conductivity of the composites as a function of the carbon nanotubes fraction at room temperature for a given frequency *f*=100 Hz and a given droplet size of 24 microns (polydispersity of 41%). The conductivity increases by several orders of magnitude with only 0.1% wt% of CNTs. This means that the material is actually in a near-percolated regime. The percolation threshold is particularly low because of the excluded volume created by the emulsion droplets [18]. The conductivity increases with increasing the CNT fraction from 10^{-6} S/m for 0.1wt% to a value of 2 10^{-3} S/m for a CNT weight fraction of 0.1wt%.The increase is expected to be monotonous, but because of the variability in experiments and sensitivity in

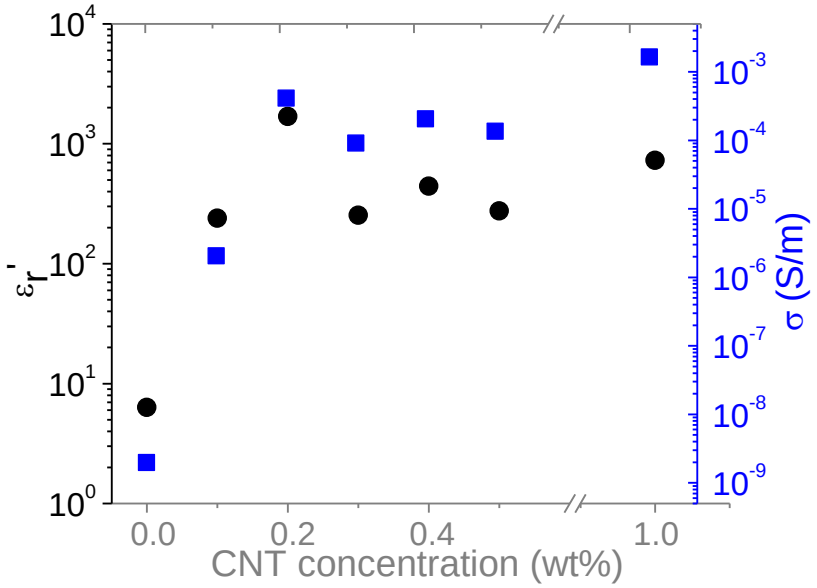

Figure 29: Relative dielectric permittivity ε_r' (black circles) and electrical conductivity (blue squares) as a function of the CNT load of nanocomposites obtained in fast drying conditions. The average droplet size is 24 µm (polydispersity of 41%) and the measurements are performed at 100Hz

near-percolated regimes some point can be slightly above or below the average trend. For example in the shown series of experiments the conductivity of the materials with 0.2wt% is slightly more conductive than the composite at 0.3wt%.

These discrepancies are due to polydispersity in droplet size of the sample, variation of the humidity of the room during the experiments. It is worth noting that such a decrease is not observed in the other samples. The relative dielectric permittivity exceeds 1000 for CNT fractions of 0.2 wt% and remains above a value of 100 for the other carbon nanotube concentrations above this weight fraction.

3) *Assessment of the emulsion based composites properties as a function of the droplet size emulsion*

As shown in the previous section, the emulsion technology proves to be a very efficient approach to reach giant dielectric constants of soft nanocomposites.

In addition, by contrast to conventional dispersion methods, the emulsion method allows tuning the inner structure of the composites by varying the size of the emulsion drops.

In order to do so, we have investigated composites made from three emulsions with mean droplet size of 6 microns and a polydispersity of 30%, 24 microns and a polydispersity of 41%, 85 microns and a polydispersity of 37%.In order to have emulsions with a size smaller than the length of the nanotubes, we complete the study by investigating composites made from latex particles with mean size equal to 180 nanometers and a polydispersity of 20%.

Figure 30 shows that all the nanocomposites display the same qualitative behavior. But significant quantitative differences are observed as a function of the droplet size. The dielectric permittivity for a given frequency and a given carbon nanotube fraction increases with decreasing the smallest droplet size.The obtained values range between 10 and 100, which are about 3 and 2 orders of magnitudes lower than the emulsion approach using 6 microns (polydispersity of 30%) droplet . It reaches a maximum for this emulsion and then decreases as a function of the droplet size. By contrast, the electrical conductivity is found to be nearly independent of the drop size.

In addition the specific surface area in the material increases with decreasing the droplet size. Both effects contribute to providing greater capacitive effects as the size of the droplets is lowered.

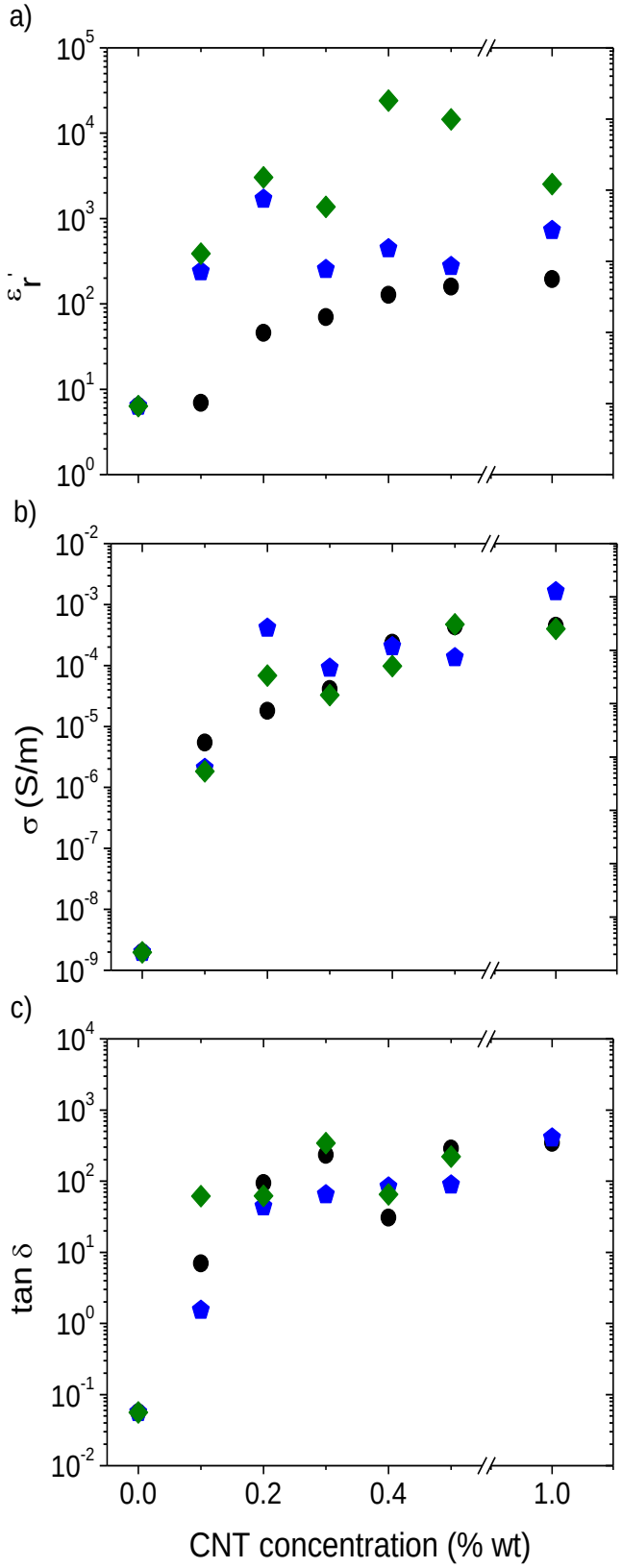

Figure 30: Dielectric properties as a function of the carbon nanotube concentration for various size of the droplets at a constant frequency of 100Hz. Black dots correspond to droplet size equal to 85 µm (polydispersity of 37%), blue pentagons to 24 µm (polydispersity of 41%), and the green diamonds to 6 µm (polydispersity of 30%). a/ dielectric constant, b/ conductivity,c/ dielectric loss defined as tan δ = $\frac{\sigma}{\omega\varepsilon'}$

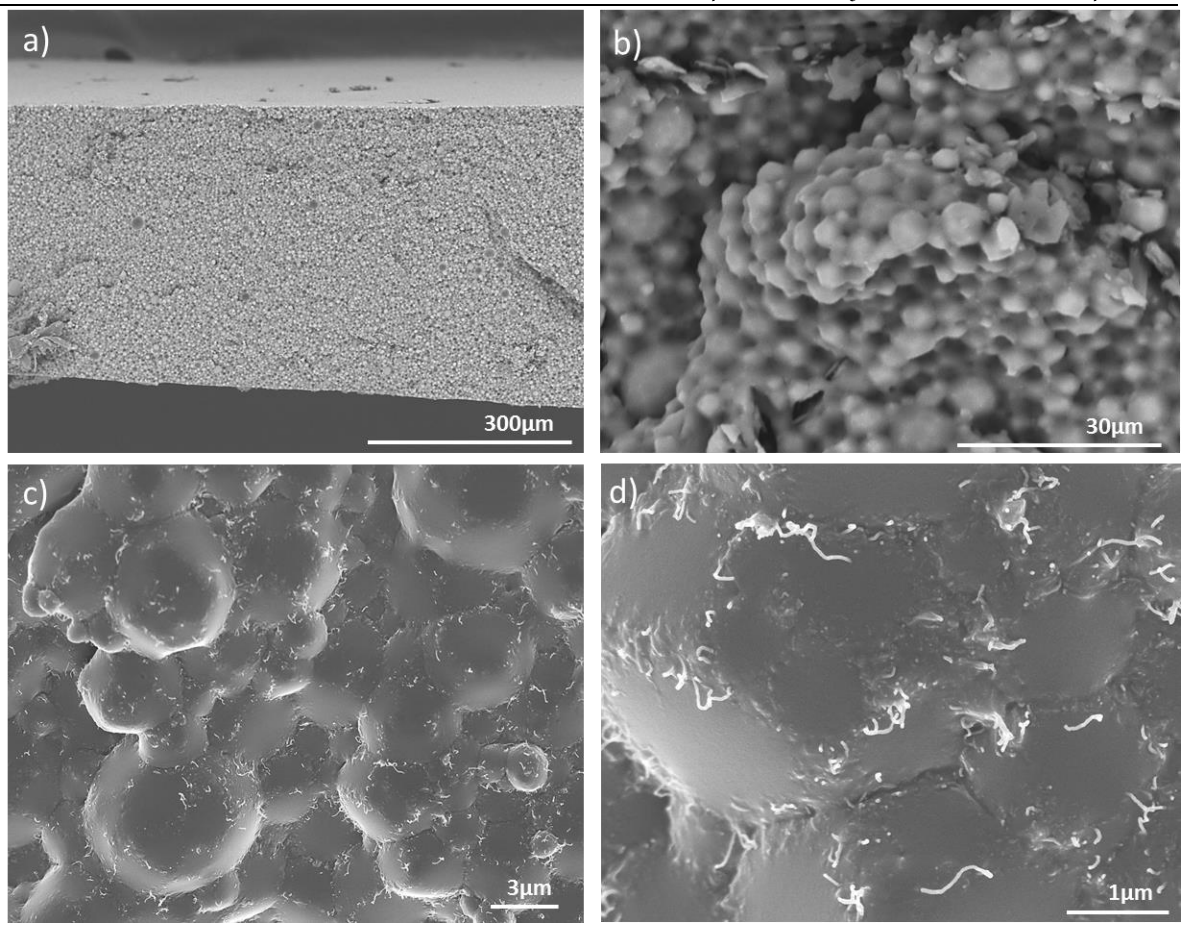

Figure 31: Scanning electron micrographs of PDMS/CNT nanocomposites containing 0.4 wt% of CNTs obtained by emulsion drying at four different magnifications a)X250 b) X2500 c) X5000 and d) X20000. Scale bars in the pictures. The droplets are facetted and the carbon nanotubes located in the Plateau borders of the emulsion

They likely explain the observed trends and the giant dielectric constants achieved in the materials with the small droplets. However, it is important to stress that the above mechanisms are expected to remain valid only when the emulsion act as a template. Particles smaller than the CNTs are not expected to play such a role.

They would be less efficient than large emulsion droplets at providing micro-capacitors and therefore giant permittivities. We couldn't formulate emulsion droplets smaller below the CNT length. Instead we have used latex particles to test the importance of the templating effect. The used latex particles have an average size of 180 nm (polydispersity of 20%).

The relative dielectric permittivity of composites made with the latex particles is considerably smaller than that of emulsion regardless the amount of carbon nanotubes. The obtained values range between 10 and 100, which are about 3 and 2 orders of magnitudes lower than the emulsion approach using 6 microns (polydispersity of 30%) droplet .

4) The optimized formulation: Dielectric response as a function of the frequency

The best properties are presently achieved for an optimum size of 6microns, which is about 10 times the average length of the CNTs. The structure of the nanocomposites made with the 6 microns (polydispersity of 30%) droplets is shown in Figure 32. The properties as a function of frequency *f* are given in Figure 32. The dielectric spectrum displays a broad dispersion in the percolation regime. Actually the dielectric constant is found to scale with frequency as $\varepsilon_r \alpha f^a$, with a critical exponent close to -0.25 (see data at 0.5 wt% for example) as expected from percolation theory [28-31]. The conductivity displays also the typical features of disordered percolating system of conductive particles in an insulating matrix [32]. The low frequency independent contribution of the free charge carriers is increased with the amount of nanotubes. As indicated above, the conductivity remains low because the percolation threshold in the present materials is itself low.

Overall the present materials exhibit a very high dielectric constant along with a low conductivity. They thus appear as ideally suited as high permittivity materials with low losses. The best compromise is achieved for a typical size of emulsion droplets that is about ten times the length of the nanotubes. In this regime and for a concentration of nanotubes of 0.4wt% the relative dielectric permittivity at 100Hz is about 2.5×10^4. This giant permittivity is associated with a conductivity of only 10^{-4} S.m^{-1} (tan δ~0.09). Compared to other materials [9, 18-20] the presently achieved properties clearly make the emulsion technology very promising for applications necessitating materials with high dielectric constants and low losses. In addition the technology leads to soft materials at low cost with an easy and scalable processing. It is therefore potentially useful for implementation of high permittivity nanocomposites in various applications including supercapacitors, MEMS, dielectric and electrostrictive actuators or sensors [1-5].

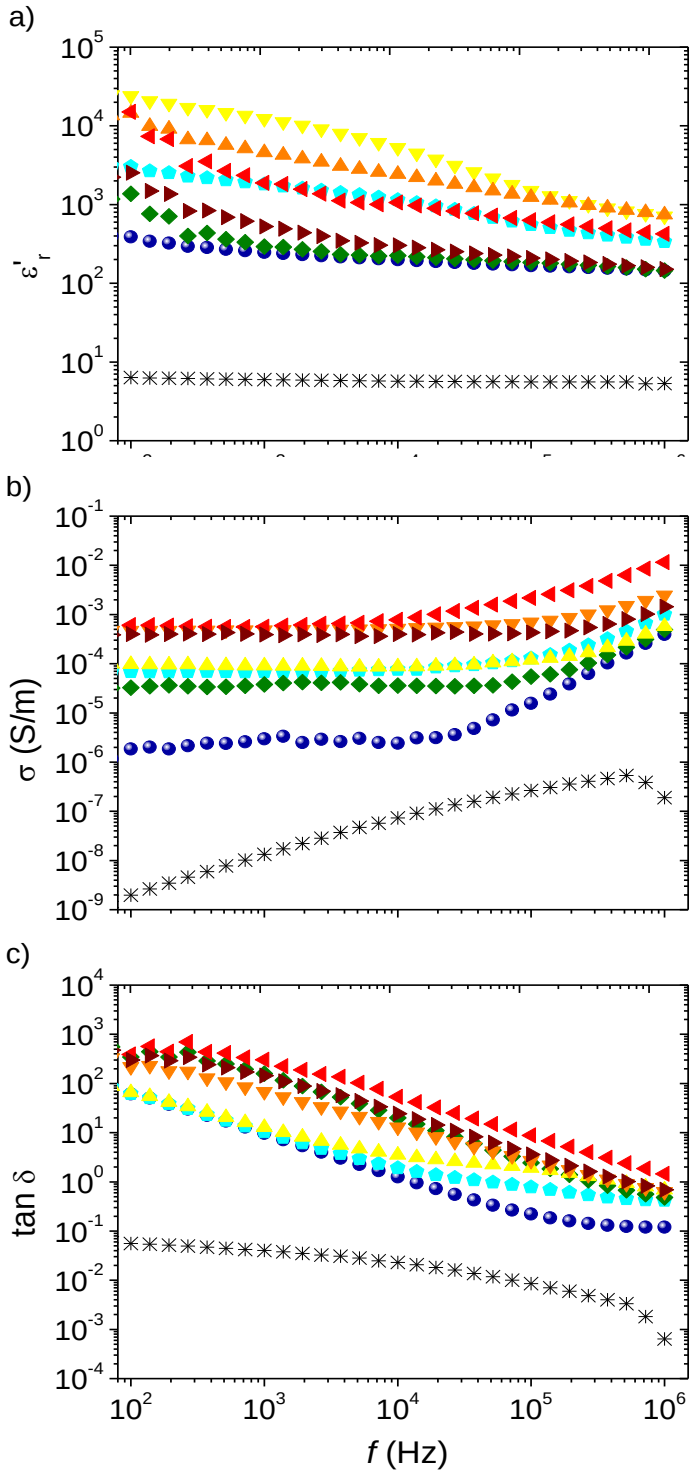

Figure 32: a) Dielectric constant and b) electrical conductivity as a function of the frequency for different CNT content : 0 wt% (cross), 0,1wt% (sphere), 0,2wt% (pentagon), 0,3wt% (diamond), 0,4wt% (down triangle), 0,5 wt% (up triangle),0.75% wt%(left triangle) and 1 wt% (right triangle). The average droplet size of the nanocomposites is 6µm, the standard deviation is 30%. a/ dielectric constant, b/ conductivity,c/ dielectric loss defined as tan $\delta = \frac{\sigma}{\omega\varepsilon'}$.

IV. Discussion

We have studied the preparation of polymer CNT nanocomposite. The use of an emulsion of curable oil and in an aqueous CNT dispersion stabilized by surfactant is a road to get materials with a high dielectric constant and a low conductivity. The reasons of this success are the followings. The main difficulty in preparing a CNT polymer nanocomposite is the dispersion of the CNT in the polymer matrix. As shown by the measurement performed on a directly processed material, CNTs do not disperse easily in the oil. In our procedure, this bottleneck is by passed by dispersing the CNTs in water in presence of surfactant. During the drying and the curing of the material, the CNTs are trapped in the plateau borders of the emulsion that build an interconnected network. This process is more efficient when the emulsion has a low continuous phase fraction. This explains why the drying conditions are of crucial importance. When the curing time is shorter than the drying time, spherical droplets are made. The space between the drops is rather large; the nanotubes cover the droplets but are not forced to build a network. By contrast when the drying time is shorter than the curing time, the CNTs are trapped in an interconnected network between facetted drops. The formation of large conductive aggregates separated by small distances creates large capacitors in the medium [7, 26]. As a consequence,the material displays a giant dielectric constant. An increase of the conductivity is also observed at high frequency due to the building of the large aggregates that are conducting.

Our second set of experiments points out that the electrical features of the network depends upon the nanotube concentration.

The conductivity increases first strongly from 10^{-9} S/m in absence of CNT to $2*10^{-4}$ S/m for a CNT weight fraction of 0.2wt%, then more gently between 0.2wt% to 1wt%. As pointed out by the microscopic observation, these two regimes are due first to the building of an interconnected network and second to an increase of the section of the conductive path. The relative dielectric permittivity exceeds 1000 for CNT fractions of 0.2 wt% and remains above a value of 100 for the greater carbon nanotube concentrations. Such giant dielectric constant arises from the formation of near percolated networks in the PDMS matrix. Indeed, the dielectric constant of composites made of conductive particles in an insulating matrix is expected to diverge at percolation. Shorts of the effective capacitors between the aggregates above percolation yield a decrease of the permittivity at high CNT concentration.

Our third set of experiments suggests that the size of the droplets is an important parameter. The dielectric permittivity is affected by the characteristic size of the aggregates of conductive particles. The experimental observation of permittivity increase with decreasing the droplet size is consistent with this expectation. The carbon nanotubes are located in the Plateau borders and nodes of the template. The conductive aggregates they form are thus separated by a characteristic distance that is equal to the bare zone. This distance is set by the average droplet size. Let us stress, that it is the inhomogeneous filling of the plateau borders network

that induces the formation of bare zones and thus the high permittivity value. The smaller the droplet size, the smaller this distance is, the higher the local capacitance.

Same explanation does not hold for conductivity. The electrical conductivity is found to be nearly independent of the drop size. This last point can be understood by considering that the conductivity is essentially dominated by the free charges brought by the carbon nanotubes and that the topologies of the networks formed by the nanotubes remain similar for different droplet sizes.

As a consequence the conductivity is expected to only depend on the amount of connected nanotubes.

It is important to stress that the above mechanisms are expected to remain valid only when the emulsion act as a template. As indicated above, particles smaller than the CNTs are not expected to play such a role. They would be less efficient than large emulsion droplets at providing micro-capacitors and therefore giant permittivities. This expectation was validates by experiments with latex beads with a diameter id 180nm.

Figure 23 compares one of our best sample (fast drying conditions, CNT concentration close or slightly above the percolation, emulsion size comparable to the length of the nanotubes) with other state of the art dielectric nanocomposites. We obtained unprecedented performances in terms of compromises of permittivity and conductivity. Our method leads to values smaller but closed to the best performance obtained using bulk polymerization of styrene monomer in presence of MWCNTs and polystyrene (PS) beads [18] for the dielectric constant. However our samples have in this situation an ultra-low conductivity which is a high improvement of the material. These electrical features come from two different reasons. First, the nanotubes are trapped in the Plateau borders of the emulsion. Near percolation, they do not build a connected structure. The large aggregates are close and form high capacities. Slightly above percolation the number of connected paths remains small. The size of the section of these paths is also low, explaining thereby a low value of the conductivity. Second, the surfactant, the sodium dodecyl sulphate, may build an isolating layer around the nanotubes limiting the electrical conductivity and improving therefore he potential of the present materials for making high permittivity nanocomposites. We recall that the use of surfactant stabilized emulsion is required to get the presently reported structures.

V. Conclusion

In this work, we proposed a new method to easily prepare carbon nanotube/ polymer nanocomposites using emulsion droplets as templating medium. As the droplets are greater than the carbon nanotubes they force the conducting particles to accumulate in the Plateau borders. This induces a decrease of the percolation threshold and the building of aggregates separated by a controlled distance roughly equal to the size of the drops. For emulsion size one order of magnitude higher than the length of the carbon nanotubes, we measure a giant permittivity larger than 20000 at 100 Hz and an electrical conductivity lower than 10^{-4} S/m corresponding to a tan δ about 100. This constitutes an important improvement in the state to the art dielectric nanocomposites. We have characterized this procedure and analyzed the role of the drying-curing procedure as well as the importance of the emulsion droplet size. We show that fast drying situation and low droplet size correspond to the optimal situation for achieving high performances.

We have proved that the emulsion formulation used as a template medium is an innovative, versatile approach to enhance the dielectric properties of the CNT nanocomposite materials. However, the choice of an organic colloidal dispersion is not limited to the carbon nanotubes. Other carbon based aqueous dispersions such as the graphene oxide (GO) dispersion seem to be a very promising approach. The following chapter is devoted to the replacement of the CNT dispersion by a the GO dispersion

References:

1. *Nalwa, H. Handbook of Low and High Dielectric Constant Materials and Their Applications; Academic Press: London, UK, 1999.*

2. *Osaka, T.; Datta, M. Energy Storage Systems for Electronics; Gordon and Breach: Amsterdam, The Netherlands, 2001.*

3. *Li, J. Y., L. Zhang, and Stephen Ducharme. "Electric energy density of dielectric nanocomposites." Applied physics letters 2007 90.13: 132901.*

4. *Barber, Peter, et al. Polymer composite and nanocomposite dielectric materials for pulse power energy storage. Materials 2009: 2.4 1697-1733.*

5. *Dang, Zhi-Min, et al. Fundamentals, processes and applications of high-permittivity polymer–matrix composites. Progress in Materials Science, 2012, 57.4 660-723.*

6. *Vigolo, B.; Coulon, C.; Maugey, M.; Zakri, C.; Poulin, P., An experimental approach to the percolation of sticky nanotubes. Science 2005, 309 (5736), 920-923.*

7. *Efros, A. L.; Shklovskii, B. I., Critical behavior of conductivity and dielectric constant near metal non-metal transition. Physica Status Solidi B-Basic Research 1976, 76 (2), 475-485.*

8. *Chang, J. F.; Liang, G. Z.; Gu, A. J.; Cai, S. D.; Yuan, L., The production of carbon nanotube/epoxy composites with a very high dielectric constant and low dielectric loss by microwave curing. Carbon 2012, 50 (2), 689-698.*

9. *Dang, Z. M.; Wang, L.; Yin, Y.; Zhang, Q.; Lei, Q. Q., Giant dielectric permittivities in functionalized carbon-nanotube/electroactive-polymer nanocomposites. Advanced Materials 2007, 19 (6), 852.*

10. *Potschke, P.; Dudkin, S. M.; Alig, I., Dielectric spectroscopy on melt processed polycarbonate - multiwalled carbon nanotube composites. Polymer 2003, 44 (17), 5023-5030.*

11. *Yuan, J. K.; Li, W. L.; Yao, S. H.; Lin, Y. Q.; Sylvestre, A.; Bai, J. B., High dielectric permittivity and low percolation threshold in polymer composites based on SiC-carbon nanotubes micro/nano hybrid. Applied Physics Letters 2011, 98 (3).*

12. *Zhang, X. H.; Liang, G. Z.; Chang, J. F.; Gu, A. J.; Yuan, L.; Zhang, W., The origin of the electric and dielectric behavior of expanded graphite-carbon nanotube/cyanate ester composites with very high dielectric constant and low dielectric loss. Carbon 2012, 50 (14), 4995-5007.*

13. *Li, Q.; Xue, Q. Z.; Hao, L. Z.; Gao, X. L.; Zheng, Q. B., Large dielectric constant of the chemically functionalized carbon nanotube/polymer composites. Composites Science and Technology 2008, 68 (10-11), 2290-2296.*

14. *Grossiord N, Loos J, Laake LV, Maugey M, Zakri C, Koning CE, et al. High conductivity polymer nanocomposites obtained by tailoring the characteristics of carbon nanotube fillers. Adv Funct Mater 2008;18 (20):3226–34.*

15. *Grossiord, N.; Kivit, P. J. J.; Loos, J.; Meuldijk, J.; Kyrylyuk, A. V.; van der Schoot, P.; Koning, C. E., On the influence of the processing conditions on the performance of electrically conductive carbon nanotube/polymer nanocomposites. Polymer 2008, 49 (12), 2866-2872.*

16. *Kyrylyuk, A. V.; van der Schoot, P., Continuum percolation of carbon nanotubes in polymeric and colloidal media. Proceedings of the National Academy of Sciences of the United States of America 2008, 105 (24), 8221-8226.*

17. Schilling, T.; Jungblut, S.; Miller, M. A., Depletion-induced percolation in networks of nanorods. Physical Review Letters 2007, 98 (10).

18. Nilesh K. Shrivastava, B.B. Khatua « Development of electrical conductivity with minimum possible percolation threshold in multi-wall carbon nanotube/polystyrene composites »CARBON 49, 2011 4571–4579

19. Chanmal, C.; Deo, M.; Jog, J., Enhanced dielectric permittivity in poly (vinylidene) fluoride/multiwalled carbon nanotubes nanocomposite thin films fabricated by pulsed laser deposition. Applied Surface Science 2011, 258 (3), 1256-1260.

20. Yuan, J. K.; Yao, S. H.; Dang, Z. M.; Sylvestre, A.; Genestoux, M.; Bai, J. B., Giant Dielectric Permittivity Nanocomposites: Realizing True Potential of Pristine Carbon Nanotubes in Polyvinylidene Fluoride Matrix through an Enhanced Interfacial Interaction. Journal of Physical Chemistry C 2011, 115 (13), 5515-5521.

21. A. Lucas, C. Zakri, M. Maugey, M. Pasquali, P. van der Schoot, P. Poulin Kinetics of Nanotube and Microfiber Scission under Sonication',. J. Phys. Chem. C 2009 113, 20599–20605

22. Pagani, G.; Green, M. J.; Poulin, P.; Pasquali, M. 'Competing mechanisms and scaling laws for carbon nanotube scission by ultrasonication', PNAS 2012, 109 (29), 11599-11604.

23. Mason, T. G. and J. Bibette, Shear rupturing of droplets in complex fluids. Langmuir 13,1997, 4600 - 4613

24. Maugey, M.; Neri, W.; Zakri, C.; Derre, A.; Nnicaud, A.; Noe, L.; Chorro, M.; Launois, P.; Monthioux, M.; Poulin, P., Substantial improvement of nanotube processability by freeze-drying. Journal of Nanoscience and Nanotechnology 2007, 7 (8), 2633-2639

25. Alibert I. Coulon C. Dielectric study of the dilute part of a SDS/brine/alcohol system: A new sequence of phases?, Europhys. Lett.,1997, 39 (5) 563-568

26. Pecharroman, C. & Moya, J.S. Experimental evidence of a giant capacitance in insulator-conductor composites at the percolation threshold. Advanced Materials, 2000 12, 294-297

27. Regev, O.,ElKati, P. N. B.,Loos, J. ,Koning, C. E. Preparation of Conductive Nanotube–Polymer Composites Using Latex Technology Adv. Mater. 2004, 16, 248–251

28. Bergman, D.J.; Imry, Y., Critical behavior of complex dielectric-constant near percolation threshold of a heterogeneous material. Physical Review Letters 1977, 39 (19), 1222-1225.

29. Stroud, D.; Bergman, D. J., Frequency dependence of the polarization catastrophe at a metal-insulator transition and related problems. Physical Review B 1982, 25 (3), 2061-2064

30. Wilkinson, D.; Langer, J. S.; Sen, P. N., Enhancement of the dielectric-constant near a percolation threshold. Physical Review B 1983, 28 (2), 1081-1087

31 Zhang, J.; Mine, M.; Zhu, D.; Matsuo, M., Electrical and dielectric behaviors and their origins in the three-dimensional polyvinyl alcohol/MWCNT composites with low percolation threshold. Carbon 2009, 47 (5), 1311-1320

32. Dyre J C. and Schrøder T B., Universality of ac conduction in disordered solids Rev. Mod. Phys. 2000, 72, 873

-The emulsion formulation enables to finely control the morphology by changing the droplet size or curing procedure, CNT loading and thus optimized the dielectric properties

-The CNT are force to segregate at the Plateau borders leading to a very close packing in between that yields huge values of the dielectric permittivity due to the Maxwell-Wagner polarization effect.

-The optimized formulation are founded at a mean droplets size about ten times higher than the average length of the CNT

-We obtain unprecedented performances and measure giant permittivity larger than 20000 at 100 Hz along with an electrical conductivity below 10^{-4} S/m corresponding to dielectric loss tan δ about 10

Chapter IV

Giant permittivity of graphene oxide - polymer nanocomposites obtained by curing an O/W emulsion

I. Introduction

1) Graphene Oxide and reduced Graphene Oxide

Graphene is a monolayer of sp^2 bounded carbon atoms that attracts interest in industry and research due to its remarkable properties such as high mechanical strength, elasticity, optical transparency, electrical and thermal conductivity, gas impermeability, environmental stability [1-7]. In order to exploit the properties of graphene, its incorporation into polymer nanocomposites is a promising route to create new functional materials. Some examples include conductive nanocomposites with antistatic properties and electromagnetic shielding, nanocomposites for organic electronics, flexible electronics, conductive inks, conductive fibers and textiles, electrostrictive nanocomposites for actuators and energy harvesting, piezoresistive nanocomposites for sensors and safety systems and electroactive nanocomposites for MEMS (micro eletro mechanical systems) [8-11].

Nevertheless difficulties in graphene processing such as insolubility in classical solvents and polymers have limited its use. A common approach to facilitate graphene processing is based on the use of graphene oxide (GO). GO is synthesized by Brodie [12], Staudenmaier [13], or Hummers [14] methods, or variations of these methods. They involve oxidation of graphitic materials. Brodie and Staudenmaier used a combination of potassium chlorate ($KClO_3$) with nitric acid (HNO_3) to oxidize graphite, and the Hummers method involves treatment of graphite with potassium permanganate ($KMnO_4$) and sulfuric acid (H_2SO_4). GO is an oxidized form of graphene monolayer bearing hydroxyl, epoxide and carboxylic groups [15-16] (Figure 33). The new functional groups make the GO sheets soluble in water and in polar solvents.

However, by contrast to neat graphene, GO is electrically insulating [17] and GO-polymer composites are not suitable for applications requiring high electrical conductivity or high dielectric permittivity. Nevertheless, reduction of GO leads to a more conductive material known as reduced graphene oxide (r-GO). The reduction process can be performed following several treatments such as chemical, electrochemical, thermal and supercritical fluids methods [18-24]. Due to its particular tunable dielectric properties, to its two-dimensional morphology and to its particular properties at interfaces [25-26] r-GO is a potential candidate to replace

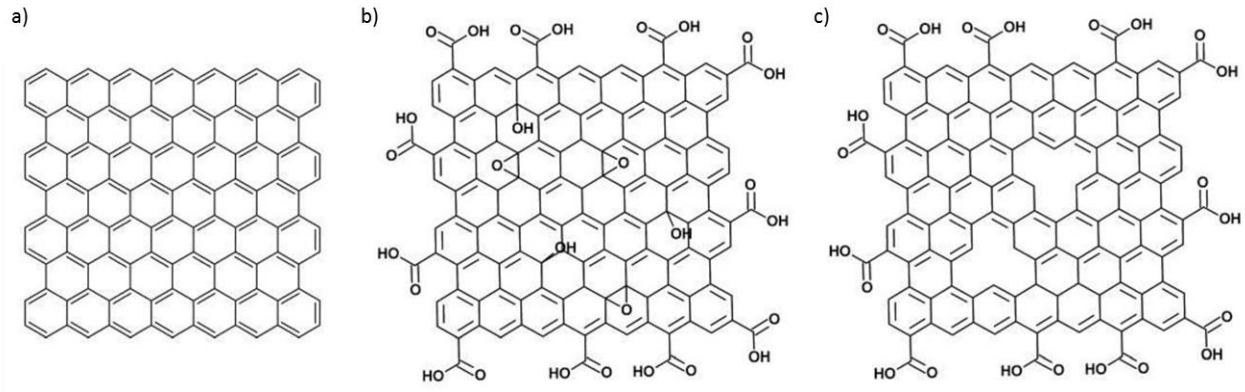

Figure 33: Graphene -based sheets. a) Graphene (G) b) graphene oxide (GO) and c) reduced graphene oxide (r-GO)

CNT in composite materials in order to develop high energy capacitors and efficient energy harvesting devices.

The most frequent technique used to convert GO into r-GO is the thermal reduction. The reduction efficiency increases with temperature. The electric conductivity of r-GO is as high 10^4 S/m when GO is reduced at about 1000°C [27]. Nevertheless, conventional thermal reduction is limited and leads to materials that are far from being as conductive as neat graphene. This is a limitation for a number of applications, but turns out to be an advantage for other applications in which a high conductivity is not sought after. These applications include energy storage or scavenging systems. However, such applications demand a good compromise between the amount of charges that can be accumulated within the composite (ε'_r) and its electrical losses (σ).

2) In situ reduction of the graphene oxide sheets within materials

In-situ reduction within the polymer composite is more convenient than *ex-situ* reduction because it doesn't involve further steps after reduction in the synthesis process of the composite. The maximal temperature allowed for the *in-situ* reduction is set by the upper temperature that the polymer matrix or solvent can sustain without being degraded. Chemically modified GO sheets [28] and non-covalent dispersion methods [29-30] have been used to make GO nanocomposites prior *in-situ* reduction. Tong *et al* [28] functionalized GO sheets with polyethylenimine (PEI) in order to enhance the compatibility between an intrinsically electrostrictive matrix such as polyvinylidene fluoride (PVDF). The PEI chains are grafted to the GO surface via the reaction between the amines and the epoxy functions. Note that at 100Hz, its permittivity is increased by a factor of five ($\varepsilon'_r = 67$) compared to the pristine PVDF material and its electrical conductivity remains as low as 10^{-8} S/m due to the lack of links between adjacent GO sheets [28].

Desmukh *et al* [30] achieved also interesting results by mixing a blend of polypyrrole/polyvinyl alcohol with GO. The increase of the dielectric permittivity for a 3 wt% GO composite is about ten times higher than the neat polymer blend ($\varepsilon'_r = 3$). When subjected to a thermal treatment, the values for the relative permittivity is as high as 150. The electrical conductivity remains as low as 2×10^{-6} S/m and the dielectric loss tan $\delta = \frac{\sigma}{\omega \varepsilon'}$ is 5 even after thermal reduction of GO. The above data is given at 100Hz.

Another interesting approach involves the use of a co-solvent of the fillers and of the polymer matrix. The resulting slurry can be casted or precipitated using a non-solvent for the polymer causing the encapsulation of the filler by the polymer. In many cases, such methodologies can lead to the aggregation of the filler and prejudice the material properties. In order to avoid this typical agglomeration Pei *et al.* [30] synthesized nanocomposites employing a co-solvent such as dimethylformamide (DMF) to disperse pristine graphene and PVDF powder in presence of an ionic liquid. The achieved materials display high permittivity and low conductivity. We

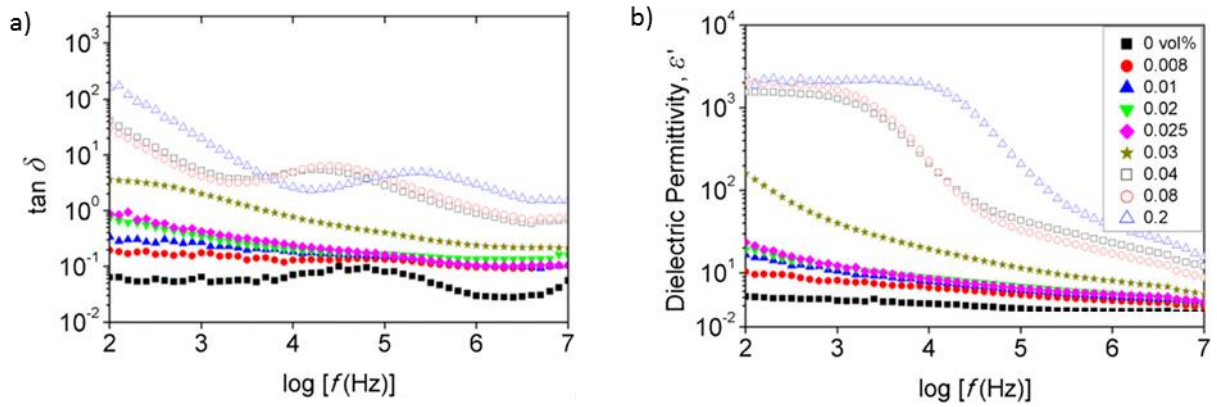

Figure 34: Dielectric permittivity (ε′) and loss factor (tan δ) of the rGO/PP composites with different volume fraction of rGO as a function of frequency at room temperature [31].

note that employing a common solvent of the GO dispersion and structuring the filler can lead to a homogenous dispersion and the structuration of the fillers network to improve the dielectric properties of the final composites.

Wang *et al* [31] proposed a simple and scalable approach that consists in mixing an aqueous dispersion of GO colloidal particles into the continuous phase of polypropylene (PP) latex aqueous suspension. Once dispersed in the continuous phase, the reduction of the GO sheets is achieved *in-situ* via a chemical treatment. The r-GO sheets are absorbed at the interface of the PP latex and remain individually dispersed. Afterwards the solvent is removed by membrane filtration and the final composite is obtained by compression molding. This approach offers a control over the structure of the composite, and leads to low percolation threshold because of the segregation of the GO sheets. Due to this latex approach, The relative permittivity of the obtained materials ε'_r is as high as $2x10^3$ and the electrical conductivity σ is about $2x10^{-3}$ S/m corresponding to a dielectric loss tan δ as high as 200 at 100Hz (Figure 34).

We note that the best reports in the literature are gathered and compared in terms of dielectric permittivity ε'_r and electrical conductivity σ (Figure 35)

3) Ex situ reduction of the graphene oxide dispersions oxide

Ex-situ reduction involves prior reduction of GO to r-GO, followed by composite formation with polymer. The advantage of reducing the GO nanoplatelets *ex-situ* is the absence of any degradation of the polymer matrix during the reduction process due to strong reducing agents or high temperatures. Various methods can be used to reduce GO. Unfortunately the restoration of electronic properties via these treatments is associated to a loss of facile processing [32-33]. Similar to graphene, r-GO is difficult to process to form homogenous polymer composites. In addition to the co-solvent approach mentioned earlier, several groups overcome this problem with new approaches. Li *et al* [33] achieve to stabilize chemically modify graphene in water through electrostatic stabilization. Using the latter approach Li *et al* [34] performed a template of high dielectric permittivity particles such as barium titanate (BT) fillers covered by either GO sheets or chemically *ex-situ* reduced r-GO sheets. Theses fillers are used by Li *et al* [34] incorporated afterwards into a PVDF matrix. For an incorporation of 50% BT-rGO powder (respectively 35%wt), the relative dielectric permittivity ε'_r, rises up to 2000 (resp. 200) and the electrical conductivity remains as low as 10^{-5} (resp.$2x10^{-7}$) S/m for the ternary r-GO-BT-PVDF composite. The corresponding dielectric loss tan δ is about 10 (resp. 0.2). As shown in Figure 35, such materials perform very well in comparison to other binary composites. Another route to overcome the difficult processing of r-GO is to combine the colloidal sheets with surfactants. Aguilar *et al* [35], first thermally reduced GO at 1000 °C. Secondly a colloidal aqueous dispersion of r-GO was prepared by ultrasonication of r-GO and dodecyltrimethylamonium bromide (DTAB) which enables the stabilization of thermally reduced particles in water. The dispersion is then added to a prevulcanized natural rubber latex. This procedure enabled Aguilar *et al* [35] to synthesize nanocomposites for which the

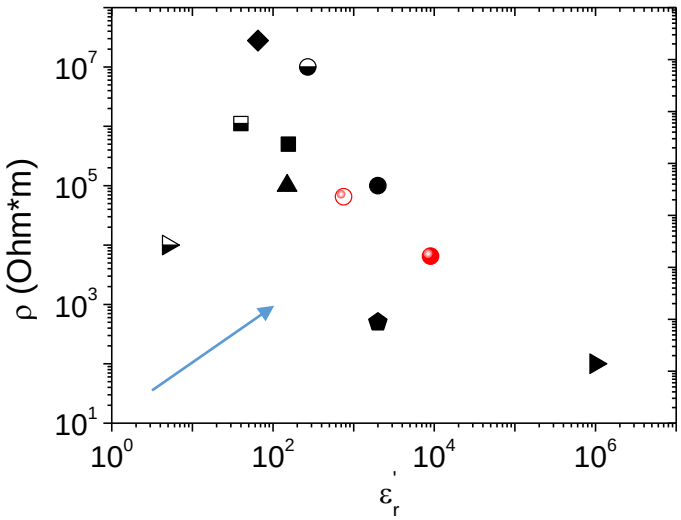

Figure 35: Comparison of the properties (resistivity vs relative permittivity) of GO based polymer composites reported in the literature. The blue arrow indicates the direction towards high permittivity and low losses materials as required in applications. The hollow symbols represent the data for GO whilst solid symbols for r-GO composites. The data is extracted among the best results of the literature: circles [34] pentagon (31), diamond (28), squares (30), and right triangle [35]. The red sphere represents the properties of the presently achieved materials. All the data are given for the same frequency of 100Hz

permittivity ε'_r is about 10^6 and the conductivity σ of about 0.01 S/m at 100Hz for a material loaded with 4wt % of r-GO.

GO sheets are segregated in between the emulsion droplets. Optimized drying and curing conditions were used to synthesize the samples. Due to the sensibility of GO to thermal annealing, the increase of temperature enables huge variations of the dielectric properties. We achieved optimized formulations with values of the dielectric permittivity as high as 10^4 and for an electrical conductivity of about $4x10^{-4}$ S/m at 100Hz for a 6wt % r-GO sample. As shown in Figure 35, the GO based composites present very good dielectric properties, when compared to the literature

The present work is focused on the development of rGO-PDMS nanocomposite materials made by an emulsion approach. The systems are obtained by mixing GO sheets and PDMS emulsion droplets in water. Composites are then made by moulding, drying and curing the emulsion. r-GO is obtained by *in-situ* thermal reduction of the composites at 200°C. According to Mattevi *et al* [24] the temperature at which the GO recovers a graphene like structure is about 1000°C. However, even at this high temperature the total proportion of the C-O bound in r-GO sheets structure is as high as 20%. At 200°C, the reduction of C-O (carboxylates and ketones) bound into C-C sp^2 is considerable and the total proportion of the C-O bound is 30%. In this work we considered that the reduction at 200°C it is not an optimized procedure, nevertheless it is a good compromise to avoid the damage of the matrix.

The dielectric permittivity of the 8wt% GO for a mean droplet size of 5µm is as high as 750 and the electrical conductivity is of only $1x10^{-5}$ S/m. When the mean droplet size is increased to 60µm, for the same GO concentration, the permittivity decreases to 100 while and the conductivity is lowered down to 10^{-6} S/m. The data is given at 100Hz

The first section of this chapter is devoted to the preparation and the characterization of the samples. The second section is focused on the assessment of the different formulation parameters. We evaluate the influence of the GO concentration at a given droplet size, the effect of the thermal treatment on the composites and the influence of the mean droplet size. Lastly we deduce optimal formulations. The final section is devoted to the comparison of r-GO and CNT composites for energy harvesting applications and to further perspectives of improvements.

II. Materials and Methods

1) Materials

The aqueous dispersion of graphene oxide was purchased from Graphenea®. The GO concentration of the raw suspension is about 0.4 wt%. The dispersion was centrifuged in order to increase the GO concentration. Twelve tubes are prepared in the following conditions: An initial mass of 10g of graphene oxide dispersion is introduced into each polypropylene round bottom centrifugation tube. The tubes are placed into a centrifuge machine (Sorval RC 6+, rotor SE-12) at 22000 rpm for 45 minutes. After centrifugation, the supernatant is removed, and the bottom phase is placed under vacuum at 100°C overnight to perform dry extracts and determine the solid content. The mean final weight fraction of the GO is about 5.84%. The mean GO sheet size is about 2-3 μm [36].

The PDMS, Sylgard 184, was purchased from Dow Corning as a kit of PDMS base and curing agent. We recall, that according to Dow Corning ® MSDS the range of temperature for stable performances is ranging [-55°C; 220°C]. This parameter is essential to avoid any degradation of the composite materials during the thermal reduction treatment.

2) Preparation of the samples

A mixture of PDMS and curing agent (20% in weight with respect to the PDMS phase) is prepared as the oily phase. We decided to choose such a ratio because the first trials using 10% in weight were too stiff and poorly deformable to remove from its molds. Emulsions are prepared by progressively adding the oil phase to an aqueous solution of SDS surfactant under mechanical stirring provided by a mechanical mixer (IKA Eurostar 40 digital). The surfactant weight fraction in the water phase is 2 wt%. Oil is added drop wise until its weight fraction reaches 85 wt%. Shear can be increased by raising the rotational speed of the mixer in order to form smaller droplets. The size of the obtained droplets is characterized using a Mastersizer Malvern 2000 particle size analyzer. Medium and large droplet sizes were respectively achieved by shearing the emulsion at rotational speeds of 800rpm and 500rpm [37]. An average droplet size of 20 microns and a polydispersity of 41.8%, respectively 60 microns and 45.1%, were obtained for the medium, respectively large, droplets. Smaller emulsion droplets are made using stronger shear in a Couette emulsification instrument [38]. A premix made of large droplets (~60 microns) is introduced in the instrument, which consists in a Couette cell with a thin gap of 100 microns. The rotation speed of the rotor is set at 681 rpm. Droplets with a mean size of 5 microns and a polydispersity of 23.9% are thereby obtained.

The emulsions are then gently mixed with a concentrated GO dispersion. The amount of added GO dispersion is varied in order to obtain different GO concentrations in the final

composites obtained after water evaporation. The concentrations of GO are ranging from 0 wt% to 8 wt%. Emulsions loaded with GO are placed in circular homemade Teflon molds that have a depth of 0.5 mm and a diameter of 19 mm. Once placed in the molds, the samples were degased in order to avoid air bubbles inside the material. The air bubbles decrease the mechanical and dielectric properties of the composite. Solid materials are obtained by evaporating water from the emulsion and by curing the PDMS polymer. The morphology of the final GO-composites for the three different mean droplet sizes are shown in **¡Error! No se encuentra el origen de la referencia.**. We note the presence of Plateau borders, which reflects the absence of coalescence and an efficient evaporation of the solvent.

As mentioned in Chapter III, drying and curing are critical stages as they take place simultaneously [37]. The higher dielectric properties and lower conductivities were obtained using fast water evaporation rates and slow curing conditions. The mold is set in an oven at 30°C for 16h. Due to a slow curing-fast drying process and to the amphiphilic character of the GO sheets [25-26] the droplets are faceted without coalescence before their solidification.

As a matter of fact, GO is known to be a poorly conductive material [17-19]. In order to increase its electrical conductivity, a thermal reduction has to be carried out. To preserve the physico-chemical properties of the PDMS matrix, we decided to proceed to the thermal annealing step at the maximum temperature recommended by the supplier: 200°C for 2h. The composites are characterized before and after the thermal reduction treatment.

3) Characterization techniques

Dielectric measurements

The alternating current (AC) electrical conductivity measurements were performed across the thickness of the molded disc samples of 19 mm in diameter and of 0.28 mm in thickness. The sample is loaded between two metallic disc electrodes that have the same diameter than the samples. The electrical conductivity was measured under a voltage of 1V applied in the frequency range of 10-10^6 Hz using a computer-controlled impedance analyzer (Materials Mates 7260). A classical calibration procedure removing the contributions of the polarization of the electrodes and of the wiring is used to determine the dielectric permittivity and the conductivity of the sample as a function of the frequency. All the experiments are performed at room temperature

Scanning Electron Microscopy (SEM) analysis

All samples were prepared as follows. Each composite was cut at its edge, then quenched in liquid nitrogen to be finally broken apart using pliers. This procedure yields a clear view of the internal morphology of the composite. The sample surface is coated with a thin (2 nm) conductive layer of Au/Pt using an Emitech SC7620 Mini Sputter Coater for better resolution of SEM imaging. A low magnification tabletop SEM Microscope Hitachi TM1000 was used to analyze the structure of the emulsion on large scale. The graphene network was visualized using a high resolution Jeol JSM 6700F SEM

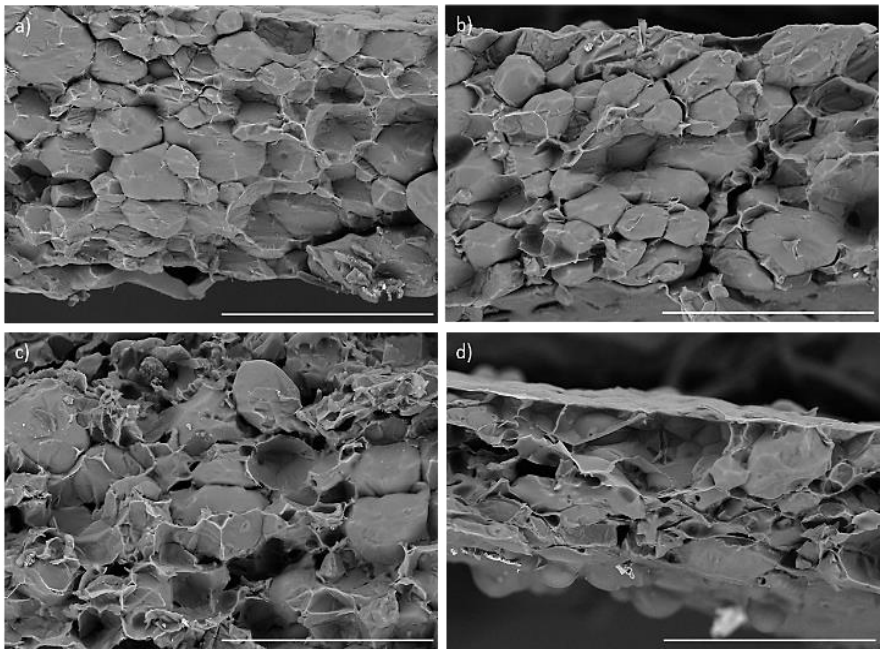

Figure 36: SEM images of the internal structure of GO based nanocomposites with increasing concentration of the filler: 1 wt%(a), 2wt% (b), 4 wt% (c) and 8wt% (d) for a mean droplet size of 60µm. All the scales bar represent 200µm

III. Results and Discussions

1) *Assessment of the emulsion based composites properties as a function of the Graphene Oxide concentration*

We formulate GO based composite materials with different concentrations of fillers: 0 wt%, 0.5 wt%, 1 wt%,2 wt % 4 wt % 6 wt% and 8wt%. The mean droplet size for these nanocomposites is 60µm. Figure 36 shows the morphology of the GO composites prepared after the curing of the PDMS –water emulsion for four different GO concentrations. The emulsion template is kept after drying and curing regardless the GO concentration. The nano-sized GO platelets surrounding the PDMS oil droplets promote their faceting. We note that the GO platelets cover the surface of the PDMS drops. However, when the GO concentration is increased, the GO sheets not only cover the droplets but start to aggregate in between the PDMS droplets at the Plateau borders as shown in Figure 36 forming a cellular structure. Figure 37 shows the relative dielectric permittivity and the electrical conductivity as a function of the GO concentration for a mean droplet size of 60µm at 100Hz. We recall that the dielectric permittivity of neat PDMS is 2.7. The composite with no GO presents a higher permittivity (ε'_r =5) presumably due to the polarization induced by remaining surfactant within the material. We note as a general trend that the permittivity increases with the GO concentration. It ranges from ε'_r =5 for 0 wt% GO to ε'_r =100 for 8 wt% GO. The electrical conductivity increases also with the GO concentration. Its values rises from 10^{-11} to 10^{-6} S/m when the GO concentration is increased from 0wt% to 8wt%. The conductivity data in Figure 37 suggest that the percolation threshold is about 1wt%. In classical percolating systems, the permittivity decreases above the percolation threshold. Here the permittivity is seen to level off. This behavior might be

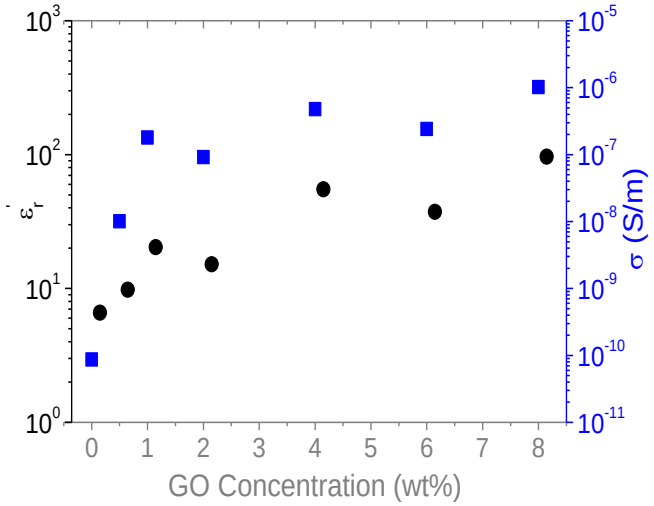

Figure 37: Relative dielectric permittivity ε'_r (black circles) and electrical conductivity σ (blue squares) as a function of the GO concentration obtained after solidification of the matrix. The average droplet size is 60µm and the measurements were carried out at 100Hz.

explained by the presence of large conductive clusters which remain not connected with the main conductive percolated network.

2) Influence of the thermal reduction on the dielectric properties of GO based composites

The increase of the GO concentration improves the dielectric properties of the composites. The droplets act as insulators between several platelets of GO considered as pseudo electrodes of electrical micro-capacitors. But GO is a poor conductor and is not ideal to provide an efficient polarization of the micro-capacitors. A thermal reduction of GO into the more conductive r-GO should lead to better properties.

The reduction of GO is macroscopically visible by a change of color. As shown in Figure 38, the poorly conductive samples are brownish. However, after the reduction process, the color of the conductive r-GO samples is completely black.

Noteworthy, the electrical conductivity as well as the dielectric permittivity remains about the same order of magnitude before and after thermal reduction below 1 wt% r-GO. Inversely, when the r-GO concentration is above 2 wt.%. The electrical conductivity and the permittivity increase significantly after thermal reduction. As shown in Figure 38 a, the permittivity is five times higher for 4wt% r-GO than 4%GO. Moreover, the values for 6 wt% and 8wt% r-GO are about one order higher than the parent GO samples. As shown in Figure 38 b, the increase of the electrical conductivity is about one or several orders of magnitudes greater depending on the r-GO content.

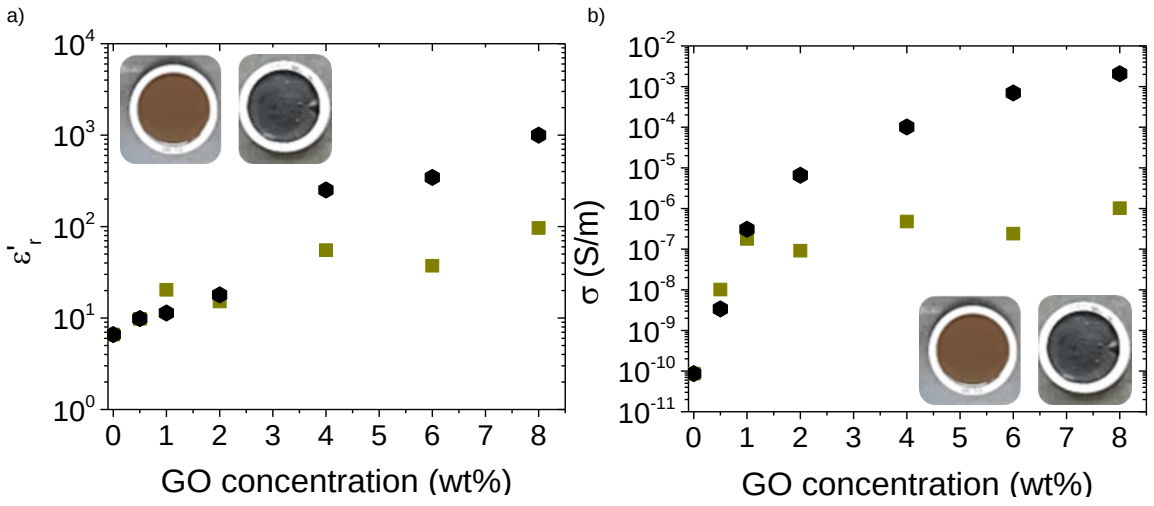

Figure 38: a) Relative dielectric permittivity ε'_r and b) electrical conductivity σ of GO (brown squares) and r-GO (black circles) nanocomposites as a function of the fillers content. The average droplet size is about 60µm and the measurements were carried out at 100Hz. The inlet show the color of the samples before and after thermal treatment

3) *Influence of the mean droplet size on the dielectric properties of r-GO based composites*

We prepared three different batches of r-GO composites containing the same concentrations of r-GO but for different mean droplet sizes. We recall, as shown in **¡Error! No se encuentra el origen de la referencia.**, that the three different mean droplet sizes are 5µm (small), 20µm (medium) and 60µm (large). We also stress that the typical r-GO platelet size is about 2-3 µm. We can therefore expect that, by contrast to medium and large droplets, droplets of 5µm play a poor templating effect.

Figure 39 b) shows the electrical conductivity as a function of the r-GO concentration for the three droplet sizes. As mentioned earlier for the r-GO 60µm composites, the electrical conductivity increases as a function of the GO concentration regardless the mean droplet size. Even though the values are slightly different, the raise of the conductivity follows the same general trend. The initial values are about 10^{-10} S/m for 0wt% r-GO while for 8wt% r-GO the values can attain 10^{-2} S/m. Once the r-GO network is built, the amount of free charges (conductivity) passing through the sample is essentially driven by the amount of r-GO, regardless the mean droplet size. This explains why there is little dependence of the conductivity on the droplet size.

However, we note an effect of the mean droplet size on the dielectric properties of the composites. An optimum is found for medium size droplets. This optimum can arise from a poor templating effect for small droplets and from finite size effects for the largest droplets. Indeed, considering that templating droplets (medium or large) set a characteristic size (Figure 40.a and b) of capacitors, one can expect a greater permittivity as the sample approaches an infinite system. It is indeed in the limit of an infinite system that the permittivity is expected to diverge at percolation. In practice, such a divergence can not be actually achieved because of finite size effects. Here, the medium (20 µm) large droplets (60µm) are a finite fraction of the

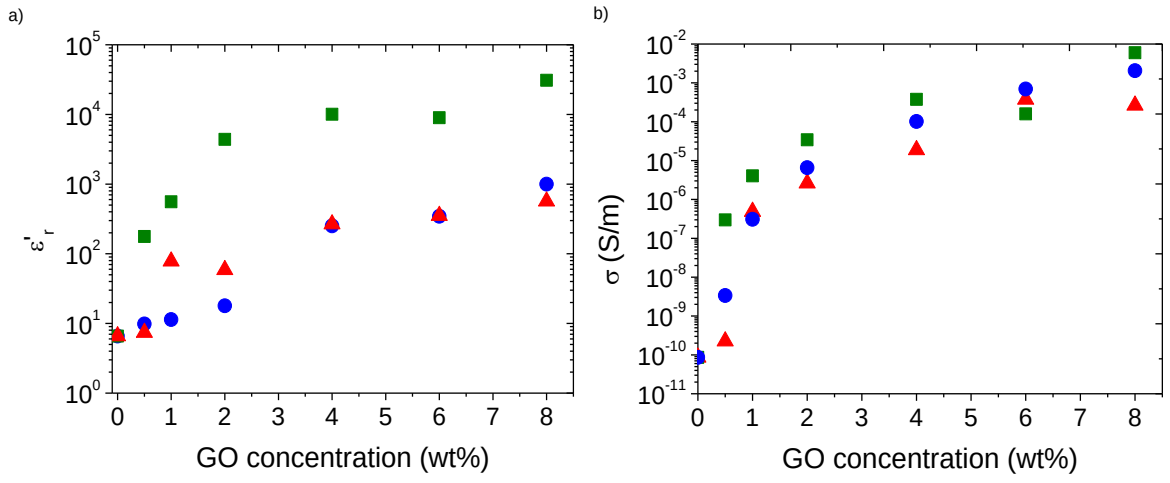

Figure 39: Relative dielectric permittivity ε'_r (a) and the electrical conductivity σ (b) as a function of the GO concentration for tree different droplet sizes: small (red triangles), medium (green squares) and large droplets (blue circles). The measurements were performed at 100Hz.

sample thickness (280 μm). The smaller this fraction the greater the permittivity as finite size effects become less pronounced with small droplets. But this trend remains valid until the droplets act as templating agents.

In addition Figure 40c and d show how the r-GO platelets aggregate at the Plateau borders to form thick r-GO stacks. The thickness of these stacks is about 20nm for 1wt% of r-GO, and about about 100 nm for 4wt% of r-GO.

4) *The optimized formulation: Dielectric response as a function of the frequency*

The 20 μm emulsion based system was shown to exhibit the greatest permittivity. This material is here investigated in more depth. Figure 41 a) shows the relative dielectric permittivity ε_r' as a function of the frequency for different r-GO concentration. The dielectric permittivity ε_r' of the blank emulsion is about 6 and independent on the frequency. It increases strongly with the r-GO concentration at a given frequency and for the entire frequency range. The dielectric relaxation is due to the Maxwell-Wagner relaxation originated from a matrix filler interface. The dielectric permittivity is found to scale as $\varepsilon_r \ \alpha \ f^a$ where *a*, is a critical exponent. Its average value for the different r-GO concentrations is about -0.5. This value is in a very good agreement with the expected theoretical value -0.5 for the percolation of 2D charges carrier [39, 40].

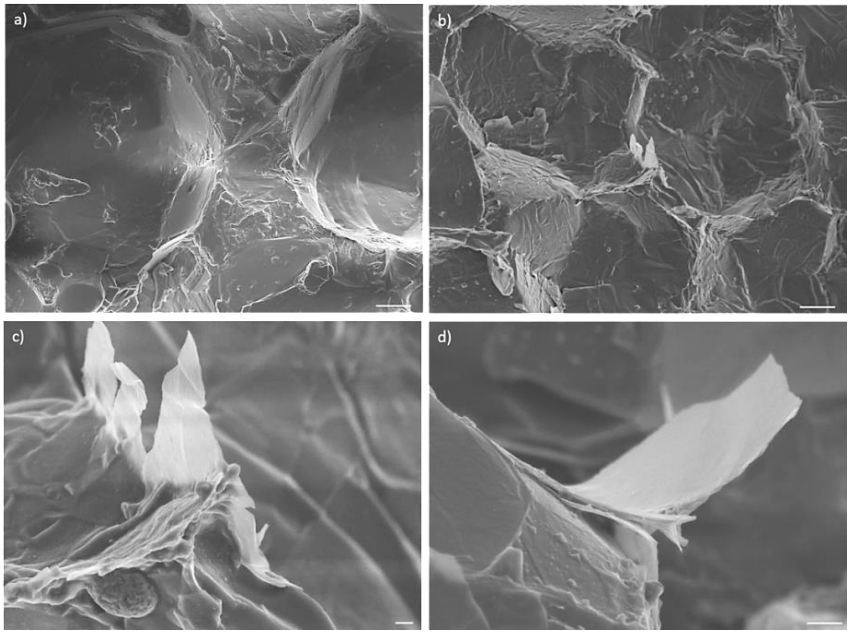

Figure 40: High resolution SEM images of PDMS–GO nanocompsites for 0wt% (a), 1wt% (b) (c) and 4 wt% (d) .We noticed that the GO sheets covers the entire PDMS droplets (a) and (b) and tend to accumulate at the Plateau borders. The scale bar for (a) and (b) represent 10μm while the bar for the quasi individual GO sheet (c) and (d) represent 1μm

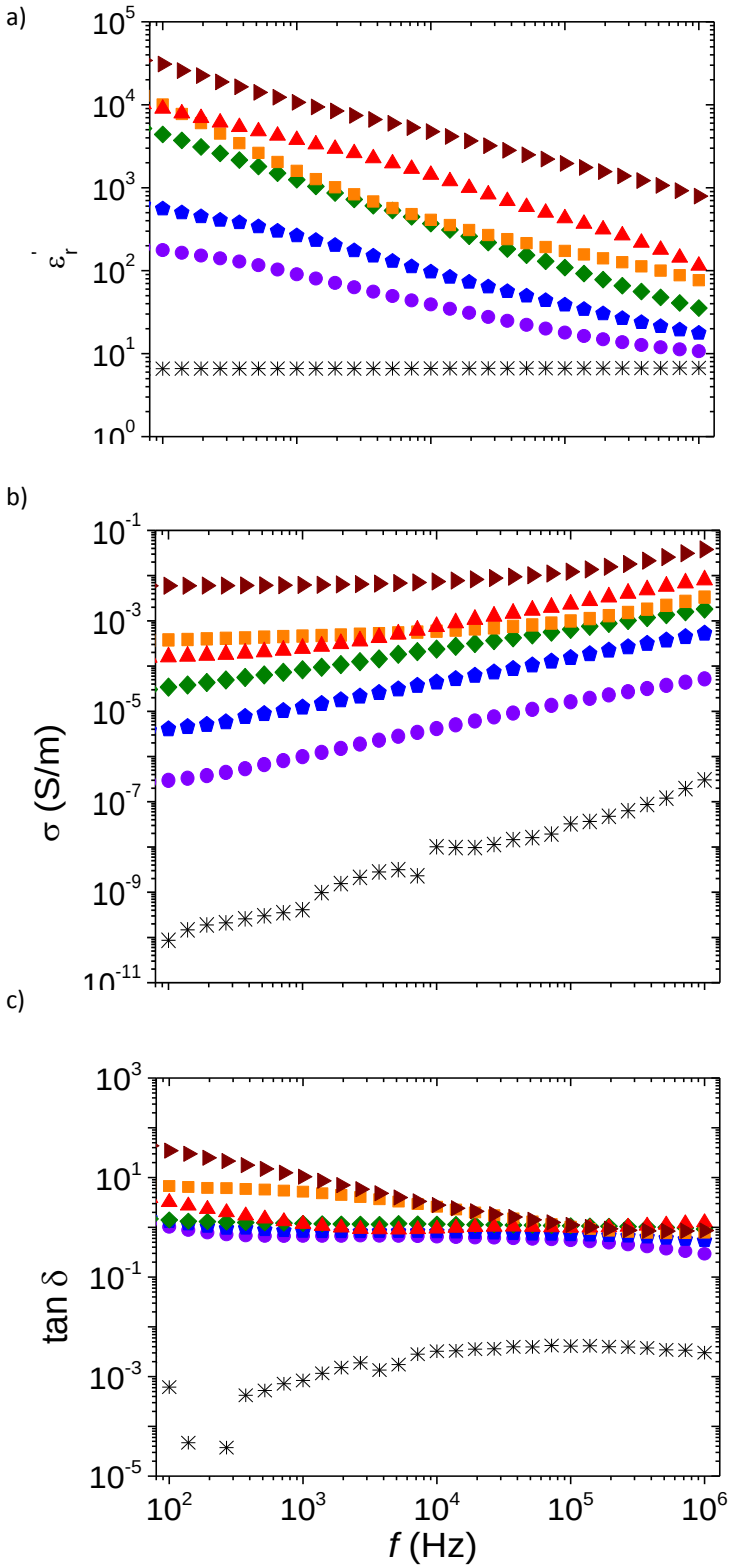

Figure 41 a) Dielectric permittivity b) electrical conductivity and c) dielectric losses as a function of the frequency for different r-GO concentration: 0 wt% (black cross) , 0.5 wt% (purple circle), 1 wt % (blue pentagon), 2 wt% (green diamond), 4 wt% (orange square), 6 wt% (red up triangle) and 8 wt %. The mean droplet size is <a>=20µm

Figure 41 b shows the electrical conductivity as a function of the frequency for different r-GO concentrations. The composite materials exhibit a different behavior as a function of the frequency and depending on the r-GO concentration. The composite without r-GO nanoplatelets shows a frequency dependence behavior. In this case, the conductivity is provided by the bounded charges and ascribed to the so called dielectric losses.

The electrical conductivity becomes frequency independent with the increase of r-GO concentration. This phenomenon arises from the contribution of free charges brought by the r-GO particles. When the r-GO concentration reaches 4, 6 and 8wt%, we observed two different slopes of the conductivity against frequency curves. At high frequencies, the electrical conductivity is frequency dependent and, at low frequencies, the electrical conductivity is constant. This behavior reflects the contribution of dielectric losses at high frequency and the dominant contribution of free charges at low frequency. Figure 41 c shows the loss tan δ as a function of the frequency for different r-GO samples. We can note that, for almost all the r-GO loaded samples, the losses are above 1 and therefore relatively large.

5) *Comparison between the r-GO and CNT nanocomposites*

We recall that Chapter III and IV are devoted to the development of organic nanocomposites using a direct (O/W) emulsion approach for their synthesis. PDMS droplets act as a templates forcing the anisotropic organic fillers to segregate at the emulsion Plateau borders; yielding high dielectric permittivity. The permittivity can be optimized by tuning of the droplet size. We found out that the highest dielectric permittivity is achieved when the mean droplet size of the composites materials are about one order of magnitude higher than the length of the filler. This optimal range corresponds to a compromise of finite size and templating effects.

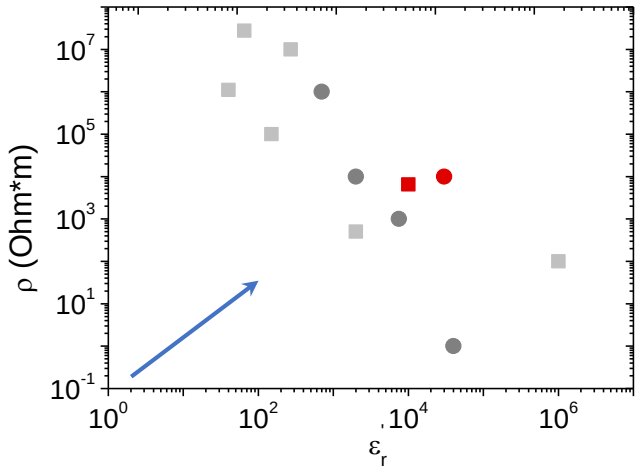

Figure 42: Comparison between state of the art high permittivity nanocomposites: light grey squares represent r-GO based composites while dark grey circles CNT composites [41] [42] [43] [44]. The red points correspond to our composite materials synthesized by an emulsion approach.

The filler concentrations for which the r-GO and CNTs display the greatest permittivities differ. Optimized r-GO loading is found for the maximum r-GO concentration (i.e. 8 wt %) which is well above the percolation threshold (1 wt%), while optimized CNT loading is found to be around the percolation threshold (0.4 wt %). CNT systems follow the theoretical mechanism in which the relative dielectric permittivity diverges around the percolation threshold. This optimum of permittivity is not seen with r-GO composites, presumably due to the presence of clusters that remain disconnected from the main conductive network. Regardless, the exact origin of this behavior we can conclude that CNT nanocomposites are probably preferable than r-GO composites for energy harvesting applications. Indeed, using a lower concentration of fillers is preferable because it reduces the degradation of mechanical properties. As a matter of fact, the present composite elastomers become brittle and fragile when the amount of fillers is high. But r-GO composites can find advantages in terms of cost and ease of processing, remaining therefore a promising material in the field.

Figure 42 show the state of the art work for r-GO and CNT nanocomposites. We note as a general trend, that the CNT composites present better performances than r-GO ones. The optimized systems developed during this thesis are highlighted in the graph with red symbols. These materials exhibit excellent compromises of permittivity and conductivity compared to previously reported materials.

IV. Conclusion

Nanocomposites loaded with r-GO display high permittivity. This permittivity is optimized with a compromise of finite size and templating effects provided by the emulsion droplets of the matrix. The optimal compromise is found for a droplet size of about 20 μm, which is an order of magnitude greater than the typical size of the r-GO sheets. The net values of permittivity and electrical conductivity place r-GO nanocomposites [45] among promising dielectric nanocomposites. Nevertheless, such high performances are obtained only at relatively high concentration, which can be a weakness as highly concentrated nanocomposites can display degraded mechanical properties. In comparison CNT based composites display better dielectric performances and lower electrical losses at even lower concentrations than r-GO based materials. Nevertheless, it is important to keep in mind that the properties of r-GO composites can certainly be further improved with a better reduction of GO. Indeed, it is known that a simple thermal reduction at 200°C is far from being optimal. Work on improvement of GO reduction is currently underway using chemical approaches or processing in supercritical fluids in collaboration with the C. Aymonier group at the Institut de Chimie de la Matière Condensée de Bordeaux.

References

1. *A. K. Geim and K. S. Novoselov, "Electric Field Effect in Atomically Thin Carbon Films " Science Vol 306 22 p 666-669*

2. *Bonaccorso, F.; Sun, Z.; Hasan, T.; Ferrari, A. C., Graphene photonics and optoelectronics. Nat Photon 2010, 4 (9), 611-622.*

3. *Ambrosi, A.; Chua, C. K.; Bonanni, A.; Pumera, M., Electrochemistry of Graphene and Related Materials. Chemical Reviews 2014.*

4. *Allen, M. J.; Tung, V. C.; Kaner, R. B., Honeycomb Carbon: A Review of Graphene. Chemical Reviews 2009, 110 (1), 132-145.*

5. *Roy-Mayhew, J. D.; Aksay, I. A., Graphene Materials and Their Use in Dye-Sensitized Solar Cells. Chemical Reviews 2014, 114 (12), 6323-6348.*

6. *Lee, Y.; Ahn, J.-H., "Graphene-based transparent conductive films". Nano 2013, 08 (03), 1330001.*

7. *Schwierz, F., Graphene transistors. Nat Nano 2010, 5 (7), 487-496.*

8. *Potts, J. R.; Dreyer, D. R.; Bielawski, C. W.; Ruoff, R. S., Graphene-based polymer nanocomposites. Polymer 2011, 52 (1), 5-25.*

9. *Sun, Y.; Shi, G., Graphene/polymer composites for energy applications. Journal of Polymer Science Part B: Polymer Physics 2013, 51 (4), 231-253.*

10. *Du, J.; Cheng, H.-M., The Fabrication, Properties, and Uses of Graphene/Polymer Composites. Macromolecular Chemistry and Physics 2012, 213 (10-11), 1060-1077.*

11. *Kuilla, T.; Bhadra, S.; Yao, D.; Kim, N. H.; Bose, S.; Lee, J. H., Recent advances in graphene based polymer composites. Progress in Polymer Science 2010, 35 (11), 1350-1375.*

12. *B. C. Brodie, « On the Atomic Weight of Graphite» Philos. Trans. R. Soc. London, 1859, 149, 249–259*

13. *L. Staudenmaier," Verfahren zur Darstellung der Graphitsäure." Ber. Dtsch. Chem. Ges., 1898, 31, 1481–1487*

14. *Hummers WS, Offeman RE. Preparation of graphitic oxide. J Am Chem Soc 1958;80 (6):1339.*

15. *A. Lerf H. He,M. Forster,J. Klinowski "Structure of Graphite Oxide Revisited"* J. Phys. Chem. B, *1998, 102 (23), pp 4477–448.*

16. *H. He, J. Klinowski, M. Forster, A. Lerf "A new structural model for graphite oxide", Chemical Physics Letters 287 1998 53–56*

17. *Z. Yanwu, S. Murali, W. Cai, X. Li, J. W. Suk, J. R. Potts, and R. S. Ruoff. "Graphene and Graphene Oxide: Synthesis, Properties, and Applications." Advanced Materials 22, # 35 2010 3906-24.*

18. *C.Y.Kong, W.-L. Song, M. J. Meziani, K. N. Tackett II, L. Cao, A.J. Farr, A. Anderson, and Y.-P. Sun. "Supercritical fluid conversion of graphene oxides." The Journal of Supercritical Fluids 61 (2012): 206-11*

19. *S. Stankovich, D.:A. Dikin, R. D. Piner, K. A. Kohlhaas, A. Kleinhammes, Y. Jia, Y. Wu; S T. Nguyen, R. S. Ruoff "Synthesis of graphene-based nanosheets via chemical reduction of exfoliated graphite oxide" Carbon 45 ,2007, 1558–1565*

20. *S. Park, J. An, I. Jung, R. D. Piner, S. J. An, X. Li, A. Velamakanni, and R. S. Ruoff. "Colloidal suspensions of highly reduced graphene oxide in a wide variety of organic solvents." Nano Lett. 9 (2009): 1593-97.*

21. S. Stankovich, R. D. Piner, X. Chen, N. Wu, S. T. Nguyen R. S. Ruoff "Stable aqueous dispersions of graphitic nanoplatelets via the reduction of exfoliated graphite oxide in the presence of poly(sodium 4-styrenesulfonate)" J. Mater. Chem., 2006,16 ,p155–158

22. I. K Moon., J. Lee, R. S. Ruoff, and H. Lee. "Reduced Graphene Oxide by Chemical Graphitization." Nature Communications 1 2010

23. G. K. Ramesha, and S. Sampath "Electrochemical reduction of oriented graphene oxide films: An in Situ RamanSpectroelectrochemical Study" J. Phys. Chem. C 113 (2009): 7985-89.

24. C. Mattevi, G. Eda, S. Agnoli, S. Miller,K. A. Mkhoyan, O. Celik, D. Mastrogiovanni, G. Granozzi,E.Garfunkel, and M. Chhowalla "Evolution of Electrical, Chemical, and Structural Properties of Transparent and Conducting Chemically Derived Graphene Thin Films" Adv. Funct. Mater. 2009 ,19,2577–2583.

25. J.Kim, L. J. Cote, F. Kim, W. Yuan, K. R. Shull, and J. Huang. "Graphene Oxide Sheets at Interfaces." J. Am. Chem. Soc. Vol. 132, No. 23, 2010

26. L. J. Cote, J. Kim, C. Vincent, J.L.Tung, F. Kim, and J. Huang."Graphene Oxide as Surfactant Sheets." Pure and Applied Chemistry 83, no 1, 2010, 95-110.

27. H. Schniepp, R. K Prud'Homme, and I.A Aksay. "Functionalized Single Graphene Sheets Derived from Splitting Graphite Oxide." J. Phys. Chem. B, Vol. 110, No. 17, 2006

28. W. Tong, Y. Zhang, Q. Zhang, X.Luan, Y. Duan, S. Pan, F. Lv, and Qi An. « Achieving Significantly Enhanced Dielectric Performance of Reduced Graphene Oxide/polymer Composite by Covalent Modification of Graphene Oxide Surface ». Carbon 94 (novembre 2015): 590-98.

29. X.Pei, G. Haoguan, W.Xiaoxi, H. Yadong , D. Yunsheng ,"Improved dielectric properties of nanocomposites based on polyvinylidene fluoride and ionic liquid-functionalized graphene". Composites Science and Technology 117 (2015) 282e288

30. K. Deshmukh, M.A. Basheer, S.K.P. Khadheer, R. R. Deshmukh, and P. R. Bhagat. « Highly Dispersible Graphene Oxide Reinforced Polypyrrole/polyvinyl Alcohol Blend Nanocomposites with High Dielectric Constant and Low Dielectric Loss ». RSC Adv. 5, n° 76 (16 juillet 2015): 61933-45.

31. D.Wang, X.Zhang, Z. Jun-Wei, Z.Jun, Zhi-Min Dang, and Guo-Hua Hu. « Dielectric properties of reduced graphene oxide/polypropylene composites with ultralow percolation threshold ». Polymer 54, n° 7 (2013): 1916-22.

32. R. Dreyer, Daniel, Sungjin Park, Christopher W. Bielawski, et Rodney S. Ruoff. « The Chemistry of Graphene Oxide ». Chemical Society Reviews 39, n° 1 (2010): 228-40.

33. D.Li, M. B. Müller, S. Gilje, R. B. Kaner, and G. G. Wallace. "Processable Aqueous Dispersions of Graphene Nanosheets." Nature Nanotechnology 3, 101 - 105 (2008)

34. Y. Li, Y. Shi, F. Cai, J. Xue, F. Chen, Q. Fu "Graphene sheets segregated by barium titanate for polyvinylidene fluoride composites with high dielectric constant and ultralow loss tangent" Composites: Part A 78 (2015) 318–326

35. H. Aguilar-Bolados, M.A. Lopez-Manchado, J. Brasero, F. Avilés, and M. Yazdani-Pedram. « Effect of the morphology of thermally reduced graphite oxide on the mechanical and electrical properties of natural rubber nanocomposites ». Composites Part B: Engineering. 2015.

36. J. Yuan, A. Luna, W. Neri, C. Zakri, T. Schilling, A. Colin, P. Poulin,"Graphene Liquid Crystal Retarded Percolation for New High-k Materials " Nature Communications 6, 8700,

37. A. Luna, J. Yuan, W. Neri, C.Zakri P. Poulin and A.Colin"Giant permittivity polymer nanocomposites obtained by curing a direct emulsion" Langmuir 10/2015; 31(44).

38. T. G. Mason, and J. Bibette, "Shear rupturing of droplets in complex fluids." Langmuir 13, 1997, 4600 – 4613

39. I.Aliga, D.Lellingera, S. M. Dudkina, P. Pötschkeb« Conductivity spectroscopy on melt processed polypropylene–multiwalled carbon nanotube composites: Recovery after shear and crystallization ». Polymer 48, 4, 9 2006 1020–1029

40. S H Chent, J Roucht, Sciortinos and P Tartaglias,"Static and dynamic properties of water-in-oil microemulsions near the critical and percolation points" J. Phys.: Condens, Matter 6 (1994) 10855-10883.

41. Dang, Z. M.; Wang, L.; Yin, Y.; Zhang, Q.; Lei, Q. Q., "Giant dielectric permittivities in functionalized carbon-nanotube/electroactive-polymer nanocomposites." Advanced Materials 2007, 19 (6), 852.

42. N. K. Shrivastava, B.B. Khatua "Development of electrical conductivity with minimum possible percolation threshold in multi-wall carbon nanotube/polystyrene composites" Carbon 49, 2011 4571–4579

43. Chanmal, C.; Deo, M.; Jog, J., "Enhanced dielectric permittivity in poly (vinylidene) fluoride/multiwalled carbon nanotubes nanocomposite thin films fabricated by pulsed laser deposition". Applied Surface Science 2011, 258 (3), 1256-1260.

44. Yuan, J. K.; Yao, S. H.; Dang, Z. M.; Sylvestre, A.; Genestoux, M.; Bai, J. B., "Giant Dielectric Permittivity Nanocomposites: Realizing True Potential of Pristine Carbon Nanotubes in Polyvinylidene Fluoride Matrix through an Enhanced Interfacial Interaction." Journal of Physical Chemistry C 2011, 115 (13), 5515-5521.

45. Nirmal Sigamani, Zoubeida Ounaies, Greg Ehlert, and Henry Sodano "Electromechanical response of reduced graphene oxide–polyvinylidene fluoride nanocomposites prepared through in-situ thermal reduction"Journal of Applied Physics 117, 154102 (2015)

-We synthesize polymer composites materials with high dielectric properties using a direct emulsion approach incorporating ellipsoid organic fillers such as graphene oxide GO sheets. When such materials are subjected to a thermal reduction, provokes the reduction of the hydrophilic groups. The so called reduced composites r-GO improved their dielectric permittivity and electrical conductivity compared to the GO composites due to better polarization of the matrix-filler interface.

-We obtain great performances and measure giant permittivity larger than $5x10^4$ and an electrical conductivity below $1x10^{-2}$ S/m at 100 Hz. The high permittivity relies on the creation of mico/nano-capacitors formed by r-GO platelets at the Plateau borders.

-An optimized formulation is found for r-GO composites when the size of the droplets is about one order of magnitude higher than the average length of the filler.

-These results are among the best results on the literature but remain lower than similar approaches performed with CNT composites.

Chapter V

Characterization of the electrostrictive coefficients M_{33} and M_{13} of polymer nanocomposites

I. Introduction

Part of the following section has already been explain in chapter I.5.iv., however we include additional information for ease of the comprehension.

1) Definition

Electrostriction is defined as the property of non-conductive materials, which develop a quadratic dependency between strain S_{ij} and electric polarization P under a constant stress τ_{ij}. The stress does not induce any electric polarization but changes the molecular structure so that its response to a field becomes modified (Figure 10a). Electrostrictive materials are passive materials which need a primary electrical source to convert mechanical energy into electricity. As for piezoelectric materials, electrostriction is described by intrinsic equations based on the thermodynamic potential, i.e. the energy exchange. The general equation of electrostriction is given by (Eq.1) [1,2]

$$D_i = \varepsilon_{ij}^T E_j + 2M_{ijkl} E_j T_{kl}$$

$$S_{kl} = s_{klij}^E T_{ij} + M_{ijkl} E_i E_j \quad (1)$$

Where s_{klij}^E are the elastic compliance coefficients, M_{ijkl} the electrostrictive coefficients, E_j the components of the electric field D_i the components of the electrical flux density and ε_{ij}^T the linear dielectric permittivity coefficients of the material. We note that the general equation can be simplified depending on the characteristics of the studied material.

In the case of an isotropic electrostrictive polymer film subjected to a stress τ_{11} and to an electrical field along its thickness direction E_3, this leads to:

$$D_1 = \varepsilon_{13}^T E_3 + 2M_{13} E_3 \tau_{11}$$

$$S_{11} = s_{11}^E \tau_{11} + M_{13} E_3^2 \quad (2)$$

This equation can be re-written as $D_1 = \varepsilon_{eff13} E_3$ where ε_{eff} is an effective dielectric permittivity that includes the contribution of mechanical stress. The resulting effective permittivity can be expressed in terms of the variation of the polarization. Consequently, the electrostrictive coefficient M_{13} is defined by Eq. 3 as the variation of the dielectric constant when mechanical stress is applied [3].

$$M_{13} = \frac{\Delta\varepsilon'_{r13}\varepsilon_0}{2\tau_{11}}, \qquad for\ \vec{E} = E_3\vec{e_3}, \qquad and \qquad \vec{\vec{\tau}} = \tau_{11}\begin{pmatrix} 1 & 0 & 0 \\ 0 & 0 & 0 \\ 0 & 0 & 0 \end{pmatrix} \quad (3)$$

Where, ε_0 is the permittivity of the vacuum, $\Delta\varepsilon'_r$ is the variation of the relative dielectric permittivity due to an external mechanical stress τ_{11} and an electrical field in the 3 direction.

Same analysis in the situation of an isotropic electrostrictive polymer film subjected to a stress τ_{33} and to an electrical field along its thickness direction E_3, leads to:

$$M_{33} = \frac{\Delta\varepsilon'_{r33}\varepsilon_0}{2\tau_{11}}, \qquad for\ \vec{E} = E_3\overrightarrow{e_3}, \qquad and \qquad \vec{\vec{\tau}} = \tau_{33}\begin{pmatrix} 0 & 0 & 0 \\ 0 & 0 & 0 \\ 0 & 0 & 1 \end{pmatrix} \tag{4}$$

Note that the coefficients M_{33} and M_{13} are equal in the case of an incompressible isotropic material.

2) Measurement of the electrostrictive coefficients M_{13}, M_{33}

Electrostriction is ascribed to the intramolecular dipoles in the polymer chains. The application of an external electric field induces the reorientation of the polar chains, resulting on a bulk deformation (Figure 43a), which persists until the electric field is removed. The measurement of this precise bulk deformation is a way to determine the electrostrictive properties of some polymers materials. Classical electrostriction experiments are generally performed on thin polymer samples coated with conducting metallic or organics layers on their two opposite faces and acting as compliant electrodes.

Figure 43 a) and b) show an electro-active polymer material in between two compliant electrodes. When an electrical field E is applied, with an intensity equal to typically 10V/µm, the thickness is reduced and consequently the width is increased in all directions. The variation of the thickness is recorded by a sensor on top of the materials enabling the determination of the strain. The electrostrictive coefficient M_{33} is obtained by dividing the strain over the square of the electric field $M_{33}=S_{33}/E_3^2$ [4].

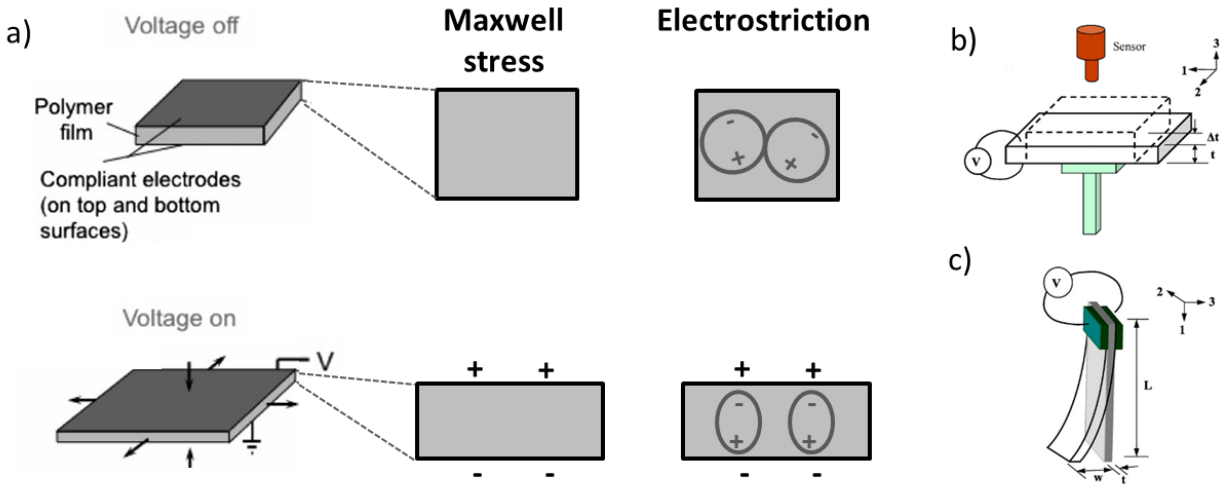

Figure 43: The strain of an electro-active polymer material can be due to different a) electromechanical mechanism: Maxwell stress (i.e free charges on the electrodes) or electrostriction (i.e. interaction between dipoles within the material). Scheme of the two characterization techniques to determine the electrostrictive coefficient Mij via an indirect approach: b) thickness (M33) or c) bending actuation (M13). Deshmukh et al [17]

Figure 10 c) shows the scheme for the measurement of the electrostrictive coefficient M_{13} (i.e. when the applied electric field is perpendicular to the strain). In this configuration the material is composed by two layers and two compliant electrodes. Due to their different thicknesses and affinity to the electric field, the layers display different states of elongation or compression, resulting in the bending of the multilayer material. The resulting deflection of the tip is employed to calculate the electrostrictive coefficient M_{13} [5].

The bending and thickness actuation (i.e. Figure 43 b) and c)) are the most commonly used characterization techniques that enables the determination of the electrostrictive coefficients, M_{33} and M_{13} respectively.

Nevertheless these methods suffer from some drawbacks.

The actuation that is measured to compute these coefficients arises from the Maxwell stress and from the electrostriction effect [6]. The Maxwell stress is driven by the interaction between free charges on the electrodes, leading to the modification of the internal electric field distribution inside the dielectric material. The electrostriction is driven by the interaction between dipoles induced inside the material (Figure 10 a). Besides, these mechanisms are difficult to separate experimentally because both induce bulk deformations that display a quadratic dependence with the electrical field. According to Kofod *et al* [7] the actuation for elastomeric materials with low permittivity $\varepsilon'_r \approx 1$, such as silicones, natural rubber latex and acrylates results mainly from Maxwell stress. On the other hand, for high permittivity $\varepsilon'_r \approx 10$ polar polymers, such as PVDF and PU, the actuation is dominated by the electrostriction mechanism [8].

The most reliable procedure to verify that the actuation is due to a pure electrostrictive effect is to corroborate that the bulk dielectric permittivity of the material is modified when the material is subjected to a mechanical stress [6, 9]. Indeed in this case, the free charges will not be involved in the variation of the dielectric constant. We anticipate that the dielectric constant has to be measured at high frequency in order to avoid polarization at the electrodes. There does not exist, to our knowledge, such experimental determination reported in the literature.

Last but not the least, the accuracy of the measurements may be biased by the heat produces due to the high values of the electric field, by the remaining polarization on the electrodes or even by the methodology to determine the deflection of the tip.

We conclude this section by noting the necessity to develop a more direct characterization technique, using a low voltage, for the assessment of the dielectric properties while a mechanical stress is applied (i.e. electrostrictive properties).

3) Intrinsic electrostrictive polymers

Neat elastic polymers have been tested with bending or thickness actuation, to explore their potential as electromechanical harvesters. Cheng *et al* [10] and Huang *et al* [11] studied the electrostrictive properties of neat polyvinylidene fluoride (PVDF) polymer polyvinylidene fluoride, trifluoroethylene (PVDF-TrFE) copolymers and polyvinylidene fluoride, trifluoroethylene, and 1, 1-chlorofluoroethylene P(VDF-TrFE-CFE) terpolymer (exclusively Huang *et al*). They expected to change the polarization of the polymer by adding different ratio of the copolymer. The approach is interesting but the values remains low to expect an interesting electromechanical harvesting. Cheng *et al.* reaches a maximum value M_{33} about $1.9x10^{-19}$ m^2xV^{-2} at 1Hz while Huang *et al* improved the M_{13} value and reach up to $5x10^{-18}$ m^2xV^{-2} for the same frequency value. Zhang *et al*, [12] studied the influence of the temperature on the electrostrictive coefficient values of PU polymers. In order to proceed to this study they increase the temperature. At 100 Hz the value M_{33} of the PU polymers, increases from $5\ x10^{-19}$ m^2xV^{-2} at 20°C to $3.5\ x10^{-18}$ m^2xV^{-2} at 80°C. Guillot *et al* [8] also performed thickness actuation in PU polymers to determine the electrostrictive coefficient M_{33} at 2 kHz. The values are broadly distributed: the lowest one is about $9x10^{-19}$ m^2xV^{-2} and the highest $7x10^{-17}$ m^2xV^{-2}. The huge difference between the values is explained by the incorporation of several average molecular weight chains within the polymer. In summary, the electrostrictive properties of neat polymer can be increased by improving the polarization at the intramolecular scale [1]. However the obtained electrostrictive coefficients remain low, typically below 10^{-16} m^2xV^{-2}. We note that the electrical conductivity for neat polymers is low and typically 10^{-12} S/m at 100Hz. In spite the relatively low electrostrictive coefficients for such materials, it has been proved that the induced polarization is used at large scale applications to perform harvesting devices. [8,10,11,12]. We expect that an enhancement on the electrostrictive properties can scale down the size of such devices. Thus, smaller energy harvesting devices can be produced, typically at the micron scale.

4) Electrostrictive nanocomposites

The approach of increasing the electrostrictive properties by changing the polarization in an electrical field is very interesting for energy harvesting devices and has been exploited remarkably for composite materials. We recall that the inclusion of conductive fillers in a dielectric matrix enhances the dielectric permittivity due to the Maxwell-Wagner polarization. Furthermore, the increase of the dielectric permittivity or more rigorously the increase of the variation of the permittivity under strain leads to an augmentation of the electrostrictive coefficient (Eq.2). Wongtimnoi *et al* include conductive carbon black (CB) particles to a PU matrix using a co-solvent such as DMF. As expected the M_{33} increases about two orders of magnitude compared to the neat polymer. The optimized material reaches a value of M_{33} of about $1,2\ x10^{-14}$ m^2xV^{-2} for a 1.5 v % of carbon black fillers for an electrical conductivity of about

10^{-5} S/m at 0.1Hz (Figure 44a). The M_{33} value remains relatively constant for studied CB concentration (Figure 44b). The values range from 3 to 8 $x10^{-15}$ m^2xV^{-2} for a CB concentration ranging from 0 to 1.25 v%. On the other hand the electrical conductivity variations are proportional to the CB content. We note that the highest electrostrictive values correspond to the samples for which the CB content is around the percolation threshold (1.4 v% and 1.5 v%). It has been proved that free charges are responsible for the electrical conductivity of the optimum formulation, i.e 1.5 v%, at low frequency (below 1 kHz).

Guiffard *et al* [13] reported a similar value for a PU matrix but instead of CB, the fillers incorporated were SiC particles. The modification of the filler leads to an average M_{33} value of about 2.5 $x10^{-15}$ m^2xV^{-2} at 0.1Hz. This value is comparable to the one obtained by Wongtimnoi *et al* [6] but for lower electrical conductivity, which is about $1.1x10^{-9}$ S/m(Figure 44). The improvement of M_{13} has been proved for PU polymers but also for other dielectric matrixes. Cottinet *et al* [14] incorporate CB to a PVDF-TrFE copolymer matrix. Herein, the value reaches 2 $x10^{-15}$ m^2xV^{-2} at 0.1Hz, corresponding about to 3 orders of magnitude greater than Huang *et al* or Cheng *et al* [10-11] neat fluorinated polymers. Noteworthy that for composite materials the applied electric field that causes the mechanical strain is reduced by an order of magnitude (i.e. 1V/µm) compared to the neat polymers. Most of the works focused on the electrostrictive properties of the composite materials reported electrostrictive values about 10^{-15} m^2xV^{-2} for electrical conductivities about 10^{-9} S/m. These values are significantly higher than neat polymer (about three orders of magnitude) but we believe that optimizing the fillers distribution and the structure of the matrix can increase the electrostrictive coefficient M_{13} or M_{33} even more.

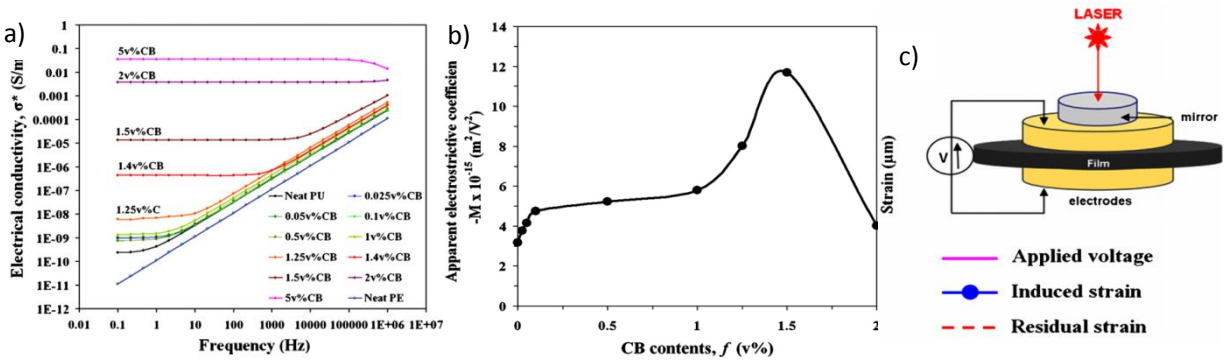

Figure 44: a) electrical conductivity as a function of the frequency b) electrostrictive coefficient as a function of the CB concentration and c) experimental set-up for the characterization of Wongtimnoi et al [6] composites

5) Highly electrostrictive nanocomposite: polyimide-SWNT

The use of single wall carbon nanotube –polyimide (PI-SWNT) composites seems to yield greater results than the rest of the composites reported in the literature. As a matter of fact, Park *et al* [5] improved the electrostrictive properties of a PI by including a highly uniform dispersion of single wall carbon nanotube SWNT to the polymer. The uniformity of the dispersion is possible due the donor-acceptor interaction between the SWNT and the PI. [15,16]. The electrostrictive coefficient M_{33} and M_{13} were determined using thickness and bending actuation respectively. The optimization of the electrostrictive coefficient was carried out by adjusting the SWNT concentration. The optimized composite, a 0.2%SWNT composite, shows a huge M_{33} value of $1.2\text{x}10^{-13}$ m^2xV^{-2}at 0.02Hz. The increase of the M_{33} value is accompanied by a high electrical conductivity of about 10^{-3} S/m. The M_{13} value is calculated using four layers bending actuation and is about the same order of magnitude. Deshmukh *et al* [17] developed a similar composite system where the out of plane and the extensional strain are used to determine the M_{33} and M_{13} coefficients. The optimized composite is found to be at 1% SWNT. Figure 45 b shows that the electrostrictive coefficient depends on the SWNT concentration and on the actuation mode (i.e. M_{13} or M_{33}). The latter nanocomposite is subjected to bending actuation the strain S_{33} is about 0.020% at E 0.05V/µm leading to a M_{13} as high as $1\text{x}10^{-14}$ m^2xV^{-2}at 0.5Hz. When this composite material is studied employing thickness actuation at 1Hz, the value of M_{33} is the highest ever reported before $9\text{x}10^{-13}$ m^2xV^{-2}. The variations that are found for the different actuation modes are explained by a preferential alignment of the fillers during the casting. The PI-SWNT electrostrictive coefficients are about six to seven orders of magnitude higher than the neat intrinsically electrostrictive polymers. In addition the electrical conductivity is about nine orders of magnitude higher than neat polymers. Deshmukh *et al* [17] stress that the high electrostrictive coefficient results from the creation of micro and nanocapacitors formed by the carbon nanotubes (CNT's) [18]. Moreover the donor acceptor interaction between fillers and matrix bring additional polarization to the system. The π–electron from the aromatic molecules of the polymer chains interacts with the

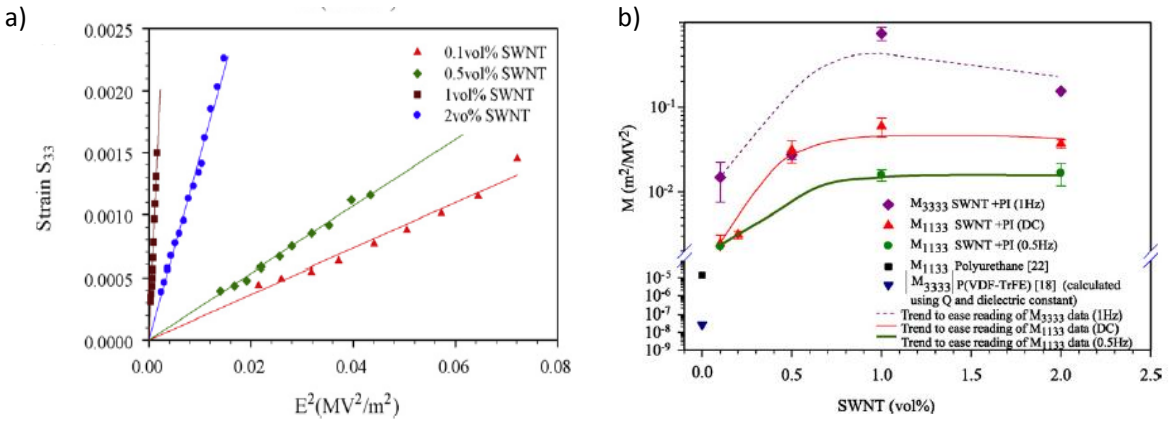

Figure 45: a) Strain of the tip deflection as a function of the applied E^2 for different SWNT contents. The slope of a) enables the determination of the electrostrictive values b) for different experimental conditions. [Deshmukh et al]

SWNT. We note that this polarization effect leads to an additional structuration of the dipoles at the nano-scale

6) *Our work*

These results clearly demonstrate the potential of organic composites to achieve efficient electrostrictive materials. But a greater degree of control of the structuration of the conductive network is still needed to improve the properties. We show in this work that the fabrication of composites using an emulsion approach and filled with CNT provides such a control and yields unprecedented performances (see Figure 46). We study a unique mean droplet size composite which is about an order of magnitude bigger than the length of the CNT. We recall that this ratio corresponds to the ideal ratio between the mean droplet size and length of the fillers to obtain a high permittivity and low losses (see chapter III and IV).

The CNTs remain literally segregated in between the emulsion droplets. Varying the CNT concentration enables the tuning of the average density of the near percolated particles at the Plateau borders. The mechanical stress enables the tuning of the interactions between the CNTs and of their ordering. The sensitivity of the composite material to mechanical stress increases with the CNT concentration and it is maximal around the percolation threshold. The formulation enables the fine control of the CNT network and its optimization.

The electrostrictive properties of the optimized materials were evaluated using a particular methodology that combines simultaneous dielectric and mechanical characterizations. The composite materials were characterized at f=100Hz and displays, for the optimum CNT concentration, a variation of the electrical conductivity about 2 orders of magnitude. Thus, the optimized composites display a variation of the relative dielectric permittivity of about $5x10^3$

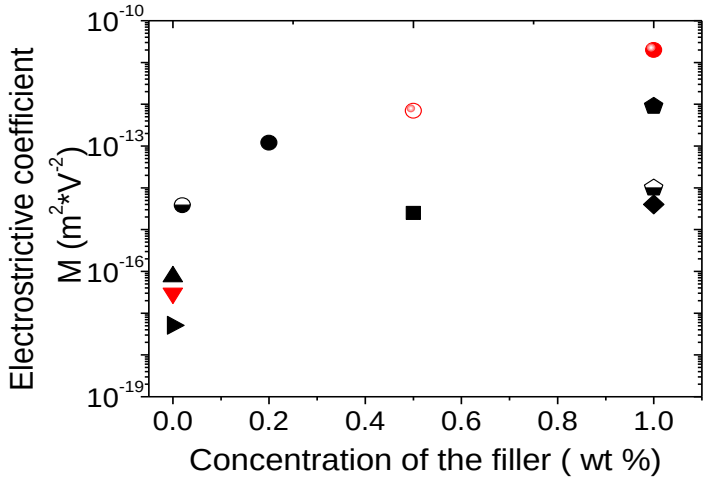

Figure 46: Comparison between the state of the art electrostrictive coefficients for polymers and composites, compared to the present work (red points). Neat polymers correspond to triangles: The circle and pentagons corresponds to PI+SWCNT composites at different SWCNT concentrations. Solid circle and pentagons are calculated M_{33} deduced from measured M_{13} coefficients. Up triangle [8], right triangle [11], circle [4] pentagon [17] and square [9] and diamond [3].

leading to an electrostrictive coefficient M_{33} of about $1x10^{-11}$ m^2xV^{-2}. This is to our knowledge

the highest value for M_{33} ever reported. We note that the electrical losses (i.e. conductivity) are improved and are about one order of magnitude lower than the best reports in the literature (10^{-4} S/m). The description and discussion of these results are provided in the followings.

The first section of the chapter presents the materials and methods used for the study. The second section is devoted to the characterization of the electrostrictive materials; this section is divided in four subparts. The first subpart is focused on the dielectric properties of composite materials with optimized structure at rest. The second subpart concerns the variations of the dielectric properties of such materials under mechanical stress for two CNT composite regimes: one well below, and one near, the percolated threshold. The third subpart deals with the validation of the new characterization technique based on a comparison with method previously used in actuation mode. The fourth part is devoted to the optimization of the electrostrictive coefficients by varying the CNT concentration and the strain rate of deformation. The final subpart presents the conclusion in which we summarize the present results and propose new approaches for energy harvesting devices

II. Characterizations of electrostriction

1) Materials

The materials are prepared and characterized following the procedures already described in Chapter II and III. We synthesize a new batch of nanocomposites that show the best results in terms dielectric permittivity (i.e. mean droplet size of 5µm loaded with CNTs). The CNT concentrations range between 0.05wt% and 2%wt%. The latter nanocomposite materials are first studied at rest and then under dynamic stress. For the study of the electrostrictive properties, we distinguish first a direct determination of the electrostrictive coefficient M_{33} and second an actuator approach for the determination of M_{13} (Chapter II). Thus, we study the impact of the mechanical stress on the dielectric properties leading to a deeper understanding of the structure-properties mechanisms.

2) Methods

i. Measurements of electrostrictive materials under dynamic stress

a. Direct determination of the electrostrictive coefficient M_{33}

The methodology consists in the manufacturing of two solid electrodes that enable the study of the dielectric properties and transfer the mechanical stress at the same time. The experimental set-up relies on assembling two electrodes into a traction machine. The home-made aluminum electrodes (Ø 40mm) were equipped with a PVC-insulator adaptor. Its main

role is to insulate the electrodes from the rest of the ZWICK 2.5 traction machine. The electrodes are connected to a Materials Mates 7260 impedance analyzer enabling the characterization of the dielectric properties under a mechanical stress imposed by the traction machine. We note that the electrostrictive material under mechanical stress acts as a variable capacitor. The average mean thickness is about 1mm and the diameter is about Ø 40mm. The dielectric properties under dynamic stress are studied at a constant frequency (f=100Hz), at 1V and following the typical compensation procedure. We stress that the electrical field provided by the impedance analyzer is very low of about 5.10^{-4} V/µm. The mechanical deformations, from Maxwell stress or electrostriction, are completely negligible compared to the forces applied by the mechanical traction machine in such conditions. The use of a low electrical field for characterizing the materials is a critical difference with the actuation mode procedure generally proposed in the literature. A low electrical field allows the electrostriction contribution to be separated from the Maxwell stress contribution.

A first electrical contact is defined when the force sensor detects a non-null positive force. For all the characterized samples a pre-strain force of about 0.5N is applied beyond the previously defined first contact point. The pre-strain ensures a good electrical contact between the electrodes and the sample. We define a mechanical cycle as the mechanical step for which the strain goes from 0% to 8% and back to 0% strain. This cycle is repeated successively 20 times. The measurements were carried out at room temperature of about 20°C. We focused a particular interest on the impact of the filler concentration on the electrostrictive coefficient M_{33}. Moreover, we study the influence of the mechanical frequency on M_{33}. Herein the mechanical frequency is defined by the speed at which the mechanical strain is applied. We evaluate two different speds, 0.5 and 0.05 mm/min.

b. Determination of the electrostrictive coefficient M_{13} in actuator mode

We remind that the studied materials are considered as isotropic, and synthesized using an incompressible matrix with a Poisson's coefficient of ν=0.5. Therefore the electromechanical properties must be direction independent. The objective is to obtain the electrostrictive coefficient M_{13} of the already tested samples (M_{33}) using an actuator mode widely used in the literature. Matching of these two coefficients would provide a validation of our present approach. The electrostrictive coefficient M_{13} is determined using the curvature of a strip in response to an electric field. The strip material is composed by two outer layers which act as compliant electrodes. The gold conductive layers (i.e. layers 2 and 3) are made using a coating sputtering technique and its thickness is of about 100nm. The layer 1 is composed by the emulsion based electrostrictive material. The layer 4 is prepared with a pure dielectric PDMS neat polymer. We recall that the layer 1 and the layer 4 present different responses to the electric field. Presently, when the multilayer stack is subjected to an electric field, the electrostrictive layer 1 is compressed and the layer 4 is elongated resulting in the bending of

the whole strip material. We note that the PDMS base and curing agent ratio for layer 4 is modified to a 7:1 ratio. The ratio used for the electrostrictive material is 10:1. The existing gradient of curing agent between the two layers enables a good adhesion between the two inner layers of the stack and prevents possible delamination problems induced by the bending of the stack. A strength-of-materials model is used to calculate the electrostrictive coefficient M_{13} from the induced curvature and the mechanical properties of the fourth-layer material [19]. Thus, the geometrical factors of the strip enable the determination of the free strain ε_a (Chap II). Taking into consideration the applied voltage V and we calculate the electrostrictive coefficient M_{13}:

$$M_{13} = \frac{\varepsilon_a (h_1 + h_4)^2}{V^2} \tag{4}$$

The constants h_1 and h_4 correspond to the thickness of the polymer layers.

The set-up that is used to characterize the electrostrictive coefficient M_{13} is shown in Figure 10. The strip composite material is subjected to a triangular AC electric field, produced by a TTi-TGA 1230 waveform generator and amplified by a TREK high voltage amplifier model 609E-6. We use plastic tweezers to safely hold the sample. The high electric field is applied through two copper electrodes. The displacement of the bilayer strip composite material induced by the electric field is recorded by a PHANTOM high speed camera MR110. The influence of the frequency was evaluated in the range of 0.5Hz -10Hz under electrical fields ranging from 0 to 1.5V/μm.

III. Results

1) Static measurements of electrostrictive material properties

We study the dielectric properties of the electrostrictive materials used at rest for comparisons with the dynamic measurements. Figure 47 shows the dielectric properties (ε_r', σ and tan δ) of the nanocomposites as a function of the frequency for different CNT concentrations. The relative dielectric permittivity ε_r' shown in Figure 47a remains constant of almost on the entire frequency range for the samples loaded with 0wt%, 0.05wt% and 0.1%wt CNT. By contrast, the permittivity of the samples loaded with 0.2 wt%, 0.5 wt% 1wt% and 2%wt present frequency dependences. The addition of conductive particles, such as CNTs, to a dielectric matrix enhances the interfacial polarization leading to an increase of the permittivity. We note that the relative permittivity values are broad and ranges from 10 to 10^4 depending on the CNT concentration at 100Hz. The permittivity increases with the CNT concentration within the range of 0 to 1 wt% CNT, as a result of the formation of micro-capacitors made of neighboring clusters of nanotubes. The permittivity of the 2wt% CNT above the percolation threshold decreases because of shorts between the previously mentioned micro-capacitors. The present observations are in agreement with the results in chapter III, confirming the repeatability of the emulsion based methodology.

Figure 47b shows the electric conductivity as a function of the frequency for different CNT samples. The electrical conductivity shows three regimes as a function of the CNT concentration. First, for CNT concentrations below the percolation threshold, the conductivity is characterized by a frequency dependence. It is observed for samples loaded with less than 0.1%wt. This behavior arises from dielectric losses due to bounded charges.

Second, for CNT concentration largely higher than the percolation threshold (i.e. 2 wt %), the sample is frequency independent since the conductivity is dominated by free-charges. The third case is for CNT concentrations around the percolation threshold. At high frequencies, the conductivity is dominated by dielectric losses due to bounded charges, while at low frequencies the conductivity is driven by the transport of free charges brought by the CNTs.

The electrical conductivity at 100Hz varies between 10^{-8} S/m at 0.1wt% and 10^{-5} S/m at 0.5wt%.

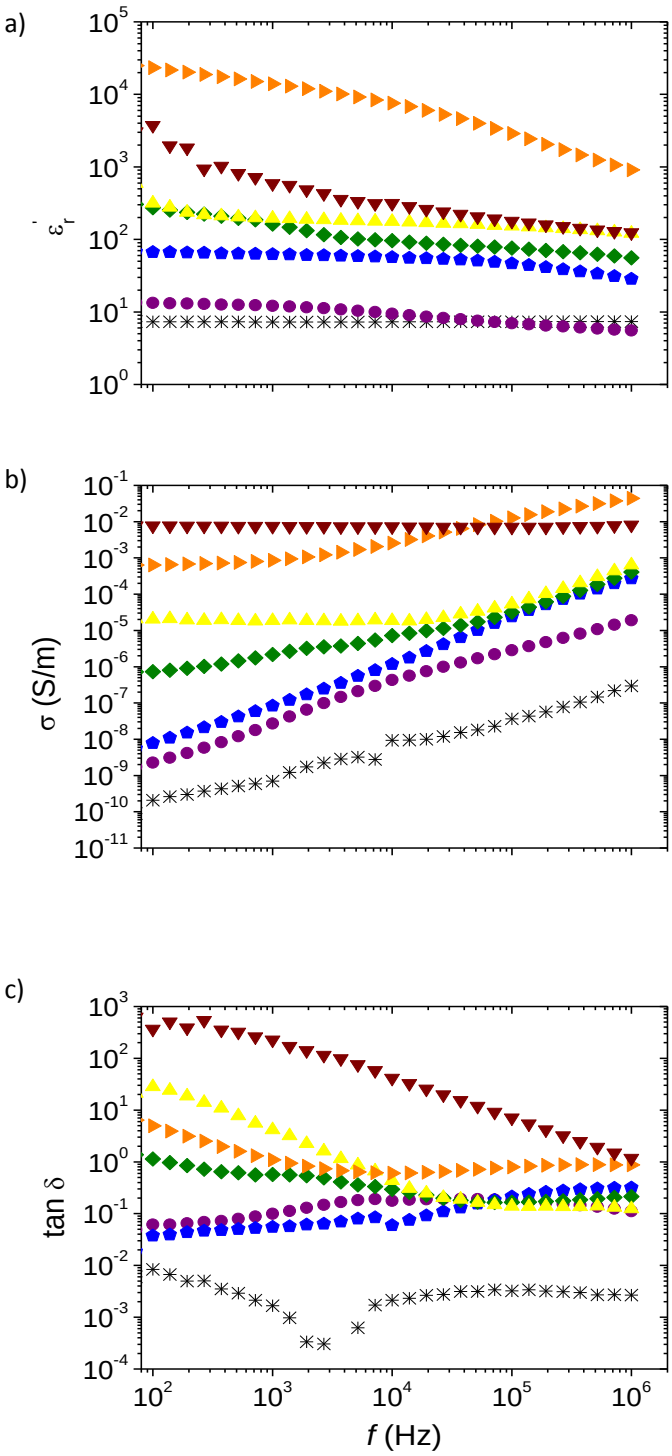

Figure 47: Dielectric permittivity a), electrical conductivity b), and electrical losses c) as a function of the electrical frequency for different CNT concentration: 0 wt% (black scross), 0.05 wt% (purple circle), 0.1 wt% (blue pentagon), 0.2 wt% (green diamond), 0.5 wt% (yellow up triangle), 1 wt% (orange right triangle) and 2 wt% (red down triangle).

The tan δ which characterizes dielectric losses is measured as a function of frequency. The data are shown in Figure 47c. The blank nanocomposite shows a low tan δ of about 10^{-2} on the entire frequency range. Due to the absence of conductive particles, no significant current leakage is found. The value of tan δ increases with the incorporation of CNT. The value of tan δ continues to rise due to the contribution of more and more conductive particles. When the CNT concentration reaches the percolation threshold, a continuous leakage path is formed. The tan δ value for the samples around the percolation threshold is about three orders of magnitude higher than that of the blank composite. For a CNT concentration largely above the percolation, the leakage due to the free charges is largely superior to the accumulated charges leading to a tan δ of about 10^3

2) *Dynamic measurements of electrostrictive material properties*

The following section is devoted to the study of electrostrictive materials under mechanical stress. Two different materials are investigated. The first one is a non-percolated composite and the second one is a percolated sample. The mechanical stress is expected to induce a percolation and de-percolation a priori associated to huge variations of permittivity and conductivity.

i. Direct determination of the electrostrictive coefficient using non percolated samples

Nanocomposites loaded with 0.1wt% CNT act as non-percolated materials since their electrical conductivity is dominated by bounded charges at 100Hz (section 1). The sample is subjected to mechanical stress that is cycled several times. The mechanical stress applied to the material is shown in Figure 48 a and is about 10^4 N/m^2 at its maximum. The applied stress is situated within the linear elastic region and its maximal value corresponds to an 8% strain. The compression of the sample results in an increase of the permittivity and of the conductivity of the material (Figure 48 b and c). The maximum of permittivity and conductivity correspond to the maximal compressive stress. The exact reason of such behavior remains speculative. Nevertheless, we consider that the material can be viewed as a collection of effective micro-capacitors formed by CNTs at the edges of the droplets and at the Plateau borders of the emulsion. The separation between the CNTs decrease when the droplets are compressed and the capacitance of the effective micro-capacitors is expected to increase. This effect may explain the increase of permittivity and electrical conductivity under compression.

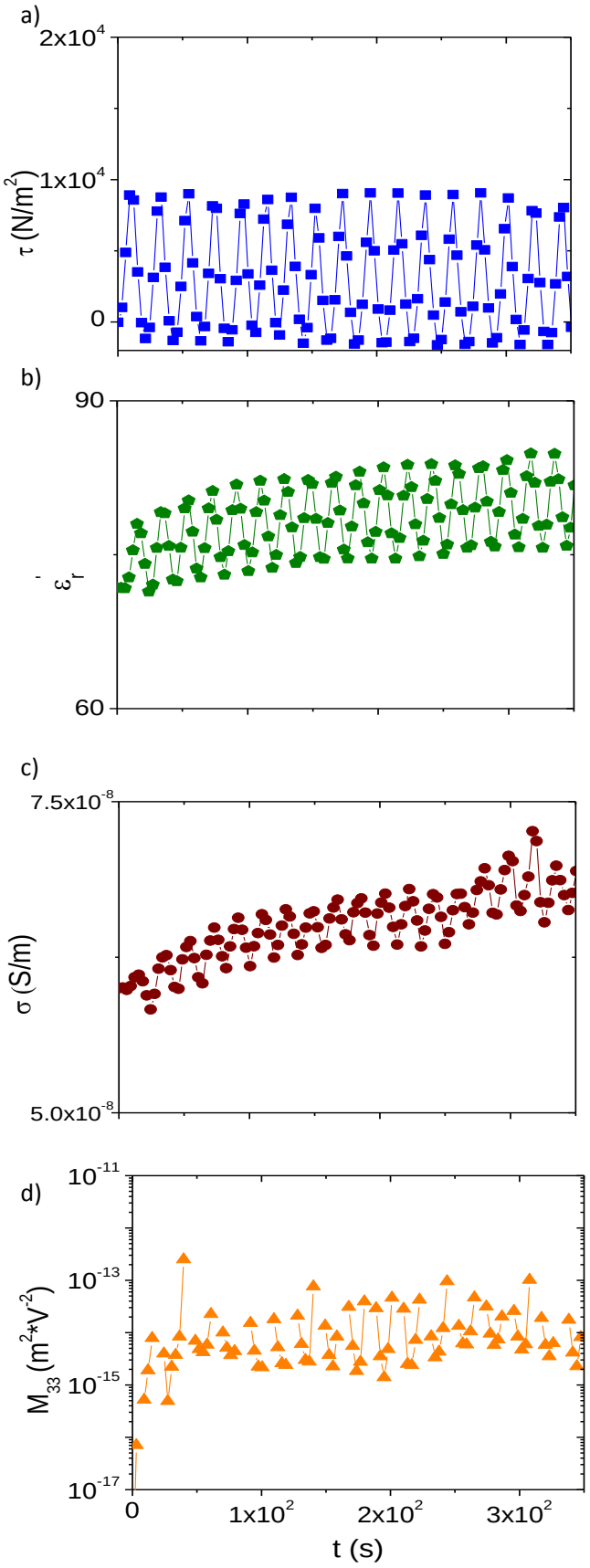

Figure 48: Nanocomposites loaded with 0.1 wt% CNT subjected to a a) mechanical stress which leads to a slight modification of its b), dielectric permittivity, c), electrical conductivity and d) electrostrictive coefficient. The measurement are performed at 100Hz

The relative variation of the dielectric permittivity $\Delta\varepsilon_r'/\varepsilon_r'$ at maximal stress is about 15% while the one of the electrical conductivity is about 12%. Such a variation normalized by the strain defines the so-called gauge factor. The latter ratio is of only about 2. This value is just above the value of 1 which corresponds to the theoretical gauge factor induced by geometrical changes.

We observe a slight increase of the mean value of the permittivity as a function of time as the material is periodically loaded and unloaded. This evolution can reflect some irreversible structural modifications.

The variations of permittivity in response to the mechanical stress allow the electrostrictive coefficient M_{33} to be measured as a function of time using Eq.3 (Figure 48 d). Note that the M_{33} fluctuations do not represent any particular physical phenomenon, but result only from the mathematical evaluation of the coefficient in the present conditions. The coefficient M_{33} is an intrinsic value of the composite which is supposed to be independent of stress in the linear elastic regime. The mean value for the 0.1 wt% CNT nanocomposite is about $3.4\text{x}10^{-15}$ m^2*V^{-2}. This value is above the electrostrictive coefficient of neat polymers (10^{-18} to 10^{-16} m^2*V^{-2}). It compares in fact well with values already reported for other nanocomposite materials (10^{-15} to 10^{-14} m^2*V^{-2}). It is believed that greater values should be achieved by using samples closer to the percolation threshold.

ii. Direct determination of the electrostrictive coefficient using near percolated and percolated samples

The following section is devoted to the study of the 1wt% CNT sample. As mentioned in section *i*, the sample presents an electrical conductivity dominated by the transport of free charges at 100Hz. The nanocomposite is subjected to a cycled mechanical stress of about $3\text{x}10^3$ N/m^2. The maximal stress corresponds to an 8% strain. We note that the Young's modulus Y of the sample is 3 times lower than the one of materials loaded with 0.1wt % CNT (Y=0.1 MPa). This result can be considered as counterintuitive. Nevertheless, due to the cellular structure of the material several explanations are possible. First some air bubbles remain trapped in the composite during the synthesis of the sample. Those could explain a reduction of the Young's modulus. In addition, the emulsion approach forces the CNT to be trapped in between the PDMS droplets, leading to a lower cohesion as the CNT concentration increase. Indeed, the nano-composites present a Young's modulus about one order of magnitude lower than bulky PDMS prepared under similar thermal conditions (Y=1MPa) [20]. We note that this decrease is beneficial to the electrostrictive coefficient M_{33} since its value increases with a drop of the Young's modulus.

We observe that the initial values of permittivity and conductivity differ from the ones measured during the study of the static properties of the materials.

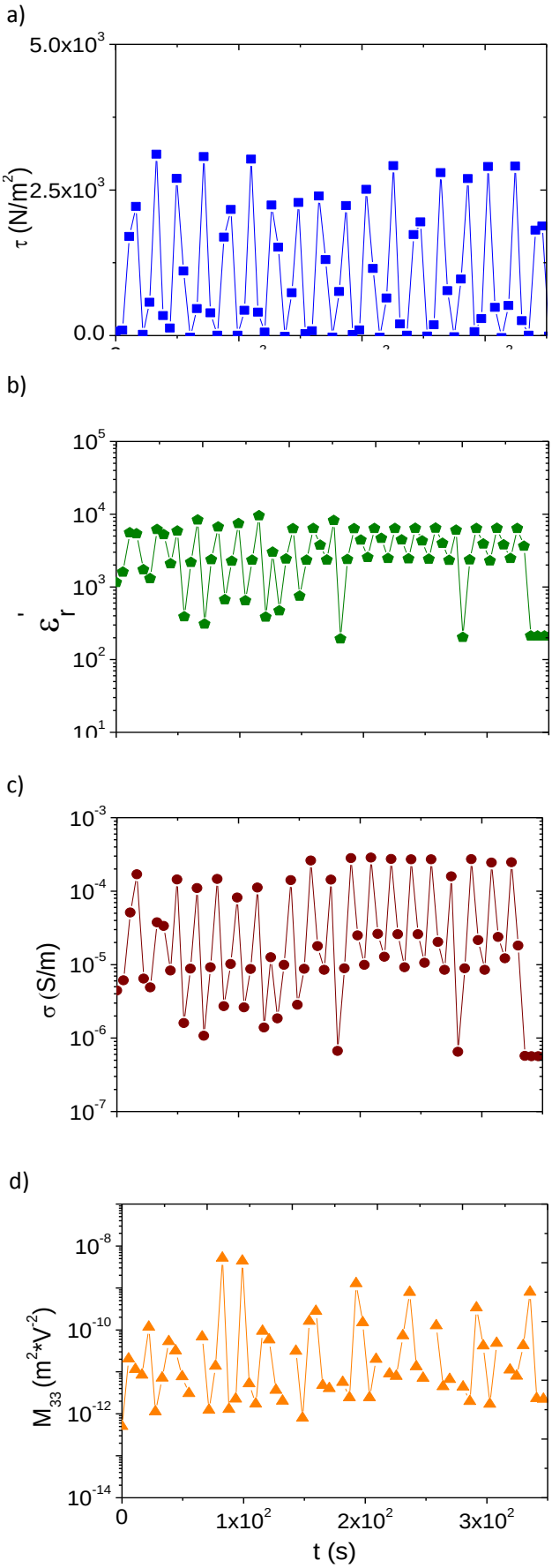

Figure 49: Nanocomposite loaded with 1 wt% cnt subjected to a a) mechanical stress which leads to a giant modification of its b) dielectric permittivity, c) electrical conductivity and d) electrostrictive coefficient.

This difference comes from the pre-strained force applied to the sample, and to a possible creep during the dynamic measurement. We mention that the acquisition of data for the traction machine and the impedancemeter present different time resolution. The plotted data points are in fact average acquisition points. As mentioned earlier, the compression subjected to the samples, reduces the distance between the CNT and leads to an increase of the capacitance. Herein, the 8% strain provokes high variations of the permittivity and of the conductivity (Figure 49 b and c). The variations of the permittivity are about one order of magnitude, and about two orders of magnitude for the electrical conductivity.

The latter variations result into giant electrostriction coefficients of about $5.3x10^{-12}$ m^2*V^{-2}, which corresponds to an improvement of about half order of magnitude compared to the previous highest reports by Deshmukh *et al* [17] and about 3 orders of magnitude in comparison with most data in the literature focused on composites[15,18]. We stress that this value is an actual measurement and not a calculated or extrapolated value [17].

For high concentration of 2%wt, the CNT network is well above the percolation threshold (see section 1 static mode). The material is not purely dielectric and behaves differently from near percolated materials. The permittivity decreases when the sample is compressed and increased when the stress is released. In other words the sign of the electrostriction coefficient is opposite to the one of non-percolated and near-percolated networks. The compression may create new contacts between nanotubes and thus decrease the number of microcapacitors inside the sample. Note that such a behavior has also been observed using GO nanocomposites [23]. Nevertheless, it is observed that the absolute value of the electrostriction coefficient of the 2wt% CNT sample is very high, presumably because of the vicinity of the percolation threshold. The absolute values of the electrostriction coefficients are shown in Figure 50 as a

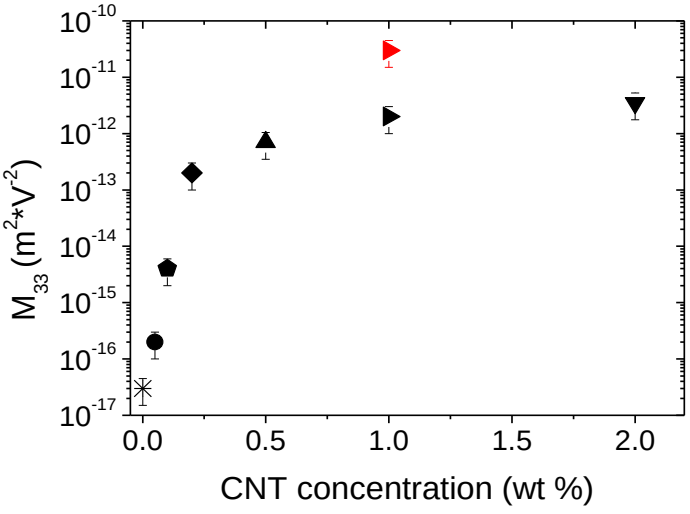

Figure 50: Absolute values of the electrostrictive coefficient M_{33}, as a function of different CNT concentrations: 0 wt% (cross), 0.05 wt% (circle), 0.1 wt% (pentagon), 0.2 wt% (diamond), 0.5 wt% (up triangle), 1 wt% (right triangles), and 2 wt% (down triangle). Red triangle shows the best result for our nanocomposites. The one decade difference between two samples at this concentration is explained by the large differences close to the percolation threshold. All measurements are performed at 100Hz.

function of the CNT concentration. The electrostrictive coefficient M_{33} varies with the CNT

concentration with an optimum at 1wt% CNT. The sample for which the CNT concentration is near the percolation threshold (1wt% CNT) yields the highest permittivity values ($\varepsilon_r' >$ 10000). The electrostrictive coefficient M_{33} of the latter sample is also the greatest and of about $1x10^{-11}m^2*V^{-2}$. The average value is calculated based on two different batches and for samples tested at 0.5 mm/min. We report two different values for M_{33} in the 1%wt CNT situation. These variations seem to be related to the use of two different batches. Slight differences of structure and chemical nature are enhanced in the percolation region. But even the lowest measured values remain exceptionally and above previously reported values for related materials [14-18].

3) *Determination of the electrostrictive coefficient M_{13} in actuator mode*

The following section is devoted in first place to the determination of the electrostrictive coefficient M_{13} as commonly done in the literature. Second, we will confront these values to the ones obtained using the more direct methodology. We study the deflection of the strip material when the electric field E is applied. The typical applied values for E are about 1V/μm and lead to the displacement of the strip (Figure 51 a and b). The bending is the result of the compression and expansion of the different layers when the electric field is applied. The strip deflection is determine using a millimeter range sheet place behind the strip. In order to verify the electrostrictive behavior of the nanocomposites, we measure the actuation response as a function of the amplitude of electrical field.

Figure 51 c shows the displacement of the strip as a function of the voltage U for a nanocomposite loaded with 0.2 wt% CNT. The displacement of the strip is proportional to U^2 regardless the frequency. We attribute the slight differences of theoretical curves corresponding to U^2 from the experimental points to uncertainties in the measurements of the maximal displacement itself. Henceforth, using the tip deflection we are able to determine the

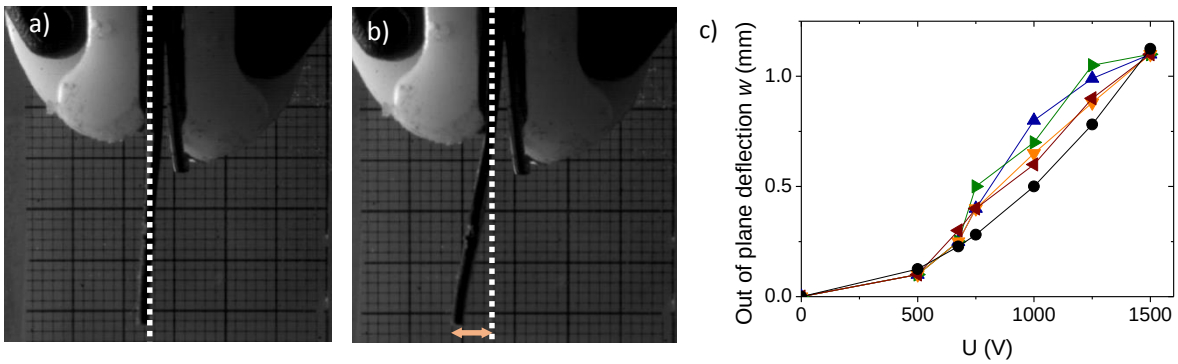

Figure 51: Comparison of the deflection of the bilayer composite tip under different voltages U: image a) corresponds to E=0 V while b) to E= 1x10³ V. The out of plane deflection w (pink arrow) enables the determination of the electrostrictive coefficient M_{13}.The small squares are 1mm side. c) The out of plane deflection of strip composites as a function of the applied voltage at different electrical frequencies for a 0.2 wt % CNT composite: Up triangle corresponds to 0.5Hz, right triangle to 1Hz, down triangle to 2.5Hz, left triangle to 7.5Hz and black circles to the square of the applied electric field

electrostrictive coefficient of the nanocomposite following Eq. 4. We obtain a mean value of $2.1x10^{-13}$ m^2*V^{-2}.

This value is about the same order of magnitude than M_{13} value reported by Deshmukh *et al* [17] for related materials, and at least one order of magnitude greater than values in other reports [13-18] (Figure 46).

We carried out similar experiments with other nanocomposite strips for non-percolated and percolated samples (i.e. 0.1 wt% and 0.5 wt%). We found out that the electrostrictive coefficient increases with the CNT concentration. The red circles in Figure 53 represent the M_{13} coefficient using the actuator mode. The values for 0.2wt% and 0.5wt% are about the same order of magnitude and among the best results compared to previous reports. As previously shown (section 2 *i*), the non-percolated CNT composites, such as 0.1wt%, are expected to present lower electrostriction coefficients compared to percolated samples. Actually the average M_{13} value measured in actuation mode is about $4.5x10^{-15}$ m^2/V^{-2}. This value is in very good agreement with the one reported above ($3.4x10^{-15}$ m^2/V^{-2}). We note that the PDMS is considered as an incompressible material (i.e. Poisson ratio ν=0.5). In this sense we expect to find similar values for the electrostrictive coefficient M_{13} and M_{33}.

Figure 52 shows the electrostrictive coefficient M as a function of the CNT for the actuator mode (i.e. M_{13}) and for the direct approach (i.e.M_{33}). We find that the values compare rather well. In addition we are able to determine the electrostrictive coefficient M_{33} of a blank material using the developed methodology. We remind that the principle of the actuation mode is based on the different response of each layer to the electric field. However, when it comes to the study of a bilayer of neat PDM and emulsion based composite with no CNT, the affinity is the too similar to induce any bending on the strip. The value of the M_{33} for the blank material (i.e. $1x10^{-17}$ m^2*V^{-2}) is about four orders of magnitude lower than the value of the percolated composites, and two orders of magnitude lower compared to the non-percolated. It is actually

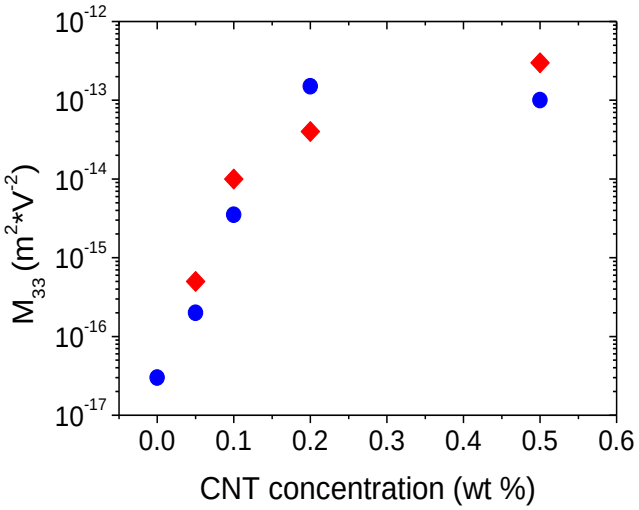

Figure 52: Electrostrictive coefficient M_{33} as function of the CNT concentration for two different compression speeds during the mechanical stress cycles: the red diamonds/blue circles correspond to a speed of 0.05 mm/min /0.5mm/min. All measures are performed at an electrical frequency of 100Hz

close to the electrostrictive coefficient of neat polymers such as PU ($7x10^{-17}$ m^2*V^{-2}) or PVDF ($8x10^{-18}$ m^2*V^{-2}) [8, 11].

We note that there is another possibility to prove the origin of the mechanism driving the actuation process. According to Wongtimnoi *et al* [6], the electrostrictive coefficient *M* is proportional to the dielectric constant and inversely proportional to the Young's modulus for materials for which $\varepsilon_r' \gg 1$

$$M_{13} \approx \frac{\varepsilon_0 * \varepsilon_r'}{Y} \tag{5}$$

Our calculations are in agreement with the latter approximation for all the samples tested using with both methodologies. Per instance, for the 0.1wt%CNT a value of 75 for the relative dielectric permittivity associated to a 0.1MPa for the Young's modulus lead to an accurate approximation of about 3.7 $x10^{-15}$ m^2*V^{-2}. We remind that the calculated value is 3.4 $x10^{-15}$ m^2*V^{-2}. As the deflection of the strip is proportional to the strain and the expression $M_{13} \approx \frac{\varepsilon_0*\varepsilon_r'}{Y}$ is validated, we assume that the Maxwell stress is negligible and the electromechanical response is dominated by pure electrostriction.

4) *Determination of the optimum electrostrictive coefficient M_{33}*

The dielectric permittivity is expected to show huge variations around the percolation threshold as seen in section 1. In addition the permittivity increases when the material is compressed. However, the interactions within the CNT network are related to the visco-elastic properties of the matrix. Hence, the electromechanical properties of the nanocomposites are expected to be time dependent [21]. We study of the dielectric properties for different CNT

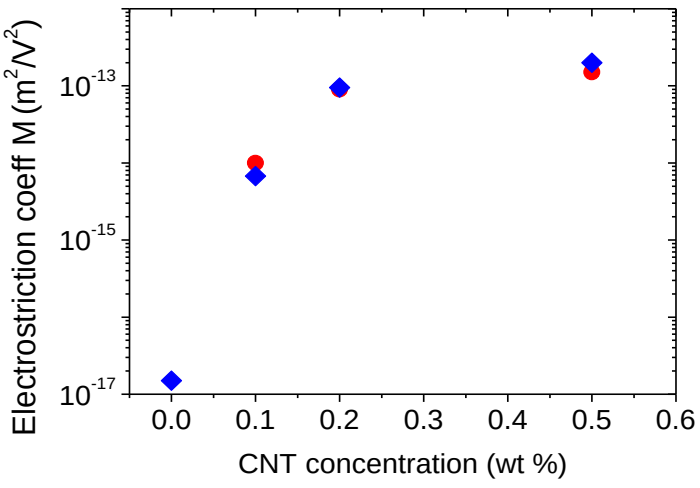

Figure 53: Comparison of the electrostrictive coefficient determine by two different set-up for different CNT concentrations. The blue diamonds correspond to the direct compression set-up (M_{33}) while the red circles correspond to the actuator set-up (M_{13}).

nanocomposites under the same mechanical stress for two different speeds of compression. Figure 53 shows the values of M_{33} for the above conditions of compression but at different rates with cycles at 15 mHz (i.e. 0.05mm/min) and cycles at 50 mHz (i.e. 0.5 mm/min).

The experimental points for each CNT concentration compare very well. An increase of the mechanical frequency by a factor 10 has no significative impact on the electrostriction coefficient M_{33} in the investigated frequency range. However, we note that we were limited by the traction machine to increase the mechanical frequency. It is clear that much lower or much greater frequencies would certainly lead to differences as observed in other studies [22].

IV. Conclusion

We developed an accurate and simple methodology to determine the electrostrictive coefficient in compression mode. This methodology enables the study of dielectric properties as a function of time when the material is subjected to a varying mechanical stress. It has been proven that emulsion based nano-composites present unprecedentedly high electrostrictive coefficients along with a decrease of electrical losses compared to the state of the art. Further studies are necessary to fully understand the involved microscopic mechanisms.

The above materials show very promising properties to develop energy harvesting devices but studies at higher mechanical frequencies are needed to validate their potential. In addition, the relatively high values of the electrical conductivity might be a critical drawback to efficiently harvest mechanical energy.

References

1. Ren, K, Y Liu, H Hofmann, et Q.M. Zhang. « An active energy harvesting scheme with an electroactive polymer ».Appl. Phys. Lett. 91, 132910 2007

2. Jean-Mistral, C., S. Basrour, et J.-J. Chaillout. « Comparison of Electroactive Polymers for Energy Scavenging Applications ». Smart Materials and Structures 19, nº 8 (6 juillet 2010): 085012. doi:10.1088/0964-1726/19/8/085012.

3. Liu, Liwu, Yanju Liu, Zhen Zhang, Bo Li, et Jinsong Leng. « Electromechanical stability of electro-active silicone filled with high permittivity particles undergoing large deformation ». Smart Materials and Structures 19, nº 11 (4 octobre 2010): 115025. doi:10.1088/0964-1726/19/11/115025.

4. Guyomar, D., P.-J. Cottinet, L. Lebrun, C. Putson, K. Yuse, M. Kanda, et Y. Nishi. « The Compressive Electrical Field Electrostrictive Coefficient M33 of Electroactive Polymer Composites and Its Saturation versus Electrical Field, Polymer Thickness, Frequency, and Fillers ». Polymers for Advanced Technologies 23, nº 6 (1 juin 2012): 946-50

5. Park Cheol, Kang Jin Ho, Harrison, Joycelyn S. Costen Robert C. ,and Lowther Sharon E. «Actuating Single Wall Carbon Nanotube–Polymer Composites: Intrinsic Unimorphs» Adv. Mater. 2008, 20, 2074–2079 DOI: 10.1002/adma.200702566

6. K. Wongtimnoi, B. Guiffard, A. Bigner-Van de Moortele, L. Severyrat, C Gauthier, J.Y. Cavaille « Improvement of electrostrictive properties of a polyether-based polyurethane elastomer filled with conductive carbon black - 1-s2.0-S0266353811000704-main.pdf ».K. Composites Science and Technology 71 (2011) 885–89.

7. Kofod G, Sommer-Larsen P, Kornbluh R, Pelrine R. Actuationresponse of polyacrylate dielectric elastomers. J Intell Mater SystStruct 2003;14:787–93.

8. Guillot, F. M., et E. Balizer. « Electrostrictive Effect in Polyurethanes ». Journal of Applied Polymer Science 89, nº 2 (11 juillet 2003): 399-404. doi:10.1002/app.12096.

9. Zhao X, Suo Z. Electrostriction in elastic dielectrics undergoing large deformation. J Appl Phys 2008;104, 123530/1–7.

10. Cheng, Z.-Y., Vivek Bharti, T.-B. Xu, Shexi Wang, Q. M. Zhang, T. Ramotowski, F. Tito, et R. Ting. « Transverse strain responses in electrostrictive poly(vinylidene fluoride-trifluoroethylene) films and development of a dilatometer for the measurement ». Journal of Applied Physics 86, nº 4 (1999): 2208-14.

11. Huang, C., R. Klein, Feng Xia, H. Li, Q.M. Zhang, F. Bauer, et Z.Y. Cheng. « Poly(vinylidene fluoride-trifluoroethylene) based high performance electroactive polymers ». IEEE Transactions on Dielectrics and Electrical Insulation 11, nº 2 (avril 2004): 299-311. doi:10.1109/TDEI.2004.1285901.

12. Zhang, Q. M., J. Su, Chy Hyung Kim, R. Ting, et Rodger Capps. « An experimental investigation of electromechanical responses in a polyurethane elastomer ». Journal of Applied Physics 81, nº 6 (15 mars 1997): 2770-76. doi:10.1063/1.363981.

13. Guiffard, B.; Seveyrat, L.; Sebald, G.; Guyomar, D. J. Phys. Enhanced electric field-induced strain in non-percolative carbon nanopowder/polyurethane composites Appl. Phys. 2006, 39, 3053–3057.

14. Cottinet, P.-J., Guyomar, D., Guiffard, B., Putson, C., and Lebrun, L.,. (2010). Modeling and Experimentation on an Electrostrictive Polymer Composite for Energy Harvesting IEEE Transactions on ultrasonics, ferroelectrics, and frequency control, Vol. 57, No. 4, pp., 0885-3010.

15. Park, Cheol, Zoubeida Ounaies, Kent A Watson, Roy E Crooks, Joseph Smith Jr., Sharon E Lowther, John W Connell, Emilie J Siochi, Joycelyn S Harrison, et Terry L. St Clair. « Dispersion of single wall carbon nanotubes by in situ polymerization under sonication ». Chemical Physics Letters 364, n° 3-4 (2002): 303-8.

16. Wise, Kristopher E., Cheol Park, Emilie J. Siochi, et Joycelyn S. Harrison. « Stable dispersion of single wall carbon nanotubes in polyimide: the role of noncovalent interactions ». Chemical Physics Letters 391, n° 4-6 (2004): 207-11.

17. Deshmukh, Sujay, et Zoubeida Ounaies. « Single walled carbon nanotube (SWNT)–polyimide nanocomposites as electrostrictive materials ». Sensors and Actuators A: Physical 155, n° 2 (octobre 2009): 246-52. doi:10.1016/j.sna.2009.07.007.

18. Z. Ounaies, C. Park, K.E. Wise, E.J. Siochi, J.S. Harrison Electrical properties of single wall carbon nanotube reinforced polyimide composites Compos. Sci. Technol., 63 (11) (2003), pp. 1637–1646

19. Singer, Ferdinand L. «Strength of Materials», Harper &Bros. , 1951, 469

20. Johnston, I. D., D. K. McCluskey, C. K. L. Tan, et M. C. Tracey. « Mechanical Characterization of Bulk Sylgard 184 for Microfluidics and Microengineering ». Journal of Micromechanics and Microengineering 24, no 3 , 2014 035017.

21. F Schneider, T Fellner, J Wilde and U Wallrabe "Mechanical properties of silicones for MEMS " J. Micromech. Microeng. 18 (2008) 065008 (9pp) doi:10.1088/0960-1317/18/6/065008

24. Sabu Thomas, Gennady Zaikov, Valsaraj "Recent Advances in Polymer Nanocomposites" CRC Press, Mar 17, 2009 - Technology & Engineering - 528 pages

23. J. Yuan, A. Luna, W. Neri, C. Zakri, T. Schilling, A. Colin, P. Poulin "Graphene Liquid Crystal Retarded Percolation for New High-k Materials" Nat Commun,-15-09449B)

-We developed an innovative technique enabling the direct assessment of the electrostrictive coefficient during mechanical stress without tedious sample preparation. The results delivered by this technique were corroborated using an actuator approach.

-We developed nanocomposite materials that yield unprecedentedly high electrostrictive coefficient $M_{33} \approx 1x10^{-11} m^2/V^2$ *and can be considered as serous candidates to energy harvesting devices.*

-The latter materials are sensitive to the mechanical stress due to a finely controlled CNT inner structure obtained by the emulsion approach. Due to this sensitivity the samples are used as actuator and sensors. It has been prove their sensibility to force, strain and electric field.

Chapter VI

Characterization of bilayers composites for the improvement of electrostrictive properties

I. Introduction

1) Bulk materials with high dielectric permittivity materials

Organic nanoparticles, such as CNT and graphene oxide platelets are known for their remarkable properties in terms of mechanical strength, elasticity, electrical and thermal conductivity, gas impermeability, environmental stability [1-2]. Henceforth these particles are used to provide and increase electrical conductivity properties of polymers. We have shown in the previous chapters that the structuration, concentration and even morphology of the nanoparticle network alter strongly the dielectric properties of composite materials. However, we also pointed out that in spite of a fine control over the inner conductive particle network, we are not yet able to overcome certain barriers using the emulsion approach. In particular it remains critical to limit dielectric and conductivity losses for efficient energy harvesting. This difficulty is a general bottleneck found in related materials reported in the literature. Figure 54 shows the best results reported in the literature in terms of high dielectric permittivity and low electrical conductivity. Optimal compromises of properties for most CNT composites [3-6], and r-GO composites [7-10] lie below a line shown by a grey dashed line in the graph of Figure 54. Data points for emulsion based composites lie above this line, displaying thereby a potential for more efficient energy harvesting. It is also interesting to note that materials made by Aguilar *et al* [11] using a particular *ex-situ* reduction of r-GO composites, and GO papers described further in this chapter, exhibit properties that differ strongly from those of other nanocomposites.

These systems indeed display an extremely high permittivity for a conductivity of about 10^{-2} S/m. This conductivity level remains rather high and the implementation of the materials in actual devices to exploit their giant permittivity may not be straightforward. This is why other

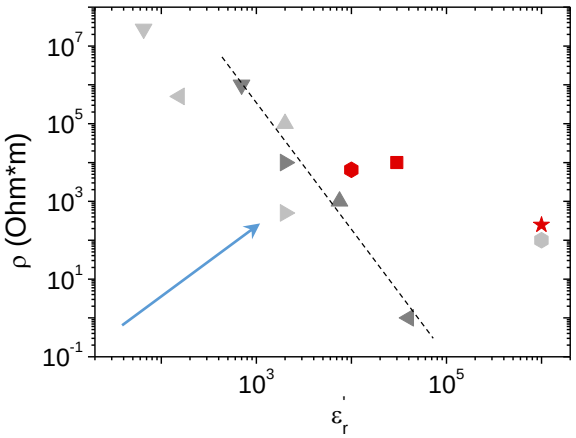

Figure 54: Comparison of properties of carbon filler based composites materials. The blue arrow indicates the direction towards high permittivities and low electrical losses. Dark grey symbols represent CNT composites: up triangle [3], left triangle [4], down triangle [5] and right triangle [6]. Light grey points correspond to GO composites: down triangle [7], left triangle [8], up triangle [9], right triangle [10] and circle [11]. The red points correspond to the best emulsion based nanocomposites: circle (GO) and square (CNT). The red star correspond to the GO paper. All the data measurements correspond to measurements at 100Hz.

approaches to limit losses still deserve a particular attention. To address this challenge, we explore in this chapter the possibility to combine different layers of materials instead of varying the structure or chemical composition of a single material.

2) Bilayer materials with high capacitance variations

Lallart *et al.* [12] proposed an approach to improve variable capacitors using a two layers system composed by a high permittivity material and a low permittivity, easily deformable, layer of variable thickness. This latter can in fact simply consist in an air gap. Figure 55 shows the scheme of the developed system which enables huge changes of capacitance in response to thickness variations. Similar changes of capacitances can be obtained with emulsion based nanocomposites, but the latter materials suffer from large losses. This is why, in the spirit of the work by Lallart *et al.*[12] we presently combine two layers of materials with distinct dielectric properties.

In order to prepare the bilayer structure we proceed as follows. The first layer is an electrostrictive material made through the emulsion approach (Figure 56a). The second layer is made of a dielectric polymer or of graphene oxide film. This second layer is deposited by spin coating or drop casting of polymer or GO solutions. Very thin layers are made in order to achieve high capacitances (Figure 56b). Each layer can be represented by an equivalent electrical circuit. The thin layer of dielectric polymer (respectively GO) will be considered in the following as a layer with a capacitance C_1 (respectively C'_1).

The electrostrictive material will be represented by a resistor-capacitor, RC_2, electrical circuit in parallel (see Figure 56a). The equivalent circuit for the bilayer structure is a capacitor C_1 or C'_1 in series with a parallel RC_2. The electrostrictive material is formulated to be as sensitive as possible to the mechanical stress so its electrical properties strongly change with the mechanical strain. When no strain is applied, the present electrostrictive material acts as an electrical insulator. In other words its resistance is very high. In such conditions, the equivalent circuit for the bilayer structure can be simply viewed as two capacitors in series (C_2 in series with C_1 or C'_1). The value of the equivalent capacitor C_{eq} is close to the capacitor with the lowest capacitance value (see Figure 56c). On the other hand, when deformed, the electrostrictive material displays an increase of permittivity but also of conductivity. It switches from an insulating to a conductive state. In fact, this is the piezoresistive behavior of the material which

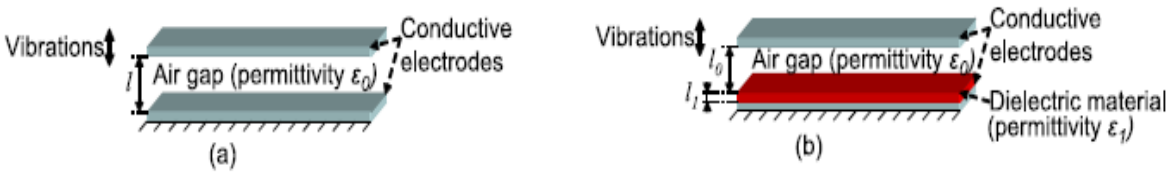

Figure 55: Electrostatic energy harvesting using a classical approach (a) and an energy conversion enhancement using a bilayer structure (b). Lallart et al [13]

is here at play. The equivalent circuit for the bilayer structure is henceforth a resistor R, in series with a capacitor C_1 or C'_1. Such a mechanical sensitive structure enables high capacitance variations due to the interchange between the different capacitance values. We expect that these variations can compare or exceed variations provided by single electrostrictive materials and at the same time provide a reduction of losses. In order to check the possibility of such improvements, we will first study the electrostrictive material alone. Afterwards, we will study the same electrostrictive material but with the thin dielectric layer on top.

The present chapter is structured as follows. The second section is devoted to the description of the materials and methods employed for the development of bilayer structures. The third section is focused on the characterizations of the material properties. This section is subdivided in four parts. The first one deals with the study of the self-standing GO films. The second and third parts are devoted to the impact of the nature of the upper layer on the electrostrictive properties of the bilayer. We study the cases of GO films and of a thin PVA layer. The fourth deals with the discussion about the potential of such systems for energy harvesting applications.

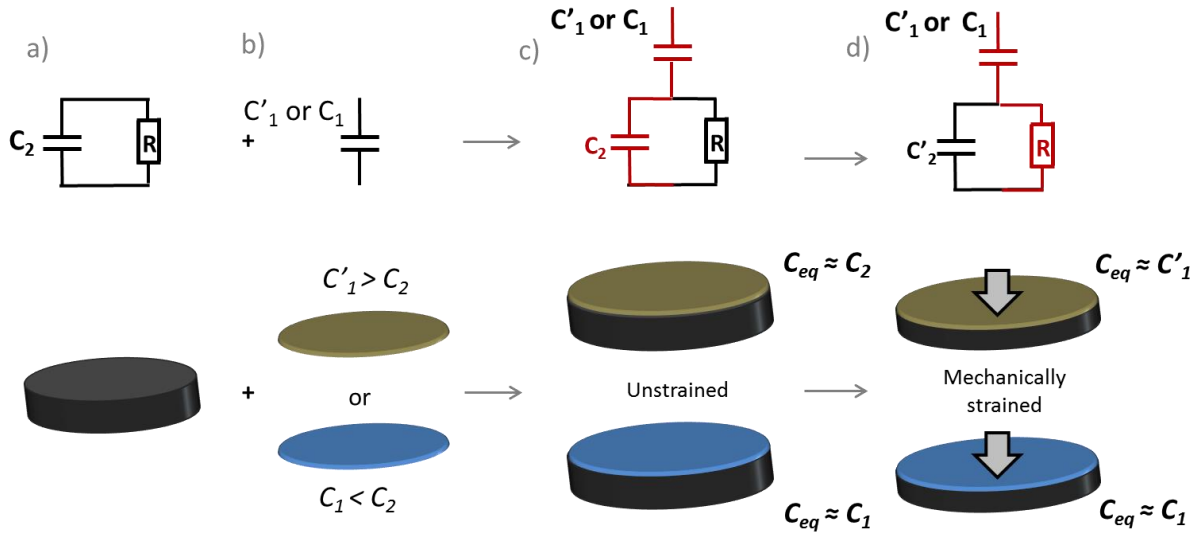

Figure 56: Scheme of the composition of the bilayer structure composite material: a) the black block represents the composite material prepared with a polymer matrix and anisotropic conductive particle. b) Blue and brown disk presents a thin-layer of polymer and graphene oxide respectively. The electrical properties of the bilayer composite material change when subjected to a mechanical strain. It can acts as a capacitor c) or as resistor d). The upper part shows the equivalent electronic circuit for each material and situation.

II. Materials and methods

1) Materials

The so called bilayer systems are composed of a layer of a dielectric material and of an electrostrictive/piezoresistive composite produced via an emulsion approach. We choose a 1wt% CNT composite because of its huge variations of electrical conductivity in response to a mechanical stress (Chap V).

Two different materials are used as the dielectric layer. The first material is the polyvinyl alcohol (PVA), which is a polymer with a low dielectric permittivity. The polymer is purchased from Sigma Aldrich (Mowiol $M_w \approx 195k$) and is dissolved in water to prepare an aqueous solution of about 8wt% PVA. The second material is an aqueous dispersion of graphene oxide (GO) platelets, which holds high dielectric permittivity when prepared as a GO paper. GO paper is a thin GO film simply obtained upon drying a GO solution. The GO dispersion is purchased from Graphenea (GO concentration of 0.4wt %).

2) Methods

We choose two materials with very different permittivities to be associated with the sensitive emulsion based composites, and to test the concept of bilayer systems. PVA, by contrast to GO paper, exhibit a low relative permittivity of about 7.5 and $5x10^{-8}$ S/m at 100Hz [13].

We study the impact of the processing conditions on the dielectric properties of GO paper to determine an optimized procedure. GO paper is obtained by drop casting 8g of the Graphenea solution in 2mm deep Ø 40mm circular Teflon molds. We prepare a self-standing GO paper at 30°C under 30%RH for 8h defining the so called "controlled" conditions. The self-standing films are then used to measure the dielectric properties of GO layer.

The GO and PVA layers used in the bilayer systems are prepared using a same methodology. The upper layer is obtained by drop casting 2mL of the PVA or GO solution. The final dielectric layers are obtained by evaporating the excess water at 30°C under 30%RH for 8h. The dielectric and electrostrictive properties are studied using the direct approach described previously (Chapter II and V). We performed the electrostrictive measurements using the same parameters: mechanical strain of about 8%, speed of 0.5mm/min, applying 1V at 100Hz to Ø 40mm diameter sample.

III. Results and Discussions

1) Study of the dielectric properties of the GO upper layer

GO paper materials have developed by casting the GO dispersion. We manufacture a self-standing GO paper by gently evaporating the water of the dispersion. Note that the GO paper can exhibit nematic-liquid crystal behavior during the evaporation process when the GO dispersion is highly concentrated and can form liquid-crystal phases [14]. After water removal, the GO sheets are restructured in a quasi-parallel configuration layer to form a GO paper. Figure 57 shows clearly the lamellar structure.

The mechanical properties of GO paper are particularly interesting. The Young's modulus is about 30 GPa and an ultimate tensile strain of only 0.6% [15]. However in spite it brittleness and high strength, the GO self-standing paper is a very flexible material. As a matter of fact, the bending of the GO paper is due to the slippage and delamination between GO sheets.

Figure 58 shows the a) dielectric permittivity and b) electrical conductivity as a function of the frequency for the GO paper. The permittivity at 100Hz is about $1x10^6$ which is particularly high. It is about two orders of magnitude higher than the state if the arte electrostrictive materials. We note that the permittivity is frequency dependent and the values at high frequency (1MHz) can decrease to a permittivity of about 70. The increase of the permittivity is followed by an increase of the conductivity. Values are ranging from $3x10^{-3}$ S/m at 100Hz to 0.5 S/m at 1MHz. The change of slope on the conductivity curves is the signature of a change of electrical conduction regime. The frequency independence regime (from 1MHz to 10 kHz) is a signature of a conductivity driven by free charges carrier.

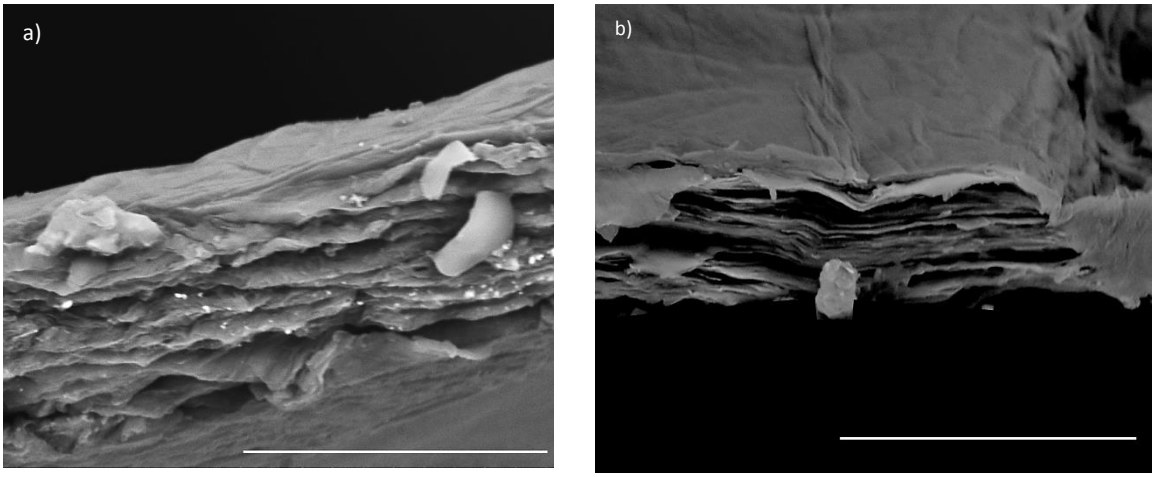

Figure 57: SEM images for a GO paper-like material from two different GO aqueous dispersions a) diluted and b) concentrated. The materials are performed under "controlled" temperature and relative humidity conditions. The scale bar represents 20µm (a) and 30µm (b). The average thickness of the self-standing material is about 10µm.

Inversely, the frequency dependence regime (10 kHz to 100Hz) is attributed to bound charges carrier. We remind, that the free charges are assimilate to electrical losses and increases with the conductivity. In analogy with a capacitor, the ability of a material to accumulate charges is inversely proportional to the distance between to plates. In the case of GO paper each GO sheet is assimilated to micro in quasi parallel configuration. The submicron confinement shown in Figure 57 of the GO sheets creates nano-capacitors which yield to high capacitance and dielectric permittivity.

It has been proved once again that the increase of the permittivity is inexorable followed by an increase of the conductivity, which is clearly a barrier for energy harvesting devices. To overcome to such a problem, we expect propose to produce a bilayer system which yields huge variation of capacitance by interchanging the capacitance of two different layers when compressed. We recall that optimized formulas of the electrostrictive materials (Chap V) are very sensitive to the mechanical stress. The electrical conductivity is increased when the material is compressed and induces by it piezoresistivity behavior. The latter behavior enables to probe any material lay on the top of the electrostrictive material. The bilayer system acts as an actual mechanical switch and as compliant electrode when compressed.

To study such a proof of principle we propose two study two different thin upper layer that are attached to the electrostrictive material. The first one a good insulator layer such as PVA and a conductive layer more conductive layer displaying permittivity values such as the GO paper. The best result will be considered as the one displaying the highest electrostrictive for the least electrical conductivity. We first study the electromechanical properties of the electrostrictive material and second we study the electromechanical properties of the bilayer composite conceived with a PVA (respectively GO) layer on top.

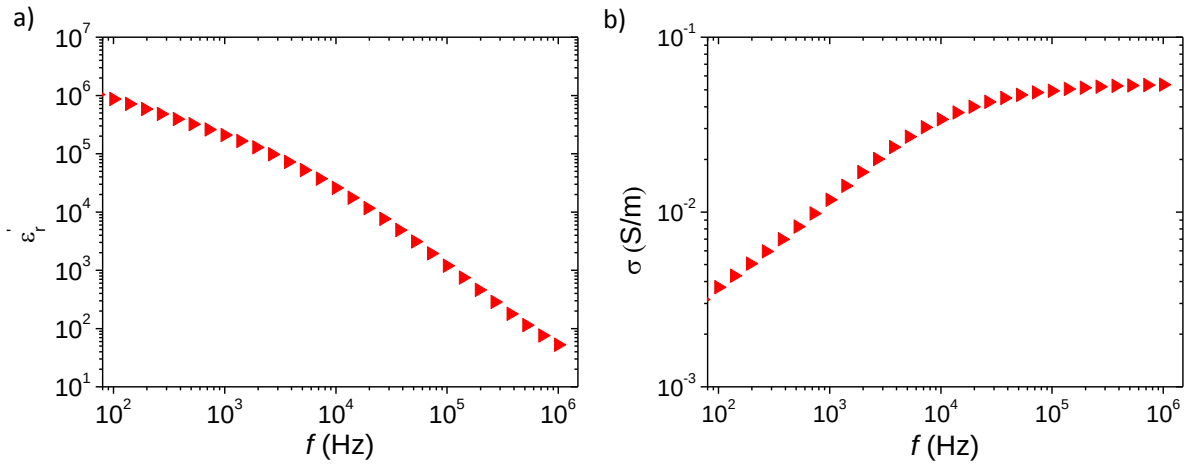

Figure 58: Relative dielectric permittivity ε_r' (a), and the electrical conductivity σ (b) as a function of the frequency. The blue circle represents the properties of the self-standing GO paper under "controlled" evaporation, while the green triangles represent the self-standing GO paper under "fast" evaporation. The red circles represent the bilayer sandwich composite which is a combination of thin GO paper and CNT based composites (black circles).

2) Study of the electrostrictive properties of the bilayer nanocomposites

i. Nanocomposite using PVA as the upper layer

The electrostrictive as well as the bilayer latter materials were subjected to the same mechanical stress which is about $1x10^4$ N/m^2 and which corresponds to a strain of about 8%. (Figure 59a). Note that no significant increase of the Young's modulus is observed when the PVA layer is added.

When the electrostrictive material is compressed the dielectric constant increases Figure 59b. This behavior is in accordance with the geometrical variation of a variable capacitor. The same behavior is observed for the bilayer structure. However the absolute variation is decreased by a factor of 2. In the case of the electrostrictive material $\Delta\varepsilon_r'$ is about 700 while for the bilayer 300. In addition, the initial (at t=0s) permittivity for the bilayer is lower. As a matter of fact the equivalent electric model of the two layer material is assimilated to RC in parallel with a capacitor in series. Herein the equivalent capacitance is about the same order of magnitude as the one of the PVA layer (i.e. 10), rather than the one of the electrostrictive material (i.e. 300) (Figure 59). Note that the relative variation of the permittivity for the bilayer material (about a factor of four) is higher than the one shown by the electrostrictive material (about a factor of two).

The decrease of the permittivity is followed by the decrease of the electrical conductivity. Figure 59 c shows that at rest (t=0s) the conductivity of the electrostrictive is high and about $5x10^{-6}$ S/m, while the one of the bilayer is decreased down to $7x10^{-8}$ S/m. When the bilayer is compressed the highest value of conductivity remains lower than the initial conductivity of the electrostrictive material. When the bilayer is uncompressed, the conductivity decreases again. The mechanical cycling is reflected on the dielectric properties the bilayer acts as predicted.

This is a very promising result since the variation of the permittivity are about the same order of magnitude $\Delta\varepsilon_r'$ few hundred's but the conductivity is considerably lowered. Taking into account these variations and the mechanical stress applied, we are able to determine the electrostrictive coefficient M_{33}. We note that the latter coefficient is about one orders of magnitude higher for the electrostrictive (i.e. $M_{33} \approx 4.5x10^{-12}$ m^2*V^{-2}) than for the bilayer (i.e. $M_{33} \approx 3x10^{-13}$ m^{2}V^{-2}) for the bilayer. However the value of the M_{33} coefficient for the bilayer material is as high as the one reported in the state of the art works. More important is the decrease of the electrical losses by at least two orders of magnitude. It has been demonstrated that the electrostrictive material can probe an upper layer of a pure dielectric polymer.

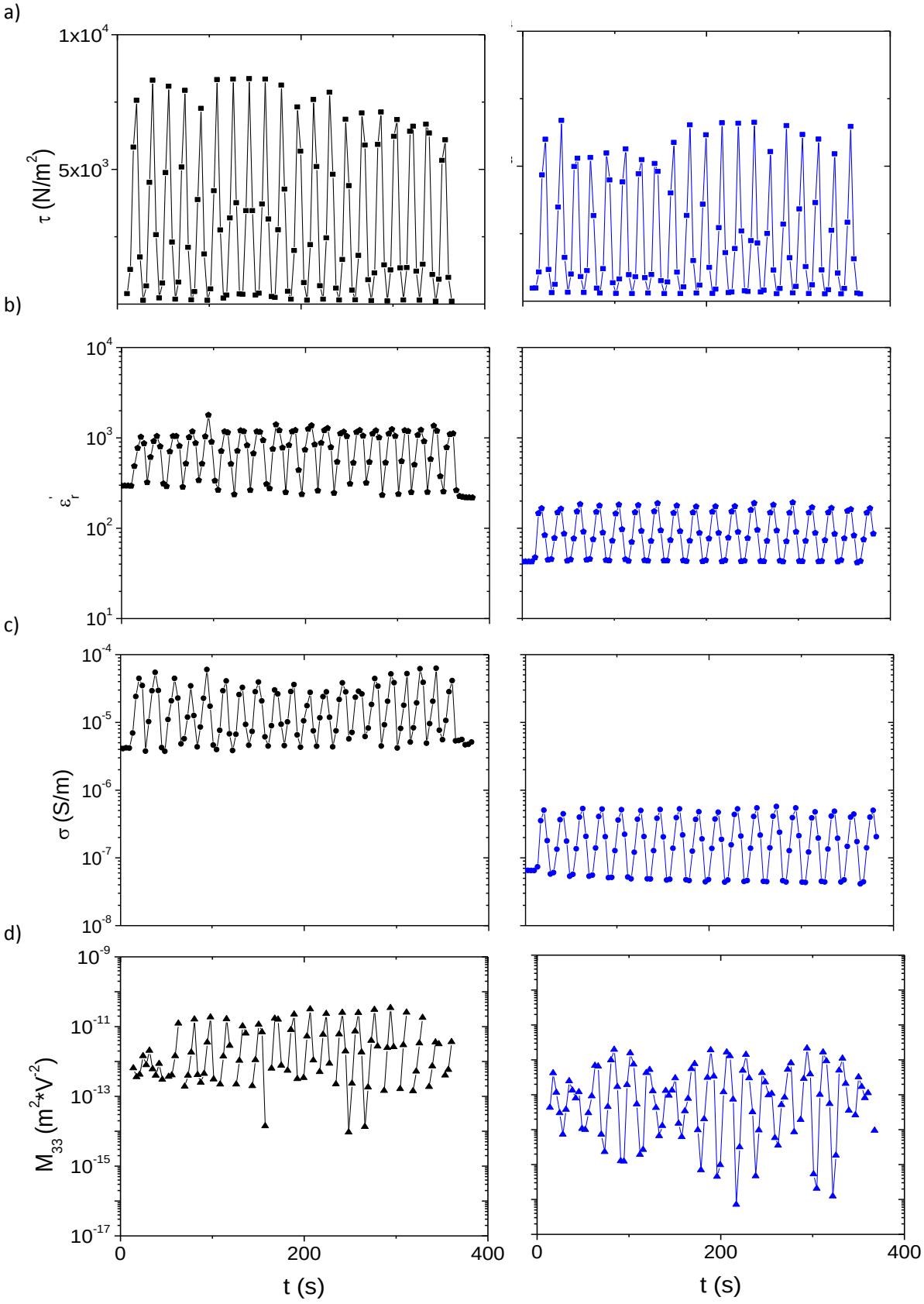

Figure 59: We apply a a) mechanical stress to a nanocomposite material loaded with 1wt%CNT (black points) and to the latter material with an upper layer of PVA (blue points) in order to study the variation of its b) dielectric permittivity, c) electrical conductivity. The latter variations enables the determination of d) the electrostrictive coefficient of each material.

ii. Nanocomposite using GO as the upper layer

In this second we choose to study the electromechanical properties of an electrostrictive for and a bilayer using the latter material with a thin layer of GO on top. We recall that the addition of the GO paper is conceived to increase the variation in terms of permittivity and electrical conductivity. Figure 60 a shows that the addition of the GO thin layer has not any variation on the mechanical properties of the electrostrictive material. Hence, the mechanical stress is about the same value (i.e. $5x10^3$ $N*m^{-2}$) for electrostrictive (black points) and the bilayer material (green points).

The compression of the electrostrictive material provokes an increase of the dielectric permittivity. The absolute variation is about $\Delta\varepsilon_r'$ few thousand's for both materials. However, we note that the variations of the bilayer material (i.e. 3000) are slightly higher than the ones of the electrostrictive material (i.e. 2000). The variation comes from the fact that 1wt%CNT is closed to the percolation threshold and yields huge but different variations in spite the same CNT concentration. The relative variation for the electrostrictive is about a factor of four while for the bilayer is about a factor of ten.

On the other hand, the conductivity of the electrostrictive material is about 10^{-5} S/m and when the material is compressed the maximum value is about one order of magnitude higher (i.e. 10^{-4} S/m). This phenomenon is due to the piezoresistive behavior of the electrostrictive material. In the other hand, the bilayer material decrease slightly the conductivity however is remains about the same order of magnitude. In fact the GO paper acts as a high permittivity layer but it does not allow to decreases the electric losses.

The electrostrictive coefficient is calculated as a function of time for the electrostrictive material (i.e. $4x10^{-12}$ m^2*V^{-2}) and for the bilayer material (i.e. $5x10^{-12}$ m^2*V^{-2}). The addition of a GO thin layer on the electrostrictive material doesn't increase significantly the electrostrictive coefficient or neither the electrical conductivity.

The addition of the GO paper is not a real advantage because we obtain basically the about the values compared to the electrostrictive material. In this sense the barriers are not overcome using a high permittivity values due to the increase of electrical losses as well.

The bilayer methodology enables to overcome a difficult barrier in terms of electromechanical properties when the proper layer is used, herein a PVA layer. We are able to keep unchanged the mechanical properties of the emulsion based nanocomposite by keeping the variation of the permittivity and reducing the electrical conductivity. We recall that in general the increase of the permittivity, due to the polarization between conductive charges and insulator matrix, is followed by an increase of the electrical conductivity.

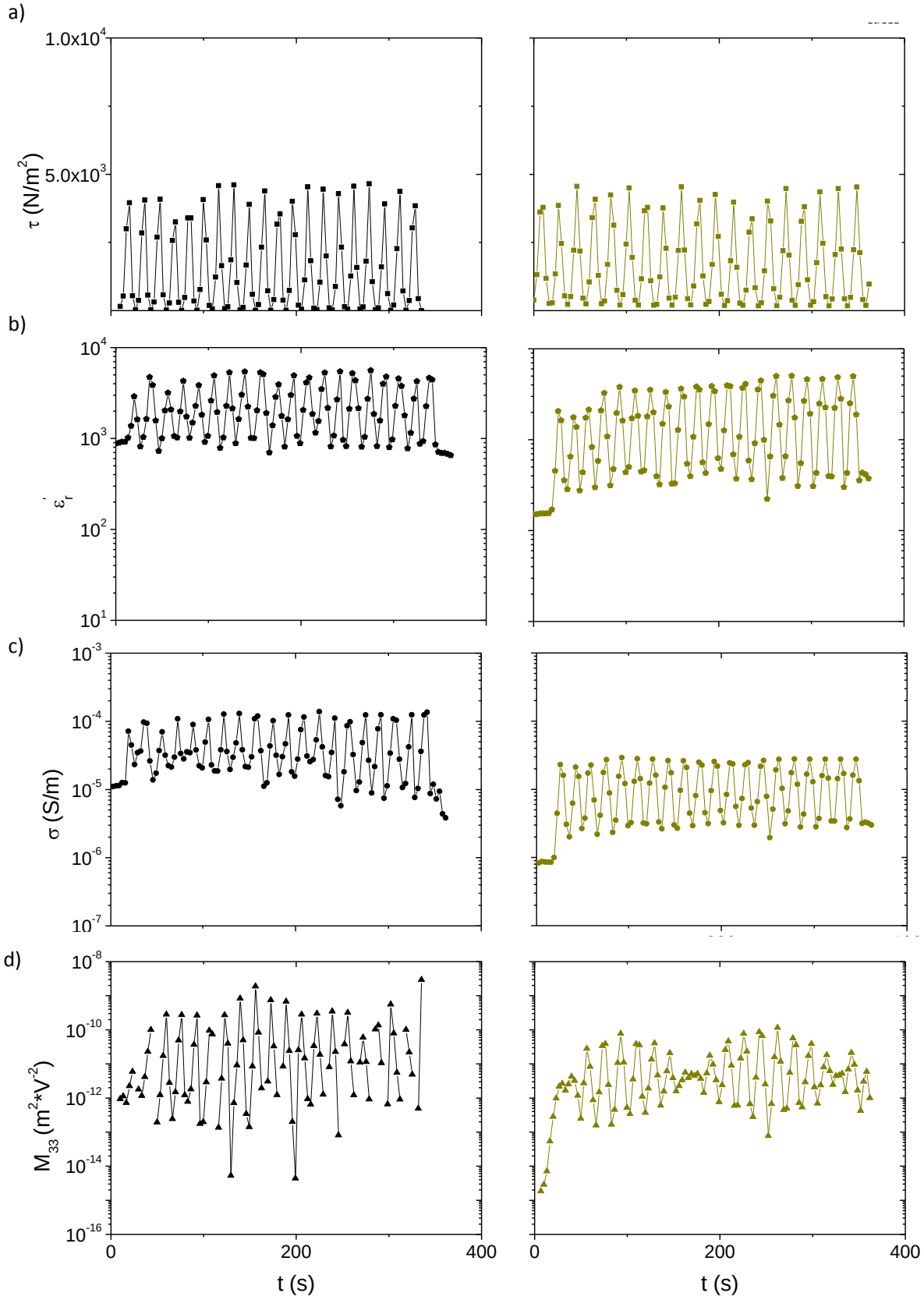

Figure 60: We apply a a) mechanical stress to a nanocomposite material loaded with 1wt%CNT (black points) and to the latter material with an upper layer of GO (green points) in order to study the variation of its b) dielectric permittivity, c) electrical conductivity. The latter variations enables the determination of d) the electrostrictive coefficient of each material.

IV. Conclusion

In this chapter, we have proved the interest of structuring the internal GO network of the composites employing the emulsion approach. Besides the values of the ratio dielectric permittivity/electrical conductivity achieved by the emulsion approach are among the best reported results on the literature.

The high permittivity was driven by the lamellar structuration of the GO platelets within the GO paper. The length scale of the inter-platelet distance and roughness are at the nanometer and micrometer scale. Thus, if we consider the GO platelets as plates of electrodes, this small distance explains the high permittivity $\varepsilon_r' = 10^6$.

The high permittivity values present GO-paper material as an excellent candidate for dielectric membranes, semi-conductor application and electrostrictive or energy harvesting devices. However, we believe it high conductivity remains an important bottleneck.

We successfully developed a bilayer material that is able to induced high variation of permittivity and lowered the electric conductivity. The electrostrictive material is used as a switch that reacts to the mechanical stress and modifies its dielectric properties. The selection of a proper upper layer enables to bypass certain barriers, very difficult to overcome with classic approaches. Thus, when the PVA is used as the upper layer of the bilayer material, we are able to keep the same electrostrictive coefficient but reducing the electrical losses when the material is subjected to a dynamic mechanical stress. Inversely when the GO paper doesn't allow such performances since the permittivity and the conductivity decreases.

References

1. *J. N. Coleman, U. Khan, W.J. Blau, Y. K. Gun'ko "Small but strong: A review of the mechanical properties of carbon nanotube–polymer composites" Carbon 44 (2006) 1624–1652*

2. *T. Kuilla, S. Bhadra, D.Yao, N-H. Kim, S. Bose, J.-H. Lee, "Recent advances in graphene based polymer composites" Progress in Polymer Science 35 (2010) 1350–1375*

3. *Dang, Z. M.; Wang, L.; Yin, Y.; Zhang, Q.; Lei, Q. Q., "Giant dielectric permittivities in functionalized carbon-nanotube/electroactive-polymer nanocomposites." Advanced Materials 2007, 19 (6), 852.*

4. *N. K. Shrivastava, B.B. Khatua "Development of electrical conductivity with minimum possible percolation threshold in multi-wall carbon nanotube/polystyrene composites" Carbon 49, 2011 4571–4579*

5. *Chanmal, C.; Deo, M.; Jog, J., "Enhanced dielectric permittivity in poly (vinylidene) fluoride/multiwalled carbon nanotubes nanocomposite thin films fabricated by pulsed laser deposition". Applied Surface Science 2011, 258 (3), 1256-1260.*

6. *Yuan, J. K.; Yao, S. H.; Dang, Z. M.; Sylvestre, A.; Genestoux, M.; Bai, J. B., "Giant Dielectric Permittivity Nanocomposites: Realizing True Potential of Pristine Carbon Nanotubes in Polyvinylidene Fluoride Matrix through an Enhanced Interfacial Interaction." Journal of Physical Chemistry C 2011, 115 (13), 5515-5521.*

7. *W. Tong, Y. Zhang, Q. Zhang, X.Luan, Y. Duan, S. Pan, F. Lv, and Qi An. « Achieving Significantly Enhanced Dielectric Performance of Reduced Graphene Oxide/polymer Composite by Covalent Modification of Graphene Oxide Surface ». Carbon 94 (novembre 2015): 590-98.*

8. *K. Deshmukh, M.A. Basheer, S.K.P. Khadheer, R. R. Deshmukh, and P. R. Bhagat. « Highly Dispersible Graphene Oxide Reinforced Polypyrrole/polyvinyl Alcohol Blend Nanocomposites with High Dielectric Constant and Low Dielectric Loss ». RSC Adv. 5, n° 76 (16 juillet 2015): 61933-45.*

9. *D.Li, M. B. Müller, S. Gilje, R. B. Kaner, and G. G. Wallace. "Processable Aqueous Dispersions of Graphene Nanosheets." Nature Nanotechnology 3, 101 - 105 (2008)*

10. *D.Wang, X.Zhang, Z. Jun-Wei, Z.Jun, Zhi-Min Dang, and Guo-Hua Hu. « Dielectric properties of reduced graphene oxide/polypropylene composites with ultralow percolation threshold ». Polymer 54, n° 7 (2013): 1916-22.*

11. *H. Aguilar-Bolados, M.A. Lopez-Manchado, J. Brasero, F. Avilés, and M. Yazdani-Pedram. « Effect of the morphology of thermally reduced graphite oxide on the mechanical and electrical properties of natural rubber nanocomposites ». Composites Part B: Engineering. 2015.*

12. *Lallart M., Cottinet P.J., Guyomar D., Lebrun L. "Electrostatic Polymers for Mechanical Energy Harvesting Journal of Polymer Sciencence part B: polymer Physics 2012, 50, 523–535*

13. *J. Zhang, M. Minea D. Zhua M. Matsuo , « Electrical and dielectric behaviors and their origins in the three-dimensional polyvinyl alcohol/MWCNT composites with low percolation threshold ». Carbon Volume 47, Issue 5, April 2009, Pages 1311–1320*

14. *J. Yuan, A. Luna, W. Neri, C. Zakri, T. Schilling, A. Colin, P. Poulin,"Graphene Liquid Crystal Retarded Percolation for New High-k Materials " Nature Communications 6, 8700,*

15. *A. Dikin, S; Stankovich, E. J. Zimney, R. D. Piner, G. H. B. Dommett, G.Evmenenko, S.T. Nguyen, and R. S. Ruoff."Preparation and Characterization of Graphene Oxide Paper." Nature 448, no 7152 (2007).*

-We found out that under optimized condition the synthesized GO self-standing paper shows dielectric permittivity as high as ε'_r 10^6 *at 100Hz but also high electrical conductivity. Such properties are explained by the small distances in between the GO platelet within the GO paper.*

-In order to overcome to the increase of the electricity with the permittivity, we developed a bilayer material composed by an upper layer and an emulsion based material. The bilayer material is able to swing between the properties of the upper layer or the electrostrictive when compressed.

- When the upper layer is used as the bilayer material is the PVA thin film, we are able to keep the same electrostrictive properties but reducing the electrical losses when the material is subjected to a dynamic mechanical stress.

Chapter VII

The power generation of electrostrictive materials using a high frequency vibrational source

I. Introduction

In the last decades considerable effort has been devoted to the development of energy harvesting devices in order to produce autonomous sensors nodes. These are highly integrated, low-power autonomous, light weight, very flexible materials that are able to transform ambient energies into electrical energy. Most of this effort has been carried out using electroactive or electrostatic materials [1, 2]. Due to their ease of manufacturing, several shapes and scales are possible. We distinguished two different scale devices: large and small scales (i.e. cm and mm scale).

i. Power generation using large scale devices

It has been proved that dielectric elastomers are able to produce low-cost, large scale energy harvesting devices with remarkable properties [3-5]. Kornbluh *et al* [4] develop two different devices to harvest the energy created by human motion and ocean waves. The first device is an electrostatic generator in a boot heel that uses the compression of the heel during walking to harvest power from human walk. This device is composed by a stack of electro-active films. The generator uses a fluid to transfer the compression of the heel to the stretching the electro-active polymer. When the heels press down, an elastomer membrane is compressed. The membrane is placed into a frame producing strain and when a voltage is applied across the electrodes it produces power. The device can produce up to 800mW. The second proof of principle is a wave energy converter. The transducers is set in a oceanographic buoy based on a suspended proof mass that stretches the electrostrictive materials as the buoy heaved the waves. When a wave passes, the outriggers of the device moves relative to the buoy and stretch the rolls using a lever arm. The material located between the rings is a dielectric material. Each element consisted of an active amount of dielectric elastomer film of 150 g, which was wrapped to form a roll with a diameter of 30 cm and a length of 20 cm (active length in the stretched condition). The strain for which each roll is subjected corresponds to the height of the wave passing through. The average strain is about 50% and yields a mean power about 0.25W. We note that bigger waves deliver peaks of power of about 1.2W. Further, we should note that these measurements were made with a high bias voltage of 2 000 V applied to the dielectric elastomer.

These are examples of state of the art proof of principle that enables the energy transduction. We stress that the relatively high power that is generated is the result of the use of a high bias voltage.

ii. Power generation using small scale devices

We find out that smaller devices are able to produce scavenge energy as well. As a matter of fact Despesse *et al* [6] developed microstructure of interdigitated silicon fingers to harvest mechanical motions in plane gap configuration. This device has a surface of 1800 mm^2 and is polarized under 120 V. Such experimental device is capable to harvest 1mW due to a narrow gap between the fingers (micron size). Basset *et al* [7] perform a similar experience but reduced the size of the experimental harvester to 66 mm^2. Using a bias voltage equal to 8 V, they measured a generated power of 61nW, about five orders of magnitude lower than Despesse *et al* [6]. We note that both studies use the same electronic system to collect the generated charges (i.e. a charge pump circuit combined with a fly-back circuit). Lallart *et al* [8] used a PVDF-based polymer loaded with carbon nanopowder. The latter nanocomposite is able to produce 415µW under a mechanical strain of about 0.5% at 100Hz. The area of the device is 1000 mm^2, the bias voltage 400 V.

The previous description of the energy harvesting devices shows that the parameters to take into account are broad. The energy harvested is size, frequency and dielectric properties dependent. In order to compare such materials, Basset et al propose a figure of merit (FOM) to normalize the power by all the significant parameters involved in the scavenging. The equation Eq.1 is written as follows

$$FOM = \frac{P}{fAU^2} \quad (1)$$

Where P is the average power, f is the external vibration frequency, A is the device area and U is the applied voltage. Table 3 shows a comparison of the best FOM in the literature for the electromechanical harvesters.

In the present chapter we validate the proof of principle proposed at the beginning of the manuscript.

Table 3 Comparison of the state of the art electromechanical energy harvesters

Author [ref]	Operating frequency f [Hz]	Device area A [mm^2]	Operation voltage U [V]	Converted power P [µW]	Figure of Merit (FOM) P/fAU^2 [$10^8 \mu W/(mm^2 Hz V^2)^{-1}$]
Despesse et al [6]	50	1800	120	$1x10^3$	80
Basset et al [7]	250	66	8	$61x10^{-3}$	6
Lallart et al [8]	100	1000	400	415	2.6
Kornbluh et al [4]	0.1	$2x10^5$	$2x10^3$	$2.5x10^5$	220

The following chapter is devoted to a preliminary study on the samples studied previously in this thesis. In the first section, we describe the electronic device allowing the energy harvesting. In the second section we demonstrate that using an emulsion based nanocomposite we are able to produce electrical power due to a mechanical stress. The third section deals with the perspective of this work.

II. Materials and Methods

i. Materials

We study the power generated by the emulsion based material loaded with CNT and GO nanoparticles previously described in Chapter II, III and IV [9]. The electrostrictive sample is resized in order to fit into the DMA sample holder. The sample holder is constituted by an aluminum support connected to the DMA, an insulating polyether ether-ketone (PEEK) polymer and an aluminum electrode on top (Ø= 20mm). The samples are disks about 1mm thickness for a diameter about Ø= 20mm.

i. Methods

An electronic circuit card constituted by two large capacitors and two diodes is developed in order to measure the power generated by the electrostrictive material used as a variable capacitor when subjected to a mechanical stress. The card is design [7,10,11] to autonomously pump the charges generated by the variable capacitor charges [12] and return it back, due to a fly-back system [1] in order to generate power.

We remind that the capacitors C_{res} (4.7µF) to C_{store} (4.7nF) and diodes D_1 to D_2 in the pump charge (red squareFigure 61) enable the control of the charges flow through C_{var} (orange square Figure 21) Once initially charged (blue square Figure 61), C_{res} provides charges to C_{var} when it voltage is minimal (D_1 on). Due to the mechanical stress the voltage across C_{var} increases and provides the generated charges due to the change of the capacitance to C_{store} (D_2 on). When the charges are given to C_{store}, therefore the voltage across C_{var} decreases and C_{res} provides again charges to C_{var} (D_1 on). In order to improve the efficiency of the system, the charges accumulated in C_{store} are returned back to C_{res} via the fly-back circuit (purple square Figure 61). **Note that the fly-back circuit contains a transistor element that is supplied by a continuous bias voltage.** After several cycles, the voltage across C_{res} should increase if the electrostrictive material within C_{var} generates energy. In order to evaluate this energy, we follow the voltage across C_{res} and C_{store} thanks to the measurement interface (green square Figure 61).

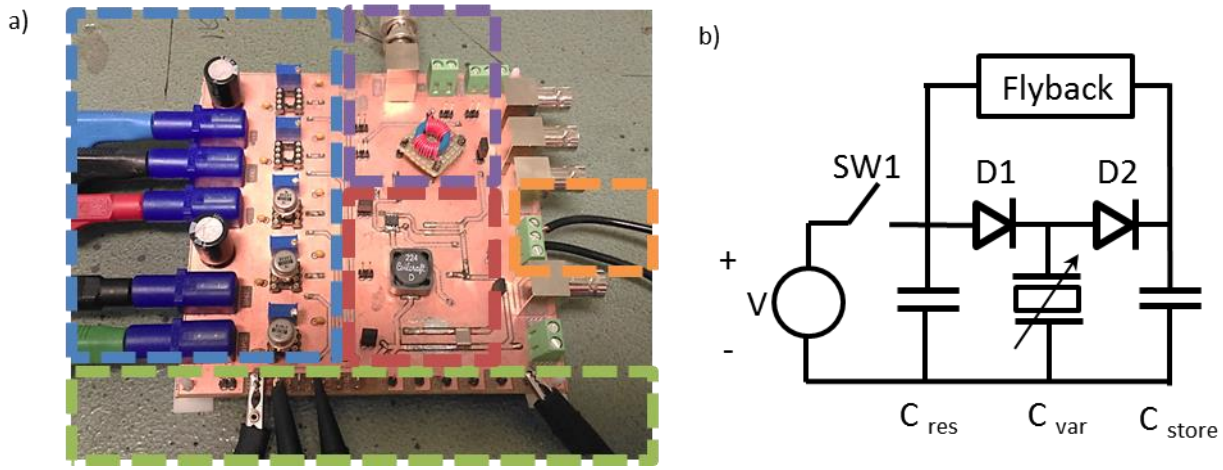

Figure 61: a) Picture of the electronic card circuit that evaluates the energy generated by a variable capacitor using an electrostrictive material. The blue square is the input for power supply of voltage followers. The green square is the measurement interface. The orange square is the input of the variable capacitance. The purple square is the external control for the fly-back circuit. The red square is composed by the core of the charge pump but C_{var} and fly-back circuits. b) Scheme of the equivalent circuit of electronic card.

The electrostrictive material is subjected to a mechanical stress applied by a DMA/SDTA861e machine. We note that the maximal mechanical strain/force applied to the samples is about 5%/15N and the mechanical frequency is about 100Hz due to the DMA instrument limits. The energy supply is ensured by Hameg HMP4040 generator. The fly-back circuit is controlled by a wave generator Agilent 33500B. The voltage across the capacitors is measured thanks to an oscilloscope Textronik DP4054B.

III. First results and discussions

We would like to stress that the following data correspond to preliminary results. In the following there is not yet a full comprehension of the phenomena and the result should be taken with such awareness. The electronic card enables the measurement of the voltage across the different capacitors. The measurement of C_{store} and C_{res} enables the study of the generation of power via the electrostrictive material used as a variable capacitance $C_{var.}$ We remind that the capacitors of the charge pump circuit are initially uncharged. In order to create electrical energy, the electrostrictive material used as variable capacitance needs to be

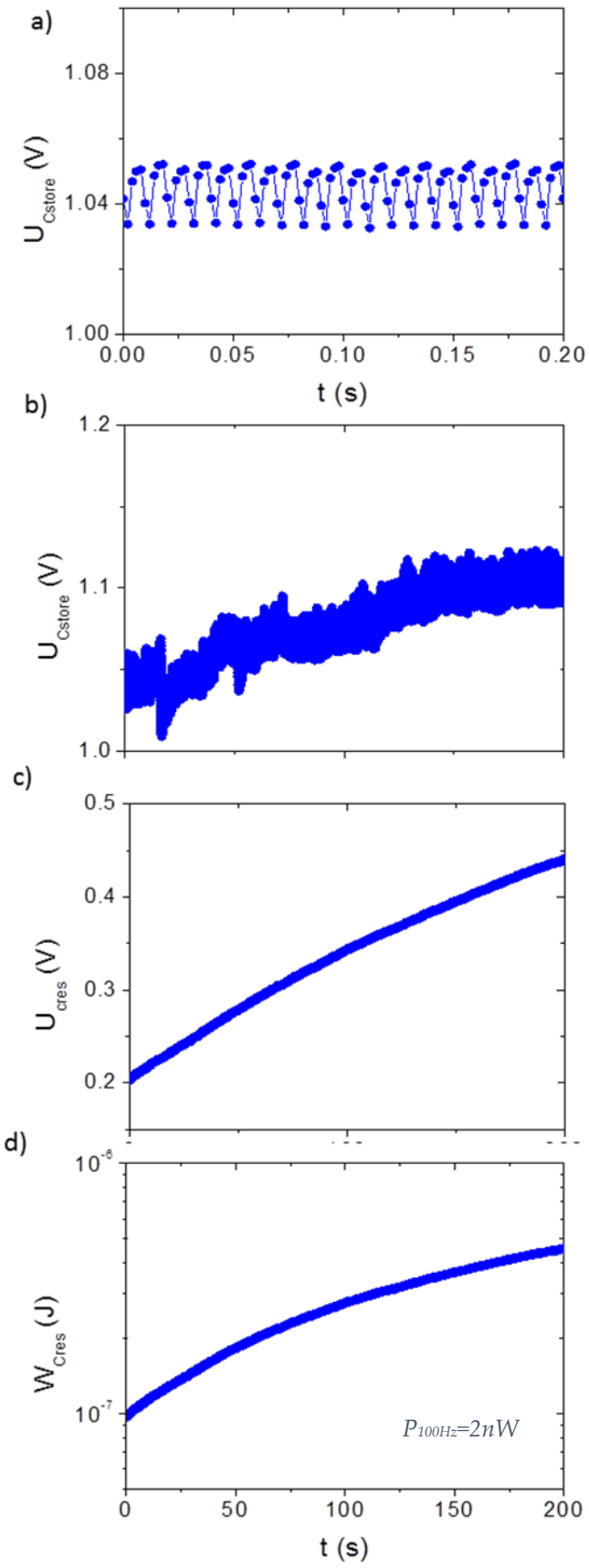

Figure 62: Measurement of the voltage across C_{store} at different time scales a) and b) to evidence the charge pump mechanism. The generated charges are re-injected to c) C_{res} enabling the conversion of energy and d) power generation The studied samples is loaded with 0.05 wt% CNT and subjected to a mechanical stress of 100Hz

polarized, therefore a bias voltage is applied. After the polarization of the variable capacitance, herein a composite material containing 0.05 wt% CNT, the power supply can be unplugged and the systems is fully autonomous. When the electrostrictive material is polarized and subjected to a mechanic stress C_{var} provides charges to $C_{store.}$ Figure 62 a and b shows the increase of the voltage across C_{store} due to the generation of charges by $C_{var.}$ We note that the voltage increases stepwise. Each step corresponds to a mechanical cycle for which C_{var} provides charges to C_{store} (i.e. D_2 is on). In addition, the voltage across C_{store} should growth until saturation as C_{var} provides charges continuously due to the mechanical stress. However according to Dudka *et al* [10] reaching the saturation reduces the efficiency of the charge pump circuit. In order to bypass such saturation, the fly-back circuit is activated every 100Hz. We note that the voltage across C_{store} increases as a function of time due to the generation of new charges. We recall that the mechanical stress is constant and set to 100Hz. Henceforth, the number of charge steps is defined by the frequency of the fly-back circuit. For a fly-back frequency of 100Hz we observe just one cycle of charge per mechanical cycle (Figure 62 b). The fly-back circuit enables to redistribute the generated charges stored at C_{store} and to retune it back to C_{res}. Figure 62c shows the voltage across $C_{res.}$ Due to a variation of the voltage across C_{store}, we are able to calculate as follows Eq1., the power generated by the system [7].

$$W_{res} = \frac{1}{2} C_{res} U_{Cres}^2 \tag{1}$$

Where W_{res} is the converted power by the system, C_{res} the values of the capacitance used as reservoir (i.e. 4.7µF) and U_{Cres} the voltage measured across C_{res}.

We note that the voltage across C_{res} increases as a function of time Figure 62 c such increase corresponds to the generation of electrical energy. Henceforth, after a mechanical stress applied to the electrostrictive material within C_{var}, the electronic circuit delivers higher charges than the initially supply by the bias voltage. Accordingly, we are able to calculate the converted electrical power using the following expression. Eq.2

$$P = \frac{\Delta W_{res}}{\Delta t} \tag{2}$$

Using a fly-back frequency equal to 100Hz, we get 2nW (Figure 62d).

We proved our ability to generate electrical energy from mechanical vibrations using an emulsion based nanocomposite.

In spite this promising results, several results remain unsolved or are unexpected.

IV. Perspectives works and barriers

First the electronic device was designed to harvest higher amount of energy. Such low values may be thus inaccurate. In particular, the use of the fly-back circuit at high frequency could harvest some energy from the transistor embedded in the circuit and re-inject it to C_{res}. Other fly-back circuits are required to test such low power values. A simple fly-back circuit including a single high resistance might be a solution.

Second we note that increasing the applied voltage leads to a decrease of the generated power. We believe that this may be due to the increases of conductivity of our samples as a function of the applied voltage. This behavior seems to be related to electrochemical reactions. Synthesis of new materials involving non-ionic surfactants or others polymers are required to test this point.

Last but not the least, the main drawback of our samples remains their high conductivity. Many of our samples have not been tested because they discharged very rapidly after the disconnection of the source (Figure 63). One possibility to bypass the issue concerning the discharge time is to modify the electronic circuit itself. Wang *et al* [14] proposed an innovative end efficient approach to enhance the pre-charge procedure. Henceforth, it is proposed to induce the bias polarization field using a ramp procedure to avoid the electric losses in the system and to keep the source connected. This procedure is even used for electrostrictive materials that are modeled by a resistance-capacitance (RC) in parallel with a resistance in series. Henceforth the approach is also valid for high dielectric losses material, for which the dielectric permittivity is high. We expect that using a similar approach will help us to gain a significant increase on the converted power.

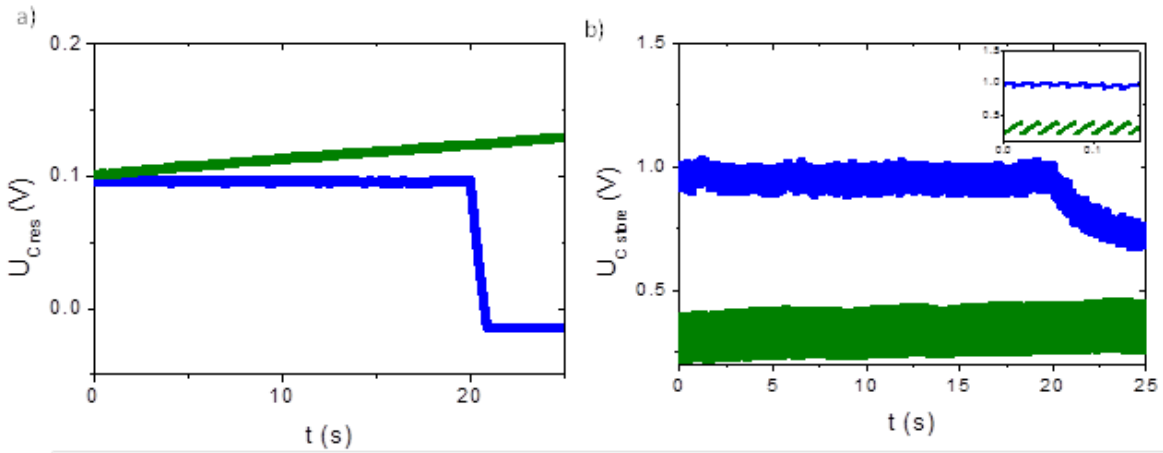

Figure 63: Voltage across a) C_{res} and b) C_{store} on the electronic circuit as a function of time. Within the variable capacitor C_{var}, two different materials, a high ($i.e. \Delta\varepsilon'_r > 100$) and a low ($i.e. \Delta\varepsilon'_r < 100$) relative dielectric permittivity, were studied. The blue points correspond to a high permittivity material ($i.e.$ 0.5 wt% cnt) while the green one to a low permittivity (i.e. 0.1%wt cnt).The inset shows the charging cycles across U store due to the mechanical stress cycles. C_{res} and C_{store} are discharged (t=20s) when the SW1 is open and the material within C_{var} is too conductive.

V. Conclusion

We have proved that the emulsion based electrostrictive materials enables the conversion of mechanical energy into electrical energy. The generated power remains low due to different barriers to overcome provoked by the nature of the surfactants and the charge pump circuit. It is worthy to mentioned that we are not yet able to convert power using the nanocomposite for which the permittivity or the electrostrictive coefficient are the highest, due to high electrical losses. Wang *et al* proposed a promising solution to harvest power from high dielectric materials. The increase is estimated up to 10^6 times higher (i.e. 1mW) by solving the bias voltage applied; however we can expect even greater power conversion by using the state of the art materials presented in Chapter III and V. The replacement of several components such as the surfactant or the curing agent on the formulation seems the easiest parameter to assess. As a matter of fact these perspectives are currently under study.

References:

1. *S. Roundy, P. K. Wright, and J. Rabaey, "A study of low level vibrations as a power source for wireless sensor nodes," Computer Communications, vol. 26, no. 11, pp. 1131–1144, Jul. 2003.*

2. *L. J., Romasanta, M. A. Lopez-Manchado, and R. Verdejo. « Increasing the performance of dielectric elastomer actuators: A review from the materials perspective ». Progress in Polymer Science. 2015*

3. *Carpi F., DeRossi D., Kornbluh R, Pelrine R., Somer-Larsen P. « Dielectric elastomers as electromechanical transducers. Fundamentals, Materials, Devices,Models, and applications of an emerging electroactive polymer Technology, Elsevier, Amsterdam,2008*

4. *Kornbluh R.D., Pelrine R., Prahlad H., Wong-Foy A.,McCoy B. Kim S., Eckerle J.,"From boots to buoys: promises and challenges of dielectric elastomer energy harvesting", Porc SPIE 7976, p797605,2011*

5. *Kornbluh R.D., Eckerle J., McCoy B., "A scalable solution to harvest kinetic energy" Newsroom ,2011 SPIE, 10.1117/25.1201106.003749.*

6. *G. Despesse, T. Jager, S. Basrour, J.J. Chaillout, B. Charlot, J.M. Léger and A. Vassilev "High damping electrostatic micro devices for vibration energy scavenging "Proc. DTIP'05 pp 386–90*

7. *P Basset, D Galayko, A Mahmood Paracha, F Marty, A Dudka and T Bourouina "A batch-fabricated and electret-free silicon electrostatic vibration energy harvester" J. Micromech. Microeng. 19 (2009) 115025 (12pp)*

8. *Lallart M, J.P.Cottinet, L.Lebrun, B. Guiffard and D. Guyomar "Evaluation of energy harvesting performance of electrostrictive polymer and carbon-filled terpolymer composites." J. Appl.Phys. 2010, 108, 034901*

9. *A. Luna, J. Yuan,C. Zakri, P. Poulin, W. Neri, A. Colin, « Giant permittivity polymer nanocomposites obtained by curing a direct emulsion. » Langmuir,10,2015;31(44)*

10. *A. Dudka , P. Basset , F. Cottone , E. Blokhina , D. Galayko "Wideband Electrostatic Vibration Energy Harvester (e-VEH) Having a Low Start-Up Voltage Employing a High-Voltage Integrated Interface" Journal of Physics: Conference Series, Volume 476, conference 1*

11. *A. Dudka , D.Galayko, P.Basset "Design of controller IC for asynchronous conditioining circuit of an electrostatic vibration energy harvester" IEEE Int Conf. on Internet of Things,2012, Workshop on energy and wireless sensors*

12. *B. C. Yen and J. H. Lang, "A Variable-Capacitance Vibration-to-Electric Energy Harvester," IEEE Transaction on Circuits and Systems–I: Regular papers IEEE, vol. 53, no. 2, pp. 288–295, 2006.*

13. *Lebrun, L., D. Guyomar, B. Guiffard, P. -J. Cottinet, and C. Putson. « The Characterisation of the harvesting capabilities of an electrostrictive polymer composite ». Sensors and Actuators A: Physical 153, no 2 (2009): 251-57.*

14. *L.Wang, M. Lallart, L. Petit, L. Lebrun,P.-J. Cottinet and D. Guyomar "Low-cost charge of electrostrictive polymers for efficient energy harvesting" Journal of Intelligent Material Systems and Structures 1–14*

-We validate the proof of principle that nanocomposite for which the inner conductive network can be controlled and tuned by an emulsion approach is able to convert mechanical energy into electrical energy. However several technical barriers and parameters remain to be solved or improved.

-A novel system of electrodes and formulation is necessary. Thanks to the versatility of the emulsion formulation we are able to replace SDS by a non-ionic surfactant and the PDMS matrix (Sylgard 184) by another system using a different curing agent.

- An optimized or enhanced pre-charged system has been recently reported enabling to the use of near percolated electrostrictive material for which the electric losses (tan δ) but specially the dielectric permittivity (ε_r') is higher.

- The ease of manufacturing of the emulsion based materials enables the scale-up of these samples and the production of low cost, energy harvester devices. Bypassing the present barriers would lead to a very promising device, to scavenge ambient energies

General conclusion

We have developed in this research work nanocomposites made via the addition of conductive nano-fillers to soft elastomeric polymers. The particularity of the herein investigated nanocomposite is that the conductive particles are initially added into a continuous phase of an emulsion. The use of an emulsion as a template enables the optimization of the internal tunable network structure of the soft nanocomposite. This approach offers opportunities to control the stiffness, level of connectedness and morphology of the networks of the conductive fillers segregated in between the emulsion droplets at the Plateau borders.

The properties of the networks are finely controlled by the synthesis parameters such as the evaporation rate and curing times, the mean droplet size and the filler concentration. The optimization of these parameters yields very high permittivity values at the vicinity of the percolation threshold. At 100Hz, a carbon nanotube based nanocomposite material loaded with 0.4 wt% presents a dielectric permittivity as high as $2x10^4$ for a corresponding electrical conductivity of 10^{-4} S/m. At the same frequency, and in the case of a nanocomposite material loaded with 8 wt% graphene oxide (GO), the permittivity is as high as $4x10^4$ for a conductivity of about $2x10^{-2}$ S/m. The latter materials present a common and remarkable morphology regarding the relative sizes of the droplets and fillers. Optimal properties were obtained for an average length of the fillers ten times smaller than the mean droplet size. The present approach is addition of being versatile is easily scalable. It can even be extended to other low-cost organic fillers such as carbon black for potential industrial applications.

We have used a simple and direct technique to characterize the electrostrictive properties of the investigated materials without tedious sample preparation. The results delivered by this technique were corroborated using a more delicate actuator approach. Contrary to the widely used actuator technique, the developed technique allows measurements at low voltage so that to the contribution of true electrostriction can be more easily characterized. The developed soft materials are found to be very sensitive to a mechanical load with an unprecedentedly high electrostrictive coefficient $M_{33} \approx 1x10^{-11}$ m^2/V^2 at 100Hz.

In spite of such high electrostrictive coefficients, the use of emulsion based nanocarbon composites energy harvesting applications remains challenging due to high electric losses. A route to limit losses consists in adding a layer of a dielectric material on top of the layer of electrostrictive material. Nevertheless, this route has also some limitations. It will be critical in future studies to optimize further the structuration of the nanocomposites. It will also be important to develop materials that are chemically more stable so that higher voltages can be used without electrochemical degradations. This will allow the storage of a greater energy density in the variable capacitors. Lastly, it will also be critical to engineer the most suitable electronics so that the energy can be efficiently converted. All these improvements will make emulsion based nanocomposites closer to actual applications of energy transducers that can be used to fulfill the energy demand of autonomous sensors networks.